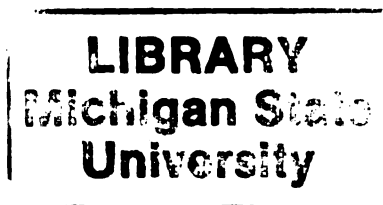




THESIS  
2  
2001



This is to certify that the

dissertation entitled

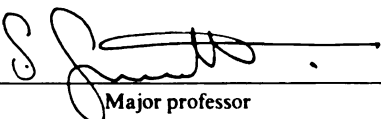
THERMAL AND PHOTOCHEMICAL REACTIONS OF FORMALDEHYDE  
ADSORBED ON Cu(100)

presented by

TODD ROBERT BRYDEN

has been accepted towards fulfillment  
of the requirements for

Ph.D. degree in Chemistry



Major professor

Date August 9, 2001

PLACE IN RETURN BOX to remove this checkout from your record.  
TO AVOID FINES return on or before date due.  
MAY BE RECALLED with earlier due date if requested.

DATE DUE	DATE DUE	DATE DUE
NOV 10 2002		

THERMAL AND PHOTOCHEMICAL REACTIONS OF FORMALDEHYDE  
ADSORBED ON Cu(100)

By

TODD ROBERT BRYDEN

A DISSERTATION

Submitted to  
Michigan State University  
in partial fulfillment of the requirements  
for the degree of

DOCTOR OF PHILOSOPHY

Department of Chemistry

2001



ABSTRACT

THERMAL AND PHOTOCHEMICAL REACTIONS OF  
FORMALDEHYDE ADSORBED ON Cu(100)

By  
TODD ROBERT BRYDEN

Thin films of polymers are promising candidates for a wide variety of technological applications including corrosion protection, chemical sensing media and photonic materials. Polymeric materials are attractive due to the potential of combining high chemical, mechanical, and thermal stability with the ability for synthetically tailoring electronic or optical properties. Current methods for producing polymeric thin films (Langmuir-Blodgett (LB) and self-assembled monolayers(SAM)) have provided few details of the polymerization reaction mechanism and thermal decomposition of the film. Additionally, many monomer systems are amenable to neither LB and SAM techniques nor direct adsorption due to the high reactivity of many surfaces. The use of a co-adsorbate to block reaction on these surfaces has the potential for controlled thin film deposition through photon and/or electron initiated polymerization.

Adsorption of formaldehyde ( $\text{H}_2\text{CO}$ ) on Cu(100) at 85 K formed an overlayer of poly(oxymethylene) (POM). For coverages up to  $1.06 (\pm 0.22) \times 10^{15} \text{ H}_2\text{CO molecules/cm}^2$  ( $\theta=0.69$ ), formaldehyde polymerized to form a monolayer of disordered POM arranged with the chain directions parallel to the surface plane. Formaldehyde formed POM with differing chain lengths; the long ( $\alpha$ ) and short ( $\beta$ ) chain species. These depolymerized to give two features in temperature-programmed desorption at

approximately 207 and 219 K, respectively. The presence of two POM species has not been observed previously in studies of H<sub>2</sub>CO adsorption on metal surfaces.

The complex desorption kinetics observed for the  $\alpha$  and  $\beta$  POM species were successfully modeled using equations based on the ratio of the average number of monomers unzipped from the chain per initiation event to the length of the polymer chain. Vibrational features were observed for the short chain ( $\beta$ ) species at  $\sim 290$ ,  $\sim 1020$  and  $\sim 1120\text{ cm}^{-1}$  that can be assigned to the  $\nu(\text{Cu-O})$ ,  $\nu(\text{C-O})$  and  $\rho(\text{CH}_3)$  modes of oxygen and methoxy endgroups, respectively. Pre-adsorbed methanol increases the proportion of short chain POM species by increasing the probability of termination for the  $\beta$  species. Lower thermal stability for adsorbed POM was observed compared to bulk POM and is believed to be related to the stability of the surface bound oxygen endgroup.

Saturating the Cu(100) surface with carbon monoxide (CO) inhibited the thermal polymerization of H<sub>2</sub>CO on Cu(100). Formaldehyde weakly adsorbed on CO/Cu(100), desorbing at 104 K, corresponding to a desorption energy of 18.2 ( $\pm 0.8$ ) kJ/mol. Irradiation of the H<sub>2</sub>CO/CO/Cu(100) surface caused the molecularly adsorbed H<sub>2</sub>CO to polymerize forming (POM). Irradiation also caused the formation of ethylene glycol. Vibrational features observed after irradiation at 870 and 3365  $\text{cm}^{-1}$  were assigned to  $\nu(\text{CC})$  and  $\nu(\text{OH})$  modes, respectively, of ethylene glycol indicating that it was formed promptly upon irradiation. The presence of ethylene glycol was confirmed by studying its adsorption on clean and oxygen-covered Cu(100). The formation of ethylene glycol was likely governed by geometric constraints present with the formaldehyde overlayer.

*To my barber...*

## ACKNOWLEDGEMENTS

There are so many people that deserve my thanks during the completion of this thesis. Of course, none of the work described here could have been done without the help and guidance of my advisor, Simon Garrett. When starting this work, I knew almost nothing about surface science and you provided the perfect atmosphere for daily discovery by always having your office door open for questions and discussions. From you I've also learned that "try it and see" is an appropriate reason for an experiment and that jaunty angles must be avoided at all costs when designing chambers and gas manifolds.

I must also thank the other members of my committee, Professors Blanchard, Baker and Swain, for listening to my ideas, answering my numerous questions and providing constructive criticism when needed.

Inheriting a nearly empty laboratory provides the opportunity to thank all those involved in the construction and repair of equipment. Russ Geyer deserves an award for all the silver soldering he did for us (and leak-tight on the first try). The rest of the machine shop (Sam, Glenn and Tom) and electronics shop (Ron, Scott and David) were also instrumental in the completion of this work. They always seemed to comply with my "emergency" requests.

Drs. Per Askeland and Kathy Severin deserve a special thanks for making my transition into graduate school go smoothly. As the only remaining Ledford students, they had a wealth of information about the department and its inhabitants.

The members of the Garrett group (Lili, Mike, Heather and Jason) were always open to discussions running the gamut from music, MSU sports, food, and occasionally, even science. They were often quite lively and I really enjoyed them. I should also thank the other members of the Garrett group (John and Mike) for keeping me abreast of the latest in fantasy sports.

Lastly, none of the work would have been possible without the help from my family. Mom, Dad, Sue, Bob, Ann and Glenn were all instrumental in my success even though you may not have understood what I was doing here. Barbara was a saint during our time in East Lansing. Between working two or more jobs and putting up with my frustration during tough experimental sessions, she deserves most of the credit for helping me with the completion of this thesis through her never ending support. I love you and thank you for helping me achieve this goal.

# TABLE OF CONTENTS

LIST OF TABLES	Page ix
LIST OF FIGURES	x
INTRODUCTION	1
1.1 Polymer Thin Films	1
1.2 Topochemical Reactions	2
1.3 Surface Topochemical Reactions	3
1.4 Influence of Co-adsorbate	6
1.5 Proposed System	7
1.6 Reaction of Formaldehyde with Metal Surfaces	10
1.7 Outline of Thesis	12
1.8 References	14
Chapter 2. Experimental	20
2.1 References	29
Chapter 3. Adsorption and Polymerization of Formaldehyde on Cu(100)	31
3.1 Introduction	32
3.2 Results and Discussion	33
3.3 Conclusions	55
3.4 References	56
Chapter 4. Evidence for Two Chain Length Distributions in the Thermal Polymerization of Formaldehyde on Cu(100)	60
4.1 Introduction	61
4.2 Results and Discussion	62
4.3 Conclusions	88
4.4 References	90
Chapter 5. Photochemistry of Formaldehyde Adsorbed on CO-saturated Cu(100)	93
5.1 Introduction	94
5.2 Results and Discussion	95
5.3 Conclusions	116
5.4 References	117
Chapter 6. Conclusions and Future Work	120
6.1 Thermal Reactions and Control of Stability	120
6.2 Photochemical Reactions	123
6.3 References	127

## **APPENDICES**

<b>Appendix A. Mass Spectra</b>	<b>130</b>
<b>Appendix B. Calculation of Electron Impact Ionization Cross-Sections</b>	<b>135</b>
<b>Appendix C. Electron Energy Loss Spectrometer and Operation Voltages</b>	<b>140</b>

## LIST OF TABLES

		Page
Table 3.1	Assignments of the vibrational bands (in $\text{cm}^{-1}$ ) observed by EELS for 0.5 L and 21 L exposures of $\text{H}_2\text{CO}$ on $\text{Cu}(100)$ at 85 K. Also shown are IR data for solid poly(oxymethylene) (POM) and $\text{H}_2\text{CO}$ .	39
Table 3.2	Assignments of the vibrational bands (in $\text{cm}^{-1}$ ) observed by EELS for 0.7 L exposure of trioxane on $\text{Cu}(100)$ at 85 K. Also shown is IR data for solid trioxane.	41
Table 4.1	Results of the fits to equations (4.5) and (4.8) for the data shown in Figures 4.2 and 4.3.	71
Table 4.2	Assignments of the vibrational losses (in $\text{cm}^{-1}$ ) observed by EELS for 1 ML coverages of $\text{H}_2\text{CO}$ and $\text{D}_2\text{CO}$ on $\text{Cu}(100)$ at 85 K; also shown are IR data for solid poly(oxymethylene- $h_2$ ) (POM- $h_2$ ) and poly(oxymethylene- $d_2$ ) (POM- $d_2$ ).	75
Table 5.1	Assignments of the vibrational bands (in $\text{cm}^{-1}$ ) observed for a 1.1 ML coverage of $\text{H}_2\text{CO}$ on CO-saturated $\text{Cu}(100)$ after 0 and 15 minutes UV irradiation. Also shown are IR data for solid $\text{H}_2\text{CO}$ and POM along with EELS data for POM on $\text{Ag}(111)$ .	102
Table 5.2	Assignments of the vibrational bands (in $\text{cm}^{-1}$ ) for the species observed following 15 minutes UV irradiation and annealing to 270 K of a 1.1 ML coverage of $\text{H}_2\text{CO}$ on CO-saturated $\text{Cu}(100)$ . Also shown are IR data for liquid $(\text{CH}_2\text{OH})_2$ along with EELS data for $(\text{CH}_2\text{OH})_2$ on $\text{O}/\text{Ag}(110)$ and $(\text{CH}_2\text{OH})_2$ on $\text{O}/\text{Cu}(100)$ .	109
Table B.1	Molecular orbital constants calculated at the Hartree-Fock level of theory with a 6-31G* basis set. These constants were used to evaluate the electron impact ionization cross-section.	137
Table C.1	Operating voltages for the ELS3000 electron energy loss spectrometer.	141



## LIST OF FIGURES

		Page
Figure 1.1	Schematic representation of a topochemical reaction on a solid lattice.	4
Figure 1.2	Crystal structure of orthorhombic POM (o-POM). Filled circles are methylene (CH <sub>2</sub> ) units.	8
Figure 1.3	Projection of the o-POM <b>b-c</b> plane onto Cu(100).	9
Figure 1.4	Schematic representation of substrate-mediated photochemistry where adsorption of photons, by the substrate, either creates a) subvacuum electrons ( $h\nu < \text{work function}$ ) or b) free photoelectrons ( $h\nu > \text{work function}$ ).	13
Figure 2.1	Sample mount.	21
Figure 2.2	Oxygen coverage on Cu(100), resulting from the directed dosing of O <sub>2</sub> at 300 K, as determined by XPS.	25
Figure 2.3	Ultraviolet/Visible spectrum of ~ 1 M NiSO <sub>4</sub> (aq) solution used as a filter for the medium-pressure Hg arc lamp.	28
Figure 3.1	Mass 29 thermal desorption spectra for increasing doses of H <sub>2</sub> CO on Cu(100). All exposures were made at 85 K. The inset shows the total integrated area for the features between 190 and 230 K as a function of exposure. Exposures are: a) 0.2 L, b) 0.3 L, c) 0.5 L, d) 0.6 L, e) 0.8 L, f) 1.1 L, g) 1.8 L, h) 2.2 L, i) 2.7 L.	34
Figure 3.2	Thermal desorption spectra for masses 2 (H <sub>2</sub> <sup>+</sup> ), 18 (H <sub>2</sub> O <sup>+</sup> ), 28 (CO <sup>+</sup> ), 29 (HCO <sup>+</sup> ), 30 (H <sub>2</sub> CO <sup>+</sup> ), and 31 (H <sub>2</sub> <sup>13</sup> CO <sup>+</sup> ) for a 1.0 L exposure of H <sub>2</sub> CO on Cu(100). Each spectrum is a separate 1.0 L exposure. All exposures were made at 85 K. Spectra are offset for clarity.	37

Figure 3.3	EEL spectra for increasing exposures of H <sub>2</sub> CO on Cu(100) at 85 K. The sample was flashed to 300 K between exposures.	38
Figure 3.4	EEL spectra of a) 0.5 L exposure of H <sub>2</sub> CO on Cu(100) and b) 0.7 L exposure of trioxane on Cu(100). Both spectra were acquired at 85 K.	40
Figure 3.5	EEL spectra as a function of annealing temperature for a 6.3 L exposure of H <sub>2</sub> CO on Cu(100). The “as dosed” spectrum is shown in a) while b) and c) were annealed to the indicated temperature. All spectra were recorded at 85 K. The shoulder at ~ 200 cm <sup>-1</sup> on the elastic peak is the lattice mode associated with the spectrum shown in a). This peak is absent in b) and c).	44
Figure 3.6	XP spectra of a) C (1s) and b) O (1s) for increasing exposures of H <sub>2</sub> CO on Cu(100) at 85 K. The sample was flashed to 300 K between exposures. Exposures were 0, 0.1, 0.2, 0.4, 0.5, 0.7, 0.9, 1.2, 2.1, 5.4, L. Vertical lines are drawn at 288.8 eV and 533.8 eV for the C (1s) and O (1s) regions, respectively.	46
Figure 3.7	Calculated coverage as a function of exposure for the adsorption of H <sub>2</sub> CO on Cu(100) at 85 K based on XPS C(1s) peak areas. Equation of linear fit is $y=0.898*x-0.082$ .	47
Figure 3.8	Enlarged view of the polymer features from the TPD spectra shown in fig. 1. A constant background was subtracted from each spectrum. Exposures ranged from 0.1 L to 1.1 L.	49
Figure 4.1	Mass 29 (HCO <sup>+</sup> ) TPD spectra for (a) 1 ML H <sub>2</sub> CO on Cu(100), (b) 1 ML H <sub>2</sub> CO after annealing to 209 K and cooling to 85 K prior to TPD and (c) 1 ML H <sub>2</sub> CO annealed to 209 K and dosed with H <sub>2</sub> CO to re-saturate the surface. A constant linear background was subtracted from each spectrum.	63

Figure 4.2	Mass 29 ( $\text{HCO}^+$ ) TPD spectra for a 1 ML coverage of $\text{H}_2\text{CO}$ on Cu(100) exposed at 85 K as a function of heating rate ( $\beta$ ). The heating rates were (a) $1.5 \text{ K s}^{-1}$ , (b) $3.8 \text{ K s}^{-1}$ , (c) $5.6 \text{ K s}^{-1}$ and (d) $8.7 \text{ K s}^{-1}$ . The solid line (—) is the raw data, the dotted lines ( $\cdots$ ) are the fits to equations (4.5) and (4.8) and the dashed line (----) is the sum of the fits.	67
Figure 4.3	Mass 29 ( $\text{HCO}^+$ ) TPD spectra for increasing coverages ( $\theta$ ) of $\text{H}_2\text{CO}$ on Cu(100) exposed at 85 K. The coverages were (a) 0.1 ML, (b) 0.3 ML and (c) 0.6 ML. The solid line (—) is the raw data, the dotted lines ( $\cdots$ ) are the fits to equations (4.5) and (4.8) and the dashed line (----) is the sum of the fits.	68
Figure 4.4	Simulated TPD spectra showing the effect of varying $\text{KL}/\text{Dp}$ . The following constant parameters were used for all spectra: $E = 90 \text{ kJ mol}^{-1}$ , $\nu = 1 \times 10^{22}$ , and $\beta = 5.6 \text{ K s}^{-1}$ .	70
Figure 4.5	Electron energy loss spectra of (a) 1 ML $\text{H}_2\text{CO}$ on Cu(100) exposed at 85 K and (b) 1 ML $\text{H}_2\text{CO}$ annealed to 209 K and dosed with $\text{H}_2\text{CO}$ to re-saturate the surface.	72
Figure 4.6	Electron energy loss spectra of 1 ML $\text{H}_2\text{CO}$ on Cu(100) exposed at 85 K and annealed to (a) 140 K, (b) 194 K, (c) 209 K and (d) 300 K. Each spectrum is a separate 1 ML $\text{H}_2\text{CO}$ dose.	74
Figure 4.7	Electron energy loss spectra of (a) 1 ML $\text{H}_2\text{CO}$ and (b) 1 ML $\text{D}_2\text{CO}$ followed by a brief anneal to 140 K.	77
Figure 4.8	Electron energy loss spectra of (a) 1 ML $\text{H}_2\text{CO}$ and (b) 1 ML $\text{D}_2\text{CO}$ followed by a brief anneal to 209 K.	79
Figure 4.9	Mass 29 ( $\text{HCO}^+$ ) TPD spectra after the adsorption of (a) 0.2 L methanol ( $\text{CH}_3\text{OH}$ ) on the Cu(100) surface pre-covered with 0.6 ML $\text{H}_2\text{CO}$ and (b) 0.6 ML $\text{H}_2\text{CO}$ on the Cu(100) surface pre-covered with 0.2 L $\text{CH}_3\text{OH}$ . The “0 L $\text{CH}_3\text{OH}$ ” spectrum is the same for both (a) and (b).	83

Figure 4.10	Electron energy loss spectra of (a) 0.2 L CH <sub>3</sub> OH, (b) 0.6 ML H <sub>2</sub> CO dosed onto the Cu(100) surface pre-covered with 0.2 L CH <sub>3</sub> OH and (c) the spectrum in (b) annealed to 209 K.	85
Figure 5.1	Temperature-programmed desorption spectra for (a) m=30 (H <sub>2</sub> CO <sup>+</sup> ) and (b) m=30 (H <sub>2</sub> CO <sup>+</sup> ) and m=34 (D <sub>2</sub> CO <sup>+</sup> ) for a 1.1 ML coverage of H <sub>2</sub> CO (D <sub>2</sub> CO) on CO-saturated Cu(100) as a function of UV irradiation time. D <sub>2</sub> CO was used to reduce coincident mass fragment interferences.	96
Figure 5.2	Electron energy loss spectra for a 1.1 ML coverage of H <sub>2</sub> CO on CO-saturated Cu(100) for (a) 0 minutes irradiation at 85 K, (b) 15 minutes irradiation at 85 K, (c) 15 minutes irradiation followed by an anneal to 270 K and (d) 15 minutes irradiation followed by an anneal to 450 K. Each spectrum constituted a separate 1.1 ML coverage of H <sub>2</sub> CO. The data were acquired at 85 K.	100
Figure 5.3	Temperature-programmed desorption spectra for m=31 (CH <sub>2</sub> OH <sup>+</sup> ) following exposures of 0.1 L, 0.2 L and 0.5 L of ethylene glycol (CH <sub>2</sub> OH) <sub>2</sub> on clean Cu(100). The inset is the TPD spectrum obtained for a 0.5 L exposure on a Cu(100) pre-covered with 0.1 ML oxygen showing a new feature desorbing at 347 K.	105
Figure 5.4	Electron energy loss spectra for (a) 0.1 L exposure of ethylene glycol (CH <sub>2</sub> OH) <sub>2</sub> on clean Cu(100) and (b) a 0.5 L exposure of (CH <sub>2</sub> OH) <sub>2</sub> on a Cu(100) pre-covered with 0.1 ML of oxygen followed by annealing to 270 K.	107
Figure 5.5	Electron energy loss spectra for (a) 1.1 ML coverage of H <sub>2</sub> CO on CO-saturated Cu(100) irradiated for 15 minutes followed by an anneal to 270 K and (b) a 0.5 L exposure of (CH <sub>2</sub> OH) <sub>2</sub> on a Cu(100) pre-covered with 0.1 ML of oxygen followed by an anneal to 270 K.	111

Figure 5.6	Electron energy loss spectra for (a) 1.1 ML coverage of D <sub>2</sub> CO on CO-saturated Cu(100) irradiated for 15 minutes followed by an anneal to 270 K and (b) a 0.5 L exposure of (CD <sub>2</sub> OH) <sub>2</sub> on a Cu(100) pre-covered with 0.1 ML of oxygen followed by an anneal to 270 K.	112
Figure 6.1	Mass=29 (HCO <sup>+</sup> ) TPD spectra showing the effect of X-ray irradiation on 1.1 ML H <sub>2</sub> CO on CO/Cu(100). Irradiation times were a) 0, b) 84 and c) 130 seconds. The X-ray wavelength was the Al K $\alpha$ ( $h\nu=1486.6$ eV) line and operated at 300 W (20 mA, 15 kV).	124
Figure 6.2	Mass=30 (H <sub>2</sub> CO <sup>+</sup> ) TPD spectra for the UV irradiation of 1.1 ML H <sub>2</sub> CO adsorbed on a surface that had been pre-covered with a saturation of poly(oxymethylene) (0.69 ML) for a) 0 minutes and b) 15 minutes UV irradiation.	126
Figure A.1	Mass spectra of a) background vacuum prior to introduction of H <sub>2</sub> CO and b) after a pressure of $\sim 1\times 10^{-9}$ Torr of H <sub>2</sub> CO was achieved within the chamber.	131
Figure A.2	Mass spectra of a) background vacuum prior to introduction of D <sub>2</sub> CO and b) after a pressure of $\sim 1\times 10^{-9}$ Torr of D <sub>2</sub> CO was achieved within the chamber.	132
Figure A.3	Mass spectra of a) background vacuum prior to introduction of trioxane (C <sub>3</sub> H <sub>6</sub> O <sub>3</sub> ) and b) after a pressure of $\sim 5\times 10^{-9}$ Torr of trioxane was achieved within the chamber.	133
Figure A.4	Mass spectra of a) background vacuum prior to introduction of ethylene glycol ((CH <sub>2</sub> OH) <sub>2</sub> ) and b) after a pressure of $\sim 1\times 10^{-9}$ Torr of ethylene glycol was achieved within the chamber.	134
Figure B.1	Electron impact ionization cross-section ( $\sigma_{EI}$ ) as a function of incident electron energy for H <sub>2</sub> CO and H <sub>2</sub> O and a comparison to previous work done for water showing the small error introduced by using a smaller basis set.	138

**Figure C.1**      **Schematic of the ELS3000 electron energy loss spectrometer.**

**142**

# INTRODUCTION

## 1.1 Polymer Thin Films

The desire to create unique surfaces with specific chemical or physical properties has focussed attention on monolayers and multilayers of organic molecules or polymers. Through innovative synthetic design, polymeric materials can combine high chemical, mechanical and thermal stability with tailored adhesion, wettability, tribological, electronic or optical properties. Hence, macromolecular thin films are promising candidates for a wide range of technological applications including corrosion protection<sup>1,2</sup> and chemical sensing media.<sup>3</sup>

Ordered polymer films with crystalline character are especially important for technological applications since they generally possess superior optical and electronic properties compared to their amorphous counterparts. Device performance is strongly dependent on defects and grain boundaries. In particular, interest in photonic materials,<sup>4,5</sup> field-effect transistors<sup>6,7</sup> and light-emitting diodes<sup>8</sup> has focussed a great deal of effort on the development of techniques for producing crystalline, macromolecular thin films on solid surfaces. The polymer thin film may be deposited onto a solid surface either pre-formed, or as a monomer adlayer followed by subsequent *in situ* polymerization. Methods investigated to date include the deposition and polymerization of unsaturated Langmuir-Blodgett (LB) films<sup>9,10</sup> and, more recently, self-assembled monolayers (SAMs).<sup>11-16</sup> In these cases, the physical structure of the polymer film is known to be influenced by the atomic arrangement of the underlying solid substrate. For example, deposition of poly(oxymethylene) (POM),  $-(CH_2-O)_n-$ , from solution onto

cleaved alkali halide single-crystals generates extended polymer chains aligned with specific substrate crystal directions.<sup>17</sup> The preferred directions appear to strongly correlate with minimal lattice mismatch between the macromolecular chain and surface unit cells.

While polymerization reactions are believed to be important in some catalytic carbon-carbon coupling reactions,<sup>18</sup> there are relatively few fundamental studies of small molecule polymerization reactions on surfaces. There is some precedent for thermal polymerization of  $\text{H}_2\text{CO}$  to POM on several metal surfaces: O/Ag(110),<sup>19</sup> Ni(110),<sup>20</sup> Pt(111),<sup>21</sup> Pd(111),<sup>22</sup> O/Rh(111),<sup>23</sup> O/Pd(111),<sup>24</sup> NiO(100)<sup>25</sup> and Cu(110).<sup>26</sup> Thermal polymerization of acetaldehyde on O/Ag(111) has also been observed.<sup>27</sup> These polymerization reactions, along with catalytic coupling reactions, are generally thought to be controlled by the relative rates of diffusion of the adsorbed monomer, initiator species and/or growing polymer chain.<sup>28</sup>

## 1.2 Topochemical Reactions

In contrast to the reactions described above, where surface diffusion largely controls the rate of the reaction, solid-state, “diffusionless” polymerization reactions have been observed. These reactions are termed topochemical because the structure of the products can be directly related to the geometric arrangement of the reactants.<sup>29</sup> Topochemical reactions are selective, rapid and stereospecific.<sup>30</sup> If the product crystal structure can be predicted from the monomer structure, such crystalline monomer to crystalline polymer transformations are considered to be topotactic in nature.<sup>29</sup> For both topochemical and topotactic reactions, a minimal amount of nuclear motion is observed



and empirical rules have been developed from experimental and theoretical investigations: reactive centers must be  $\leq 4 \text{ \AA}$  apart and unsaturated moieties must be nearly parallel.<sup>29,31</sup>

While the ideas of topochemical reactions may only be applicable in solid materials, it has been shown that a solid surface can exert a high degree of control over the polymerization and subsequent deposition of a polymer thin film. In such epitaxial polymerizations, structural information is conferred upon the first adsorbed polymer layer by the substrate and, in some cases, polymer morphologies are observed that are otherwise unobtainable from solution polymerization followed by crystallization.<sup>32-35</sup>

### 1.3 Surface Topochemical Reactions

We hope to use the substrate to order the monomer intentionally prior to polymerization. If the structure of the adsorbed monolayer matches closely with that of the polymer unit cell, the probability of a topochemical reaction occurring increases. We have chosen a system where a favorable packing geometry exists, as will be discussed below. Many small molecules are known to form well-ordered monolayers with high symmetry on transition metal surfaces increasing the possibility of parallel double bonds.<sup>18</sup> Additionally, the nearest-neighbor distance of most of the transition metals is  $< 4 \text{ \AA}$ ,<sup>36</sup> satisfying another of the rules for topochemical reactions. This is shown schematically in Figure 1.1 where the monomeric units are arranged on a lattice. Upon initiation, the monomer units are allowed free rotation and are oriented for reaction to form the polymer lattice.

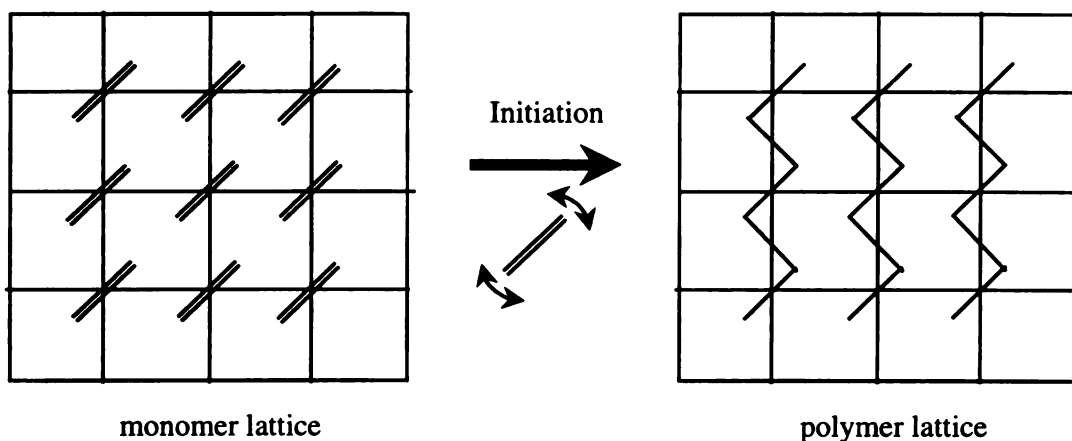


Figure 1.1 Schematic representation of a topochemical reaction on a solid lattice.

In terms of topochemical reactions, there are several differences between an adsorbed monolayer and a crystalline solid that will affect the polymerization reaction. Diffusion of adsorbates on metal surfaces is typically fast (at least 2 orders of magnitude greater than liquid diffusion coefficients) making the overlayer dynamic and less robust than the crystalline phase.<sup>37</sup> The fast diffusion could disrupt the monomer order prior to polymerization, which will lessen the chance for topochemical reaction. Also, due to interadsorbate and adsorbate-substrate interactions, unique monolayer structures may be formed that may increase or decrease the probability of a topochemical reaction. For example, bulk crystalline trioxane has been observed to photopolymerize topochemically however the structure observed for monolayer trioxane adsorbed on Cu(111) ( $\sim 15$  Å separation between molecules)<sup>38</sup> would probably preclude such a reaction from occurring based on the empirical rules.

Mechanistic factors will also affect the polymerization reaction on a surface. Successful creation of initiators and chain propagation along a specific direction in accordance with the structure of the overlayer will be crucial to formation of the polymer. The surface polymerization could suffer similar problems to solution polymerizations:

inhibition of initiation and premature termination and/or chain transfer reactions. However, the rapid addition of monomers in a topotactic polymerization may be much faster than termination events. Indeed, in solid-state polymerization reactions, monomer addition may occur on a time scale as short as  $10^{-13}$  s.<sup>39,40</sup> Even in the topochemical polymerization of crystalline formaldehyde to crystalline poly(oxymethylene), where the monomer moves a large distance ( $\sim 0.5$  Å), the addition of monomer was found to occur every  $10^{-5}$  s at 80 K.<sup>40</sup> This is faster than the rate seen for solution-phase free radical polymerization where addition occurs on the time scale of  $10^{-2}$ - $10^{-4}$  s at room temperature.<sup>41</sup>

Using the surface to align reactants was first shown for  $2\text{H}_2\text{S} \rightarrow \text{H}_2 + 2\text{HS}$ <sup>42</sup> and  $2\text{HX} \rightarrow \text{H}_2 + \text{X}_2$  ( $\text{X}=\text{Cl}$  and  $\text{Br}$ )<sup>43</sup> on  $\text{LiF}(001)$  where photochemical product energies and yields were markedly different than those seen in the gas-phase. The photochemistry of  $\text{HX}$  is thought to occur through an aligned  $\text{HX}$  dimer where the close proximity of the two  $\text{HX}$  molecules is afforded by adsorption on the  $\text{LiF}$  surface. Also, the photooxidation of  $\text{CO}$  on  $\text{Pt}(779)$  occurs by dissociation of co-adsorbed  $\text{O}_2$  at step-edges, which are aligned to oxidize  $\text{CO}$  adsorbed at step-edges preferentially.<sup>44</sup> The chemistry need not be photon driven. The observed probability of non-terminal addition of deuterium atoms to 1-butene adsorbed on  $\text{Cu}(100)$  was found to be greater ( $\sim 5\times$  more) than that seen in the gas-phase and was ascribed to a steric effect based on the adsorption geometry of the molecule.<sup>45</sup>

For most of the systems which have been investigated to date, little is known about the adsorbed monolayer structure prior to polymerization, the polymer morphology or the details of the reaction mechanism. Moreover, the correlation between the atomic

arrangement of the substrate and polymer has not been studied systematically. We are interested in elucidating the polymerization initiation, propagation and termination mechanisms operative for ordered monolayers of unsaturated small molecules, and the influence of the surface on the polymer film order, chain length, conformation and stability. Ultimately, control of some or all of these processes may enable the design of high-quality crystalline polymer thin films. To our knowledge, the possibility of controlling polymerization through the use of a surface acting as a reaction "template" (topotactic reaction) has not been investigated.

#### 1.4 Influence of Co-adsorbate

In addition to studying polymerization reactions on clean surfaces, co-adsorbed species offer the potential to control both the chain length and endgroups of the resulting polymer. In solution polymerizations, chain transfer agents are used to control the molecular weight distribution of a polymerization and determine the endgroup.<sup>41</sup> On a surface, the co-adsorbate may participate in the reaction through initiation and/or termination events; in either case, the endgroup identity may be determined by the co-adsorbate. Endgroup stability of a polymer adsorbed on a surface is known to have a large impact on the thermal stability of the polymer. For example, bulk polyimide made from pyromellitic dianhydride (PMDA) and oxydianiline (ODA) is stable at temperatures up to 500 °C.<sup>46,47</sup> However, polyimide films made from reactive adsorption of PMDA and ODA on Cu(110) decompose at ~ 280 °C.<sup>48,49</sup> The thermal stability of the film is limited by the reactivity of the carboxylate endgroups bound to the surface, but the

decomposition pathway and the influence of the substrate on the endgroup stability have not been correlated.

A co-adsorbate may also be used to control reactivity of the substrate with respect to the monomer. Direct adsorption of the monomer is a simple alternative to LB and SAM methods. However some metal substrates are too reactive to form the polymer thin film through direct adsorption. For example, formation of POM films from  $\text{H}_2\text{CO}$  is not possible through LB and SAM methods and direct adsorption of  $\text{H}_2\text{CO}$  on Fe(100) causes decomposition, and not polymerization, of the adsorbed  $\text{H}_2\text{CO}$ .<sup>50</sup>

Carbon monoxide is an obvious choice for use as the co-adsorbate to control the reactivity of the substrate because it forms a well-ordered monolayer on Cu(100) at 85 K<sup>51</sup> and is only weakly chemisorbed, desorbing molecularly at  $\sim 180$  K.<sup>52</sup> Co-adsorbed carbon monoxide (CO) is known to influence the chemistry observed on surfaces. For example, co-adsorbed CO has been found to increase the stability of ethynylidyne on Ru(001),<sup>53</sup> decrease the stability of the methyl hydrogen atoms of toluene on Ru(001),<sup>54</sup> perturb the decomposition pathway of methylamine on Ru(001)<sup>55</sup> and promote the decomposition of saturated hydrocarbons on Ni(755).<sup>56</sup>

## 1.5 Proposed System

The system chosen for study is the adsorption of formaldehyde on Cu(100). Formaldehyde is an ideal molecule for studying polymerization reactions due to its low activation energy for polymerization ( $\sim 12$  kJ/mol) and the fact the reaction can be self-initiated without the use of an initiator species. Also, the gas, solution and solid-state reactions of formaldehyde have been studied extensively.<sup>39,40,57,58</sup>

Gaseous  $\text{H}_2\text{CO}$  has a  $S_1 \leftarrow S_0$  ( $\pi^* \leftarrow n$ ) band origin at 3.49 eV<sup>57</sup> and can dissociate, upon UV irradiation, via two channels:  $\text{H}_2\text{CO} \rightarrow \text{H}_2 + \text{CO}$  (molecular) and  $\text{H}_2\text{CO} \rightarrow \text{H}^\bullet + \text{HCO}^\bullet$  (radical). The molecular channel has its threshold at 3.52 eV. Polymerization is not expected to be initiated by the molecular photoproducts. The radical channel, whose threshold is at 3.73 eV, may initiate the polymerization through reaction of the radical species with molecular  $\text{H}_2\text{CO}$ .

Formaldehyde can be polymerized to form POM via cationic, anionic and free radical routes.<sup>58</sup> Poly(oxymethylene) can also be formed through ring opening of the cyclic trimer (1,3,5-trioxane) and tetramer (1,3,5,7-tetraoxane) of  $\text{H}_2\text{CO}$ . Both orthorhombic (o-POM) and trigonal (t-POM) crystal structures have been observed for POM in which the POM chains form helices.<sup>59</sup> In t-POM, the helical conformation is designated  $D(10\pi^9)$  while the o-POM conformation is  $D(\pi)$ .<sup>60</sup> The crystal structure of o-POM is shown in Figure 1.2. For t-POM, only one chain per unit cell is present.

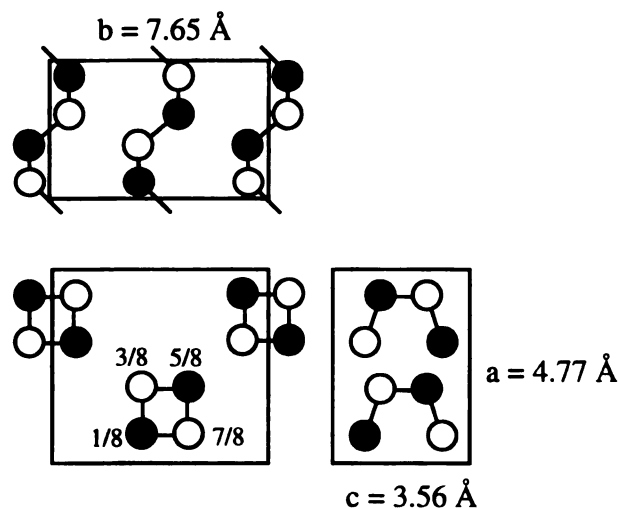


Figure 1.2 Crystal structure of orthorhombic POM (o-POM). Filled circles are methylene ( $\text{CH}_2$ ) units.

The unit cell parameters of the Cu(100) surface match well with those of crystalline o-POM. The *c* dimension of the polymer unit cell (3.56 Å) is only about 1 % smaller than the bulk copper unit cell ( $a_0=3.61$  Å),<sup>36</sup> and the *b* dimension (7.65 Å) is about 6 % larger than  $2a_0$ . This is shown schematically in Figure 1.3 where the **b-c** plane is projected onto the Cu(100) surface plane. The close match of unit cells increases the probability for a topochemical reaction.

The helical conformation observed in the solid-state may not be observed on the Cu(100) surface due to the strong adsorbate-surface interactions. The nearest-neighbor distance for copper (2.55 Å) matches closely with that of the oxygen-oxygen repeat distance (2.49 Å) for POM in a planar zigzag conformation. This conformation has not been observed experimentally due to dipole-dipole repulsion of the neighboring C-O-C units. The helical conformation has been calculated to be ~ 7 kJ/mol lower in energy than the planar zigzag structure.<sup>61</sup>

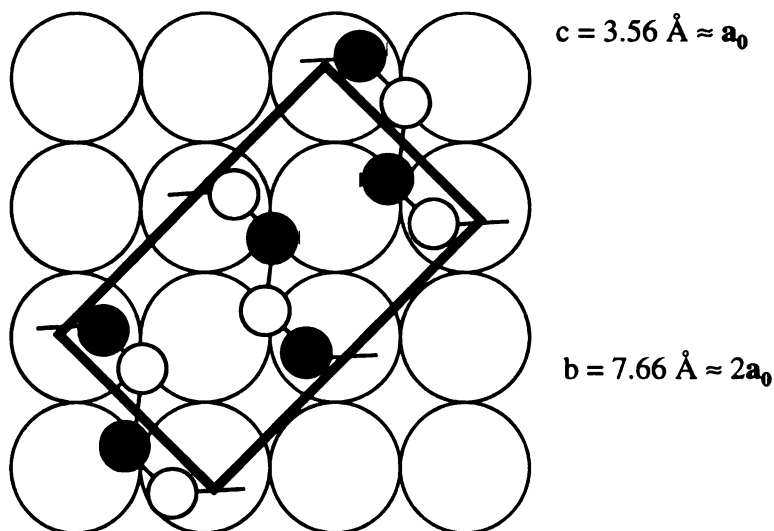


Figure 1.3 Projection of the o-POM **b-c** plane onto Cu(100).

It has been shown that in the solid-state photochemistry of formaldehyde, a high degree of order prior to irradiation is essential for long chain growth of POM. Formaldehyde has been observed to undergo photopolymerization ( $\gamma$ -rays) in the solid-state down to temperatures as low as  $\sim 4$  K producing high molecular weight, crystalline polymer.<sup>39,40</sup> In contrast, no POM was detected after irradiation of amorphous films of  $\text{H}_2\text{CO}$  at 10 and 77 K and, only after doping with  $\text{Cl}_2$  were oligomers formed ( $\sim 6$  monomer units).<sup>62,63</sup>

## 1.6 Reaction of Formaldehyde with Metal Surfaces

As was mentioned previously, the adsorption of  $\text{H}_2\text{CO}$  on metal surfaces has been investigated. Non-dissociative adsorption has been observed on clean  $\text{Ag}(110)$ ,<sup>19,64</sup>  $\text{Ag}(111)$ ,<sup>65</sup>  $\text{Au}(110)$ <sup>66</sup> and  $\text{Zn}(0001)$ <sup>67</sup> at temperatures below 100 K. Reactive adsorption of formaldehyde was found to occur on  $\text{O}/\text{Ag}(110)$ ,<sup>19,64</sup>  $\text{Ni}(110)$ ,<sup>20</sup>  $\text{O}/\text{Zn}(0001)$ ,<sup>67</sup>  $\text{Ru}(001)$ ,<sup>68</sup>  $\text{Rh}(111)$ ,<sup>23</sup>  $\text{Fe}(100)$ ,<sup>50</sup>  $\text{Pt}(111)$ ,<sup>21</sup> and  $\text{Pd}(111)$ <sup>22</sup> with  $\text{H}_2$ ,  $\text{CO}$  and POM being formed. When POM has been observed, it has been speculated the interaction of  $\text{H}_2\text{CO}$  with surface-bound oxygen forms either a formyl species ( $\text{HCO}$ )<sup>68</sup> or a dioxymethylene ( $\text{H}_2\text{CO}_2$ )<sup>64</sup> species which then participates in the polymerization process. The oxygen probably arises due to dissociation of the  $\text{H}_2\text{CO}$  upon adsorption. Oxygen has the ability to act as a nucleophile as well as create Lewis acid sites in its immediate vicinity.<sup>64,69</sup> Both can initiate the polymerization of formaldehyde.<sup>58</sup> Also, partial thermal polymerization was observed on  $\text{Cu}(110)$  at 90 K but the effect of adsorbed oxygen was not addressed.<sup>26</sup>



There has been one investigation on the photopolymerization of formaldehyde adsorbed on a metal surface. Dai *et al.* polymerized formaldehyde adsorbed on Ag(111) using nanosecond pulses of 355 nm radiation.<sup>65,70,71</sup> Formation of POM was observed at 80 K for coverages from 0.1 to 1 monolayer (ML) of adsorbed H<sub>2</sub>CO. In the absence of irradiation, no polymerization was observed. Also, no polymerization was observed upon exposure to 532 nm radiation suggesting a non-thermal initiation mechanism.<sup>70</sup> Below 60 K, no polymerization occurred after irradiation, presumably due to reduced diffusion of H<sub>2</sub>CO or initiator species. However, polymerization did occur after these irradiated samples were annealed to higher temperatures.<sup>71</sup> This is indicative of a diffusion-limited process and not a topochemical reaction.

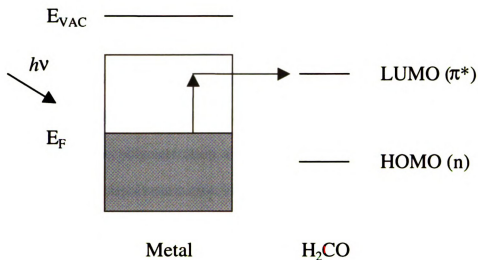
Recent results by Dai *et al.* have shown laser-induced polymerization of formaldehyde on Ag(111) occurs through photoexcited electrons generated within the substrate.<sup>72,73</sup> Substrate sub-vacuum electrons have been observed to initiate chemistry of adsorbates as well as stimulate desorption.<sup>74-77</sup> This is represented schematically in Figure 1.4a where photons ( $h\nu < \text{work function}$ ) are absorbed by the substrate creating hot electrons. These electrons can tunnel to empty states of the molecular adsorbate, inducing chemistry. In Figure 1.4a, the placement of the lowest unoccupied molecular orbital (LUMO) of H<sub>2</sub>CO is somewhat arbitrary as it is not generally known, *a priori*, how the orbitals of the adsorbate line up with the surface. If photon energies greater than the work function are used, free photoelectrons may attach to the LUMO of H<sub>2</sub>CO and also induce chemistry. This is shown in Figure 1.4b. However, for the photopolymerization of H<sub>2</sub>CO on Ag(111), the photon energies used were less than the work function.

If sub-vacuum electrons can initiate polymerization, then electrons from the vacuum side should initiate polymerization as well. Dai *et al.* have found this to be true.<sup>78</sup> Low energy ( 0-20 eV ) electrons were used to irradiate the sample, at 80 K, with polymerization occurring at all electron energies. The substrate sub-vacuum and vacuum side electrons are thought to attach to H<sub>2</sub>CO forming an unstable negative ion state. This negative ion dissociates into CH<sub>2</sub> and O<sup>-</sup> on Ag(111) which is in contrast to H<sub>2</sub>CO<sup>-</sup> gas phase dissociation into H<sup>-</sup> and HCO.<sup>78</sup> Either CH<sub>2</sub> or O may be responsible for the polymerization. In light of the thermal polymerization observed on oxygen covered surfaces, oxygen is more likely to initiate the polymerization.

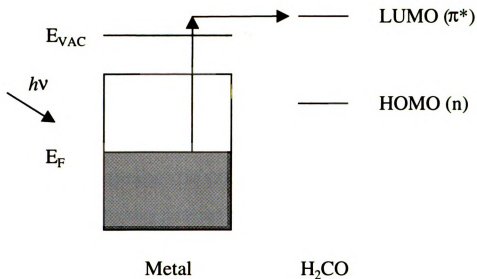
The work performed by Dai's group indicates polymerization of formaldehyde on Ag(111) is strongly temperature dependent. Topochemical polymerization reactions are not diffusion-limited processes and thus Dai's work should not be considered topochemical in nature. Also, neither the ordering of the monolayer, with respect to the substrate, nor the resulting polymer conformation was investigated. Information regarding both will be important for realizing some of the goals of the work described in this dissertation.

## 1.7 Outline of Thesis

The first step in the work described within this thesis was to study the adsorption of formaldehyde on Cu(100) at cryogenic temperatures ( $\leq 85$  K). This is discussed in Chapter 3. We have shown that at 85 K, H<sub>2</sub>CO spontaneously polymerizes to form a saturated monolayer of POM.<sup>52</sup> The POM depolymerizes, forming molecular formaldehyde which desorbs promptly, between 190 and 220 K. A small amount of H<sub>2</sub> is



a) Creation of subvacuum electrons followed by tunneling to LUMO of  $\text{H}_2\text{CO}$ .



b) Creation of vacuum electrons followed by attachment to  $\text{H}_2\text{CO}$ .

Figure 1.4 Schematic representation of substrate-mediated photochemistry where adsorption of photons, by the substrate, either creates a) subvacuum electrons ( $h\nu < \text{work function}$ ) or b) free photoelectrons ( $h\nu > \text{work function}$ ).

observed to desorb from the surface and is believed to arise from  $\text{H}_2\text{CO}$  dissociating on the clean Cu(100) substrate. A clean surface is obtained after heating to 300 K.

Two different POM species are formed from the thermal polymerization of  $\text{H}_2\text{CO}$  on Cu(100) at 85 K.<sup>79</sup> This is the subject of Chapter 4. Two separate chain lengths are produced in the polymerization and the depolymerization kinetics have been modeled using standard depolymerization kinetic equations. The differences between the ratio of degree of polymerization and the average number of monomer units depolymerized at each initiation step separate the long and short chain POM species. Also, we have used co-adsorbed methanol to preferentially form the shorter species and confirm the identity of the endgroups.

Chapter 5 describes the use of a co-adsorbate, carbon monoxide, to control the reactivity of the Cu(100) with respect to formaldehyde adsorption.<sup>80</sup> A saturation coverage of CO inhibits the thermal polymerization of  $\text{H}_2\text{CO}$  on Cu(100) at 85 K. Upon irradiation with UV photons, molecularly adsorbed  $\text{H}_2\text{CO}$  reacts to form POM and ethylene glycol, which has not been observed previously in the photochemistry of adsorbed formaldehyde. The CO desorbs prior to POM depolymerization offering the possibility for forming patterned polymer films through photopolymerization, followed by desorption of monomer (from the unirradiated areas) and the CO spacer layer.

## 1.8 References

- (1) Laibinis, P.; Whitesides, G. *J. Am. Chem. Soc.* **1992**, *114*, 9022.
- (2) Zhao, M.; Liu, Y.; Crooks, R.; Bergbreiter, D. *J. Am. Chem. Soc.* **1999**, *121*, 923.

- (3) Harsanyi, G. *Polymer Films in Sensor Applications*; TECHNOMIC: Lancaster, PA, 1995.
- (4) Lemoine, V.; Pocholle, J.; Le Barny, P.; Robin, P. In *Molecular Nonlinear Optics*; Zyss, J., Ed.; Academic Press: Boston, 1994; pp 379.
- (5) Lytel, R.; Lipscomb, G.; Thackara, J.; Altman, J.; Elizondo, P.; Stiller, M.; Sullivan, B. In *Nonlinear Optical and Electroactive Polymers*; Prasad, P., Ullrich, D., Eds.; Plenum Press: New York, 1988; pp 415.
- (6) Katz, H.; Bao, Z. *J. Phys. Chem. B.* **2000**, *104*, 671.
- (7) Xu, G.; Bao, Z.; Groves, J. *Langmuir* **2000**, *16*, 1834.
- (8) Grell, M.; Bradley, D. *Adv. Mater.* **1999**, *11*, 895.
- (9) Ejaz, M.; Yamamoto, S.; Ohno, K.; Tsujii, Y.; Fukuda, T. *Macromolecules* **1998**, *31*, 5934.
- (10) Shirai, E.; Urai, Y.; Itoh, K. *J. Phys. Chem. B.* **1998**, *19*, 3765.
- (11) Ford, J. F.; Vickers, T.; Mann, C.; Schlenoff, J. *Langmuir* **1996**, *12*, 1944.
- (12) Sun, F.; Castner, D.; Grainger, D. *Langmuir* **1993**, *9*, 3200.
- (13) Kim, T.; Chan, K.; Crooks, R. *J. Am. Chem. Soc.* **1997**, *119*, 189.
- (14) Chan, K.; Kim, T.; Schoer, J.; Crooks, R. *J. Am. Chem. Soc.* **1995**, *117*, 5875.
- (15) Balasubramanian, K.; Cammarata, V. *Langmuir* **1996**, *12*, 2035.
- (16) Batchelder, D.; Evans, S.; Freeman, T.; Haussling, L.; Ringsdorf, H.; Wolf, H. *J. Am. Chem. Soc.* **1994**, *116*, 1050.
- (17) Mauritz, K.; Baer, E.; Hopfinger, A. *J. Polym. Sci.: Macromol. Rev.* **1978**, *13*, 1.
- (18) Somorjai, G. *Introduction to Surface Chemistry and Catalysis*; Wiley and Sons: New York, 1994.
- (19) Stuve, E.; Madix, R.; Sexton, B. *Surf. Sci.* **1982**, *119*, 279.

- (20) Richter, L.; Ho, W. *J. Chem. Phys.* **1985**, *83*, 2165.
- (21) Henderson, M.; Mitchell, G.; White, J. *Surf. Sci.* **1987**, *188*, 206.
- (22) Davis, J.; Barteau, M. *J. Am. Chem. Soc.* **1989**, *111*, 1782.
- (23) Houtman, C.; Barteau, M. *Surf. Sci.* **1991**, *248*, 57.
- (24) Davis, J.; Barteau, M. *Surf. Sci.* **1992**, *268*, 11.
- (25) Truong, C.; Wu, M.; Goodman, D. W. *J. Am. Chem. Soc.* **1993**, *115*, 3647.
- (26) Sexton, B.; Hughes, A.; Avery, N. *Surf. Sci.* **1985**, *155*, 366.
- (27) Sim, W.; Gardner, P.; King, D. *J. Am. Chem. Soc.* **1996**, *118*, 9953.
- (28) Bent, B. E. *Chem. Rev.* **1996**, *96*, 1361.
- (29) Thakur, M. In *Encyclopedia of Polymer Science and Engineering*; Wiley and Sons: New York, 1989; Vol. 15; pp 362.
- (30) Wright, J. *Molecular Crystals*; Cambridge University Press: Cambridge, 1987.
- (31) Salcedo, R.; Sansores, L.; Valladares, A.; Likhatchev, D.; Aleandrova, L.; Ogawa, T. *Polymer* **1996**, *37*, 1703.
- (32) Yamashita, Y.; Shimamura, K.; Kasahara, H.; Monobe, K. *Syn. Met.* **1987**, *17*, 253.
- (33) Lando, J.; Baer, E.; Rickert, S.; Nae, H.; Ching, S. In *Initiation of Polymerization*; 212 ed.; Bailey, F. E., Ed.; American Chemical Society: Washington, DC, 1983; Vol. 212.
- (34) Sano, M.; Lvov, Y.; Kunitaki, T. In *Annual Review of Materials Science*; Tirrell, M., Kaufman, E., Giordmaine, J., Wachtman, J., Eds.; Annual Reviews: Palo Alto, 1996; Vol. 26; pp 153.
- (35) Sano, M.; Sasaki, D.; Kunitake, T. *Macromolecules* **1992**, *25*, 6961.

- (36) *CRC Handbook of Chemistry and Physics*, 76 ed.; CRC Press: Boca Raton, 1995-1996.
- (37) Seebauer, E.; Allen, C. *Prog. Surf. Sci.* **1995**, *49*, 265.
- (38) Hofmann, M.; Wegner, H.; Glenz, A.; Woll, C.; Grunze, M. *J. Vac. Sci. Technol. A* **1994**, *12*, 2063.
- (39) Gol'danskii, V.; Benderskii, V.; Trakhtenberg, L. In *Advances in Chemical Physics*; Progovine, I., Rice, S., Eds.; Wiley and Sons: New York, 1989; Vol. 75; pp 349.
- (40) Gol'danskii, V. *Ann. Rev. Phys. Chem.* **1976**, *27*, 85.
- (41) Odian, G. *Principles of Polymerization*, 3 ed.; Wiley and Sons: New York, 1991.
- (42) Bourdon, E.; Das, P.; Harrison, I.; Polanyi, J.; Segner, J.; Stanners, C.; Williams, R.; Young, P. *Faraday Discuss. Chem. Soc.* **1986**, *82*, 343.
- (43) Cho, C.; Polanyi, J.; Stanners, C. *J. Chem. Phys.* **1989**, *90*, 598.
- (44) Tripa, C.; Yates, J. *J. Chem. Phys.* **2000**, *112*, 2463.
- (45) Yang, M.; Teplyakov, A.; Bent, B. *J. Phys. Chem. B.* **1998**, *102*, 2985.
- (46) Kambe, H. In *Aspects of Degradation and Stabilization of Polymers*; Jellinek, H., Ed.; Elsevier: Amsterdam, 1978; pp 393.
- (47) Feger, C.; Franke, H. In *Polyimides: Fundamentals and Applications*; Ghosh, M., Mittal, K., Eds.; Marcel Dekker: New York, 1996; pp 759.
- (48) Haq, S.; Richardson, N. *J. Phys. Chem. B.* **1999**, *103*, 5256.
- (49) Plank, R.; DiNardo, J.; Vohs, J. *Phys. Rev. B.* **1997**, *55*, 10241.
- (50) Hung, W.; Bernasek, S. *Surf. Sci.* **1996**, *346*, 165-188.
- (51) Tracy, J. *J. Chem. Phys.* **1972**, *56*, 2748.
- (52) Bryden, T.; Garrett, S. *J. Phys. Chem. B.* **1999**, *103*, 10481.
- (53) Sasaki, T.; Kawada, F.; Aruga, T.; Iwasawa, Y. *Surf. Sci.* **1992**, *278*, 291.

- (54) Rauscher, H.; Menzel, D. *Surf. Sci.* **1995**, 342, 155.
- (55) Sasaki, T.; Aruga, T.; Kuroda, H.; Iwasawa, Y. *Surf. Sci.* **1992**, 276, 69.
- (56) Orita, H.; Kondoh, H.; Nozoye, H. *Chem. Phys. Lett.* **1994**, 228, 385.
- (57) Moore, C.; Weissnar, J. *Ann. Rev. Phys. Chem.* **1983**, 34, 525.
- (58) Walker, J. F. *Formaldehyde*, 3rd. ed.; Reinhold Publishing Corp.: New York, 1964.
- (59) Tadokoro, H. In *Macromolecular Reviews*; Peterlin, A., Goodman, M., Okamura, S., Zimm, B., Mark, H., Eds.; Interscience: New York, 1967; Vol. 1; pp 119.
- (60) Helical symmetry is specified by the nomenclature  $X(2m\pi/n)$  where X is the point group (C or D), m is the number of turns of the chain per unit cell and n is the number of monomer units per chain per unit cell).
- (61) Tadokoro, H.; Kobayashi, M.; Mori, K. *Rep. Progr. Polymer Phys. Japan* **1965**, 8, 45.
- (62) Mansueto, E.; Ju, C.; Wight, C. *J. Phys. Chem.* **1989**, 93, 2143-2147.
- (63) Mansueto, E.; Wight, C. *J. Photochem. Photobiol. A:Chem.* **1991**, 60, 251.
- (64) Barteau, M.; Bowker, M.; Madix, B. *Surf. Sci.* **1980**, 94, 303-322.
- (65) Fleck, L.; Ying, Z.; Feehery, M.; Dai, H.-L. *Surf. Sci.* **1993**, 296, 400.
- (66) Outka, D.; Madix, R. *Surf. Sci.* **1987**, 179, 361.
- (67) Sen, P.; Rao, C. *Surf. Sci.* **1986**, 172, 269-280.
- (68) Anton, A.; Parmeter, J.; Weinberg, W. *J. Am. Chem. Soc.* **1986**, 108, 1823.
- (69) Madix, R. *Science* **1986**, 233, 1159-1166.
- (70) Fleck, L.; Feehery, W.; Plummer, E.; Ying, Z.; Dai, H. *J. Phys. Chem.* **1991**, 95, 8428.



- (71) Fleck, L.; Ying, Z.; Dai, H.-L. *J. Vac. Sci. Technol. A* **1993**, *11*, 1942.
- (72) Fleck, L.; Howe, P.; Kim, J.; Dai, H. *J. Phys. Chem.* **1996**, *100*, 8011.
- (73) Ying, Z.; Fleck, L.; Dai, H. In *Laser Spectroscopy and Photochemistry on Metal Surfaces*; Dai, H., Ho, W., Eds.; World Scientific Publishing Company: Singapore, 1995.
- (74) Mieher, W.; Ho, W. *J. Chem. Phys.* **1989**, *91*, 2755.
- (75) Zhou, X.; Coon, S.; White, J. *J. Chem. Phys.* **1990**, *92*, 1498.
- (76) Ying, Z.; Ho, W. *Phys. Rev. Lett.* **1990**, *65*, 741.
- (77) Hoffman, A.; Guo, X.; Yates, J.; Gadzuk, J.; Clark, C. *J. Chem. Phys.* **1989**, *90*, 5793.
- (78) Fleck, L.; Kim, J.; Dai, H.-L. *Surf. Sci.* **1996**, *356*, L417.
- (79) Bryden, T.; Garrett, S. *Langmuir* , in press.
- (80) Bryden, T.; Garrett, S. *J. Phys. Chem. B.* , in press.

## Chapter 2 Experimental

*Ultrahigh Vacuum Chamber (UHV).* The experiments to be described were conducted in two connected stainless steel ultrahigh vacuum chambers. Each chamber was separately pumped by a 270 L/s ion pump. The first chamber, spherical in shape, was equipped with a 1-200 amu quadrupole mass spectrometer (QMS) (VG Masstorr 200 DX), an ion gun for noble gas ion sputtering (Phi 04-161 gun, 20-005F controller) and a molecular leak valve (Varian 9515106). This chamber was also equipped with a dual anode X-ray source (VG 3EXR2) and hemispherical electron energy analyzer (VG CLAM2) for X-ray photoelectron spectroscopy (XPS). The pressure was measured by a nude ion gauge. After being baked for ~ 48 hours at ~ 120 °C, the base pressure was typically  $2 \times 10^{-10}$  Torr. The other chamber was double  $\mu$ -metal shielded and housed a high resolution electron energy loss spectrometer (EELS) (LK Technologies LK3000). The  $\mu$ -metal shielding is necessary to reduce the stray magnetic fields present within the chamber to < 35 mG.<sup>1</sup>

The sample was mounted at the end of a long-travel (500 mm) manipulator capable of x, y, z, and  $\theta$  motion (Thermionics 910438NW) which was connected to the spherical chamber. The sample mount was constructed in-house and is shown in Figure 2.1. The mount was connected in vacuum to the threaded end of the manipulator through a Macor block. Macor is a machinable ceramic material that provided both thermal and electrical isolation for the sample mount. Additional thermal and electrical isolation was provided by the cryobreaks (ISI 9611004). The sample was held to the molybdenum sample block by two tungsten clips which provided good thermal and

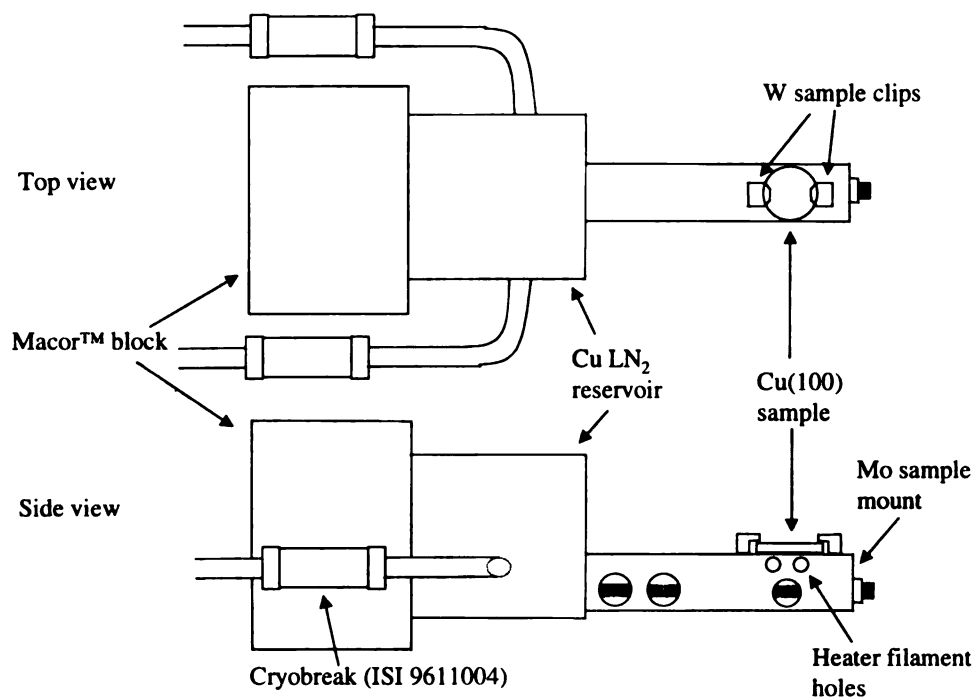


Figure 2.1 Sample mount.

mechanical contact to the mount. The Mo mount was secured to the copper liquid nitrogen (LN<sub>2</sub>) reservoir via a threaded molybdenum rod and nut. The sample temperature was monitored using an E-type thermocouple placed between one of the clips and the front face of the sample. To ensure fast response and low thermal load on the sample, the thermocouple junction was kept as small as possible (OMEGA Engineering, 0.13 mm diameter). The sample could be cooled to 85 K by drawing LN<sub>2</sub> through the reservoir using a small diaphragm pump. The sample was heated indirectly by using a tungsten filament (Alfa Aesar, 0.25 mm diameter). The heater filament was wound (25 turns each side) around a small diameter rod and inserted into alumina tubes (Kimball Physics Al<sub>2</sub>O<sub>3</sub>-TU-C-500) prior to being inserted into the heater filament holes

in the mount. In this fashion, the sample could be heated to  $> 800$  K. All cryogen and electrical lines in vacuum were covered in braided silica sheathing and connections were made via a 2.75 in. multiport flange (MDC MMF275-5-133) attached to the manipulator. Also, the entire mount could be electrically biased via a copper wire attached to the mount.

*Sample Preparation.* The Cu(100) sample (Monocrystal, Inc.  $> 99.99995$  % purity) was cleaned by cycles of argon ion sputtering and annealing. The sample was heated to 680 K, at which time argon was admitted into the chamber to a pressure of  $5 \times 10^{-5}$  torr. The ion pumps were turned off and a gate valve opened to pump the chamber via a turbomolecular pump (Varian V-80) connected to a gas manifold system. The sputtering was begun with the following conditions: 1000 eV, 15 mA emission,  $\sim 25$   $\mu$ A current onto the sample mount. The sample mount geometry prevented a measure of ion current directly onto the sample. Sputtering continued for 15 minutes, at which time the ion gun was turned off and the sample was allowed to anneal at 680 K for 10 minutes prior to cooling to  $\sim 300$  K for analysis. During the post-sputter anneal, the ion pumps were turned on when the pressure was  $< 1 \times 10^{-6}$  torr. The sample was considered clean when XPS and EELS showed no contamination present.

*Generation of Formaldehyde and Dosing.* Gas-phase  $\text{H}_2\text{CO}$  ( $\text{D}_2\text{CO}$ ) was prepared by pyrolysis of paraformaldehyde (Aldrich, 95%) or paraformaldehyde- $d_2$  (Aldrich, 99% atom) using a previously described method.<sup>2</sup> Two Nupro stainless steel in-line gas filters (SS-4F-7), with the sintered filter elements removed, were packed with  $\sim 2$  g paraformaldehyde and  $\sim 3$  g of dried  $\text{MgSO}_4$ . Both materials were constrained within the filters with glass wool that had been deactivated with trimethylchlorosilane.

The filter assembly was attached to the gas line between the molecular leak valve and the gas manifold by a T-connector. The leak valve, gas lines, and the manifold were heated to  $\sim 100\text{ }^{\circ}\text{C}$  to prevent condensation of the  $\text{H}_2\text{CO}$  which was generated, along with water, by heating the filter assembly to  $\sim 60\text{ }^{\circ}\text{C}$ , via heating tape. The water was trapped by the  $\text{MgSO}_4$  prior to introduction into the vacuum chamber. Residual gas analysis of the vapor introduced into the chamber indicated  $\sim 6\%$   $\text{H}_2\text{O}$  contamination. Removal of the drying agent,  $\text{MgSO}_4$ , reduced the water content of the gas to  $\sim 3\%$ . No effect on the chemistry of  $\text{H}_2\text{CO}$  on  $\text{Cu}(100)$  by the water was observed.

The majority of experiments were performed by cooling the sample to  $T \leq 85\text{ K}$  and backfilling the UHV chamber with  $\text{H}_2\text{CO}$  for a predetermined time (background dosing). Exposures of  $\text{H}_2\text{CO}$  are quoted in langmuirs ( $1\text{ langmuir} = 1\text{ L} = 10^{-6}\text{ Torr} \cdot \text{s}$ ) and are uncorrected for ion gauge sensitivity. Directed dosing was accomplished by dosing through a  $1/8^{\text{th}}$  in. O.D. stainless steel tube connected to the molecular leak valve (the gasket assembly within the leak valve was threaded for 8-32 and the tube was soldered to a 8-32 bolt that had been drilled through). The sample was moved away from the end of the doser and dosing was performed by opening the leak valve, while monitoring the most abundant fragment by the QMS, until a constant pressure was achieved. The base pressure, as monitored by the ion gauge, rose by only  $\sim 2 \times 10^{-10}\text{ Torr}$ . Once the QMS signal stabilized, the sample was moved under the doser for a predetermined time. The doser-sample distance was  $\sim 4\text{ mm}$ . Based on background dosing experiments involving  $\text{H}_2\text{CO}$ , enhancement factors of  $\sim 300$  were calculated for directed dosing using the stainless steel tube.

*Preparation of O/Cu(100).* Oxygen-covered Cu(100) surfaces were prepared by dosing dioxygen (AGA, UHP grade) through the 1/8<sup>th</sup> in. O.D. stainless steel tube onto the Cu(100) at 300 K. The oxygen coverage as a function of dosing time is shown in Figure 2.2. A dose time of 300 s was used to prepare a coverage of 0.1 ML as indicated by XPS analysis. At this coverage, oxygen forms a disordered overlayer with the oxygen atoms in 4-fold hollow sites as determined by photoelectron diffraction.<sup>3</sup> A single loss was observed in EEL spectra at 335 cm<sup>-1</sup> (corresponding to  $\nu(\text{Cu-O})$ ) which matches closely with previous investigations of O/Cu(100) where a loss was observed at 340 cm<sup>-1</sup> for a coverage of 0.11 ML.<sup>4</sup>

*X-ray photoelectron spectroscopy (XPS).* The surface chemical composition was determined by XPS. All XP spectra were collected using the Al K $\alpha$  X-ray line ( $h\nu=1486.6$  eV) operated at 300 W (15 kV, 20 mA) and an analyzer pass energy of 100 eV. Photoelectrons were collected at a take-off angle of 75° from the surface normal to maximize surface sensitivity. Spectra were referenced to the Cu (2p<sub>3/2</sub>) peak from clean Cu(100) at 932.7 eV.<sup>5</sup> Typically, photoemission data (Cu (2p), O (1s) and C (1s) regions) were acquired in less than 2 minutes. In order to calculate the C(1s) and O(1s) XPS atomic sensitivity factors for our instrument, single point calibration experiments were performed using a saturation exposure of CO (Matheson, 99.99 %) on the clean Cu(100) surface. This system is known to form a saturated monolayer coverage of 0.57 ML (0.57 CO molecules per Cu atom) at 85 K.<sup>6</sup> Measurement of the C (1s):Cu (2p<sub>3/2</sub>) XPS peak intensity ratio for a CO-saturated monolayer allowed us to calculate an absolute carbon atom concentration for any measured C (1s):Cu (2p<sub>3/2</sub>)

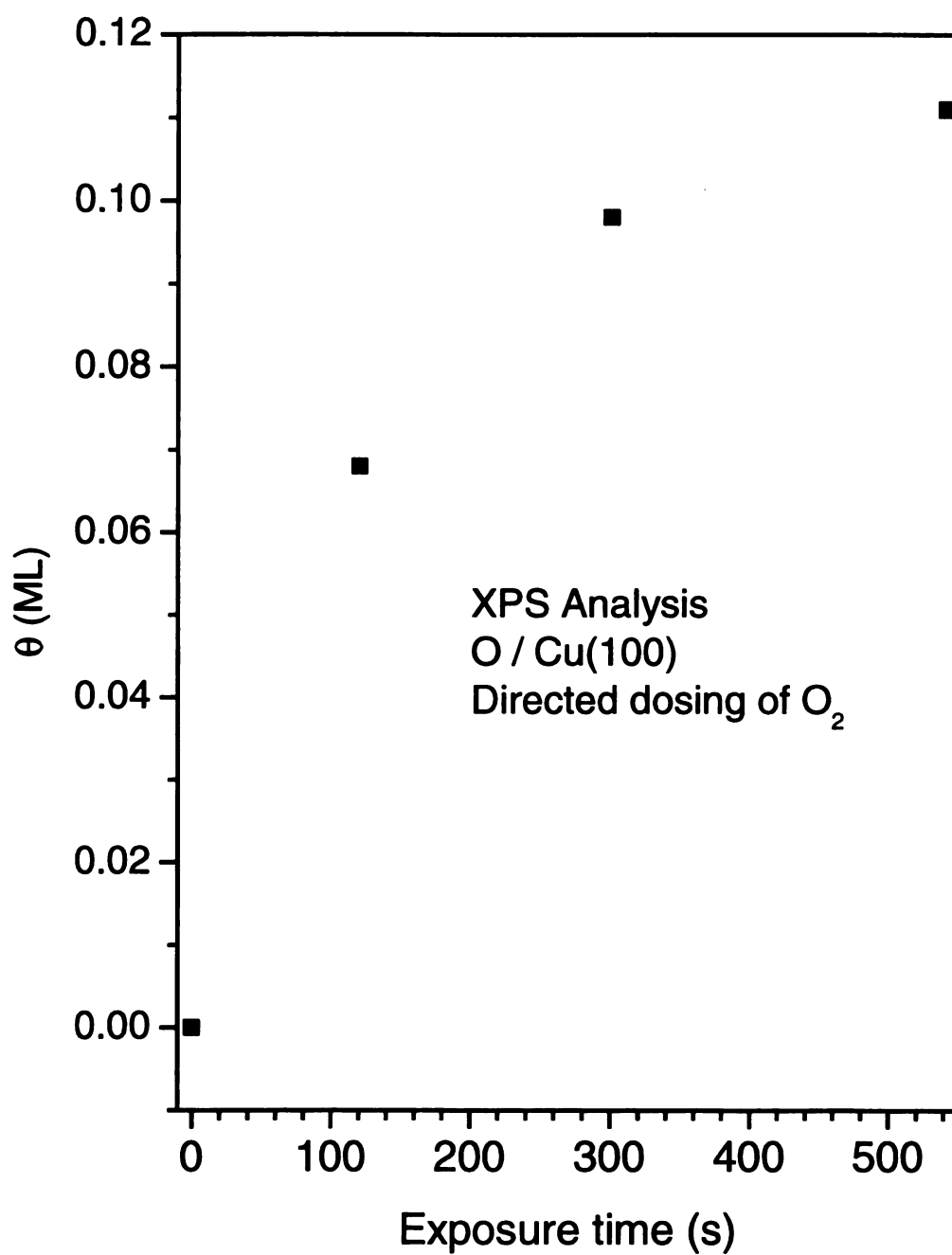


**Figure 2.2** Oxygen coverage on Cu(100), resulting from the directed dosing of O<sub>2</sub> at 300 K, as determined by XPS.

or O(1s):Cu (2p<sub>3/2</sub>) XPS ratio. This method was used to determine the absolute number of H<sub>2</sub>CO molecules for a given exposure.

*Electron Energy Loss Spectroscopy (EELS).* The clean and adsorbate-covered surface was characterized by high resolution electron energy loss spectroscopy (EELS). In a typical EELS experiment, a monoenergetic beam of electrons is scattered off a surface. The majority of electrons scatter elastically, but, a small fraction interact with the surface-adsorbate system and lose quanta of energy corresponding to vibrations of the system.<sup>1,7</sup> For the experiments described here, the dominant interaction was assumed to be dipolar. In this scattering mechanism, the electron scatters inelastically from the long-range dipole field produced by the adsorbate. This interaction changes the momentum minimally and, as such, the electrons that have lost energy are detected very close to the elastic peak (specular direction).

Electron energy loss spectra were acquired in the specular scattering geometry ( $\theta_i = \theta_s = 55^\circ$ ) with a primary electron beam energy of 6.1 eV. The elastically scattered beam from the clean Cu(100) surface was typically 24-32 cm<sup>-1</sup> (3-4 meV) full width at half maximum (FWHM). Under these conditions, currents onto the Cu sample were approximately 300 pA and count rates from the clean Cu(100) surface were >10<sup>6</sup> Hz. From the adsorbate-covered surface, the FWHM ranged from 32-64 cm<sup>-1</sup> (4-8 meV) with count rates of 10<sup>3</sup>-10<sup>5</sup> Hz.

*Temperature-Programmed Desorption (TPD).* The adsorbate-covered surface was characterized by TPD. During TPD experiments, the adsorbate-covered surface was heated at a linear rate (4.2 or 5.7 K·s<sup>-1</sup>) and the desorbing molecules characterized by mass spectrometry. The surface was positioned such that the surface normal was in



direct line-of-sight of the QMS. Molecules were transmitted to the mass spectrometer through a 2 mm diameter aperture in a stainless steel shroud enclosing the ionizer. The shroud ensured the majority of desorbing species originated from the surface and not the sample mount. While heating, a  $-70$  V potential was applied to the sample to prevent electrons from the mass spectrometer ionizer inducing adsorbate chemistry.

The rate of desorption for an adsorbate is equal to the rate of change of coverage ( $\theta$ ) with respect to temperature ( $T$ ) and can be described by the Polanyi-Wigner equation

$$\text{Rate of desorption} = \frac{d\theta}{dT} = \frac{v\theta^n}{\beta} \exp\left(\frac{-E_d}{k_B T}\right) \quad (2.1)$$

where  $v$  is the preexponential,  $n$  is the order of desorption,  $\beta$  is the heating rate and  $E_d$  is the energy of desorption. For zero-order desorption ( $n=0$ ), Arrhenius plots of  $\ln(\text{rate})$  versus  $T^{-1}$  yield values for  $E_d$  and  $v$ . Redhead<sup>8</sup> showed that for a first-order process  $E_d$  can be estimated from the peak desorption temperature ( $T_m$ ) using equation (2.2)

$$E_d = RT_m \left[ \ln\left(\frac{vT_m}{\beta}\right) - 3.46 \right] \quad (2.2)$$

and assuming a value for  $v$  (usually  $10^{13} \text{ s}^{-1}$ ). Equation (2.2) has been found to vary by only  $\sim 2\%$  when  $v$  falls between  $10^8$  and  $10^{13} \text{ s}^{-1}$ .<sup>9</sup> These two analyses represent only a few of the procedures cited in the literature.<sup>9-11</sup>

*Photochemistry.* The adsorbate-covered surface was exposed to unpolarized ultraviolet (UV) radiation from a medium-pressure Hg arc lamp (Oriel 6286) operated at 350 W. The lamp was equipped with an aqueous visible/infrared filter ( $\sim 1 \text{ M NiSO}_4$ ) which transmitted photon energies in the range 5.4-3.9 eV (230-320 nm). The UV/Vis

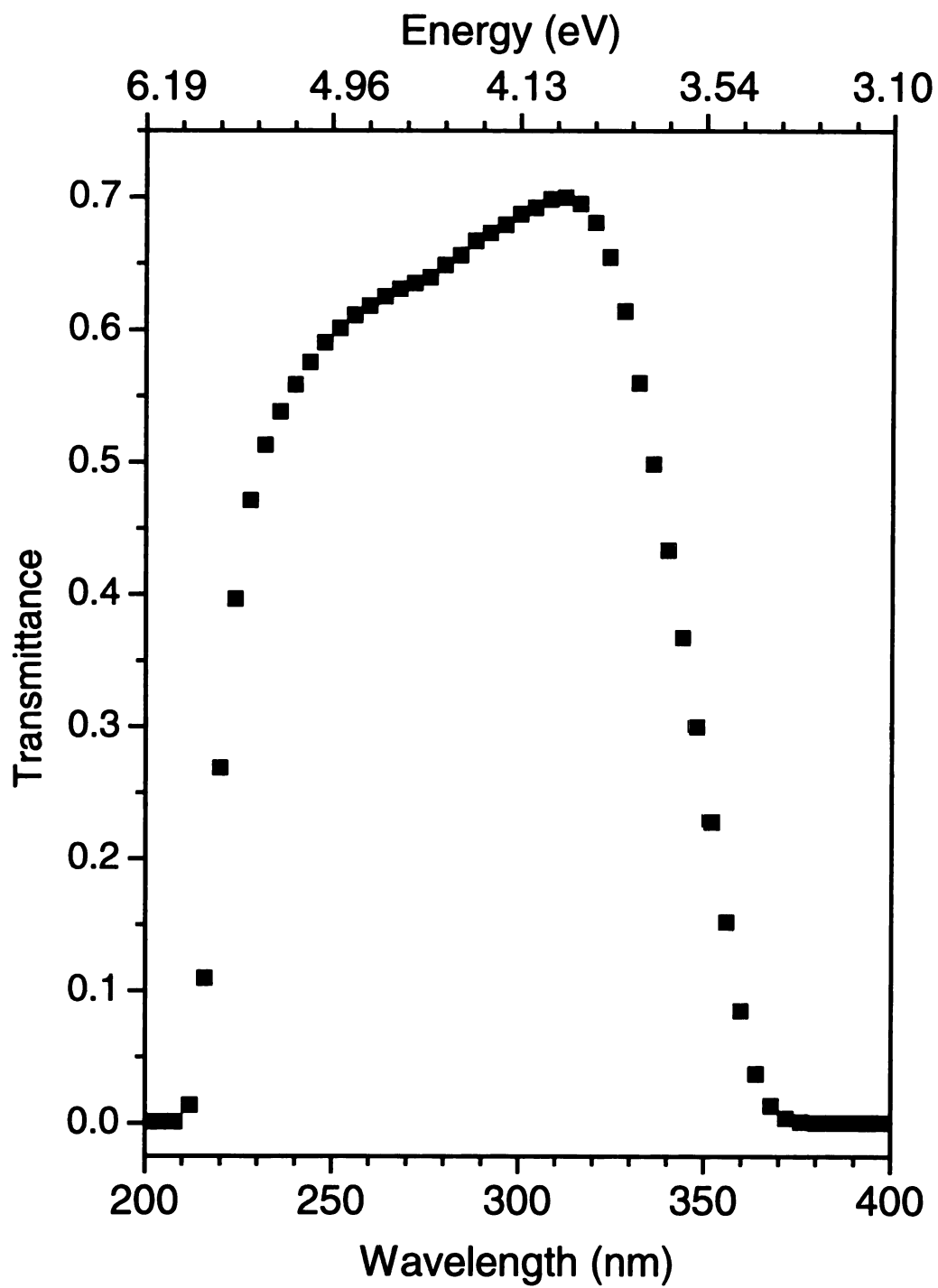


Figure 2.3 Ultraviolet/Visible spectrum of ~ 1 M  $\text{NiSO}_4$  (aq) solution used as a filter for the medium-pressure Hg arc lamp.

spectrum of a  $\sim 1$  M  $\text{NiSO}_4$  solution is shown in Figure 2.3. The UV light was introduced into the UHV chamber through a fused quartz window. The angle of incidence of light was  $45^\circ$  with respect to the surface normal. Irradiation of the chamber and sample mount was minimized through the use of an aperture affixed to the window and irradiation of the sample with a power of  $\sim 9 \text{ mWcm}^{-2}$  resulted in a temperature rise of  $\sim 2$  K. All irradiations were performed at  $T \leq 85$  K.

## 2.1 References

- (1) Ho, W. In *Investigations of Surfaces and Interfaces - Part A*; Rossiter, B., Baetzold, R., Eds.; Wiley and Sons: New York, 1993; Vol. 9A.
- (2) Terentis, A.; Waugh, S.; Metha, G.; Kable, S. *J. Chem. Phys.* **1998**, *108*, 3187.
- (3) Kittel, M.; Polcik, M.; Terborg, R.; Hoeft, J.; Baumgartel, P.; Bradshaw, A.; Toomes, R.; Kang, J.; Woodruff, D.; Pascal, M.; Lamont, C.; Rotenberg, E. *Surf. Sci.* **2001**, *470*, 311.
- (4) Sueyoshi, T.; Sasaki, T.; Iwasawa, Y. *J. Phys. Chem. B.* **1997**, *101*, 4648-4655.
- (5) Seah, M.; Smith, G. In *Practical Surface Analysis*; Briggs, D., Seah, M., Eds.; Wiley and Sons: New York, 1990; Vol. 1; pp 531.
- (6) Tracy, J. *J. Chem. Phys.* **1972**, *56*, 2748.
- (7) Ibach, H.; Mills, D. L. *Electron Energy Loss Spectroscopy and Surface Vibrations*; Academic Press: San Diego, 1982.
- (8) Redhead, P. A. *Vacuum* **1962**, *12*, 203.
- (9) de Jong, A.; Niemantsverdriet, J. *Surf. Sci.* **1990**, *233*, 355.
- (10) Koch, K.; Hunger, B.; Klepel, O.; Heuchel, M. *J. Catal.* **1997**, *172*, 187-193.

(11) King, D. *Surf. Sci.* **1975**, *47*, 384.

### Chapter 3 Adsorption and Polymerization of Formaldehyde on Cu(100)

#### Abstract

The adsorption of formaldehyde ( $\text{H}_2\text{CO}$ ) on clean Cu(100) at 85 K has been studied using electron energy loss spectroscopy (EELS), X-ray photoelectron spectroscopy (XPS), and temperature programmed desorption (TPD). For coverages up to  $1.06 (\pm 0.22) \times 10^{15}$   $\text{H}_2\text{CO}$  molecules/ $\text{cm}^2$ , formaldehyde spontaneously polymerized to form a monolayer of disordered poly(oxymethylene) (POM), arranged with the chain directions parallel to the surface plane. Thermal decomposition/desorption of the polymer monolayer occurred by two routes, producing peaks in temperature programmed desorption (TPD) at approximately 200 K and 215 K. These features were produced by *molecular*  $\text{H}_2\text{CO}$  generated via depolymerization of the polymer. The 200 K and 215 K features displayed apparent zero- and first-order desorption kinetics, corresponding to estimated activation energies for depolymerization of  $75 (\pm 10)$  and  $53.9 (\pm 0.5)$  kJ/mol, respectively. The presence of *two* polymer desorption peaks is attributed to chain conformational differences present within the monolayer, and has not been previously observed in studies of formaldehyde adsorption on metal surfaces. Large exposures of  $\text{H}_2\text{CO}$  on this surface formed multilayers of molecular formaldehyde on top of the first polymer layer. The second layer desorbed at 105 K and subsequent layers at  $\sim 100$  K.

### 3.1 Introduction

Compared to Langmuir-Blodgett (LB)<sup>1,2</sup> and self-assembled monolayer (SAM)<sup>3-8</sup> techniques, direct adsorption of monomer followed by polymerization, either thermally or through initiation with photons or electrons, offers a simple, rapid and solvent-less route to the formation of polymer thin films. However, for most of the systems which have been investigated to date, little is known about the adsorbed monolayer structure prior to polymerization, the polymer morphology or the details of the reaction mechanism. Elucidation of the polymerization initiation, propagation and termination mechanisms operative for ordered monolayers of unsaturated small molecules, and the influence of surface electronic and crystallographic structure on the polymer film order, chain length, conformation and direction(s) in relation to specific crystal directions may ultimately enable the design of high-quality crystalline polymer thin films.

There have been relatively few fundamental studies of small molecule polymerization reactions on surfaces even though this type of reaction plays a large role in Fischer-Tropsch catalysis.<sup>9,10</sup> While the adsorption of formaldehyde on Cu(100) has not been investigated (the focus of this chapter), there is some precedent for thermal polymerization of H<sub>2</sub>CO to poly(oxymethylene) (POM) on several metal surfaces: O/Ag(110),<sup>11</sup> Ni(110),<sup>12</sup> Pt(111),<sup>13</sup> Pd(111),<sup>14</sup> O/Rh(111),<sup>15</sup> O/Pd(111),<sup>16</sup> NiO(100)<sup>17</sup> and Cu(110).<sup>18</sup> Thermal polymerization of acetaldehyde on O/Ag(111) has also been observed.<sup>19</sup> In addition to thermal polymerization, ultraviolet photons or low-energy electrons have been shown to initiate polymerization of other small molecules adsorbed at metal substrates: TCNQ,<sup>20</sup> dinitrobenzene,<sup>21</sup> thiophene,<sup>22,23</sup> formaldehyde<sup>24,25</sup> and styrene.<sup>26</sup>

### 3.2 Results and Discussion

*Temperature Programmed Desorption (TPD).* The adsorption of formaldehyde on Cu(100) was studied by TPD. Figure 3.1 shows a series of  $m=29$  ( $\text{HCO}^+$ ) TPD spectra for increasing exposures of  $\text{H}_2\text{CO}$  (for clarity, not all exposures shown). At 0.2 L  $\text{H}_2\text{CO}$  exposure, desorption peaks of approximately equal intensity were observed at 197 K and 212 K. With increasing exposure of  $\text{H}_2\text{CO}$ , both peaks increased in intensity. However, the 197 K peak shifted to higher peak desorption temperatures, but the 212 K peak remained at approximately the same peak desorption temperature. The total area of these two peaks, as a function of exposure, is shown in the inset of Figure 3.1. The area increases linearly up to an exposure of approximately 0.9 L and then reaches a constant value. Separate fits of the increasing and constant regions intersected at  $0.87 (\pm 0.14)$  L, which can be related to coverage, as discussed below.

For a 1.1 L  $\text{H}_2\text{CO}$  exposure, the two desorption features merged into a broad peak at approximately 205 K, and a new peak was observed at 105 K. For exposures  $>2.2$  L, an additional peak at 100 K grew in that did not saturate with increasing exposure. Based on previous investigations,<sup>18</sup> the 105 K and 100 K features are associated with desorption of molecular  $\text{H}_2\text{CO}$  from the second and subsequent monolayers, respectively. The feature observed at 84 K is attributed to desorption from the heating filament and the large, broad background observed between 100 K and 180 K is attributed to desorption from the sample mount.<sup>27</sup>

Figure 3.2 shows TPD spectra for a 1.0 L  $\text{H}_2\text{CO}$  exposure on Cu(100) measured at masses corresponding to hydrogen ( $m=2$ ,  $\text{H}_2^+$ ), water ( $m=18$ ,  $\text{H}_2\text{O}^+$ ), carbon monoxide

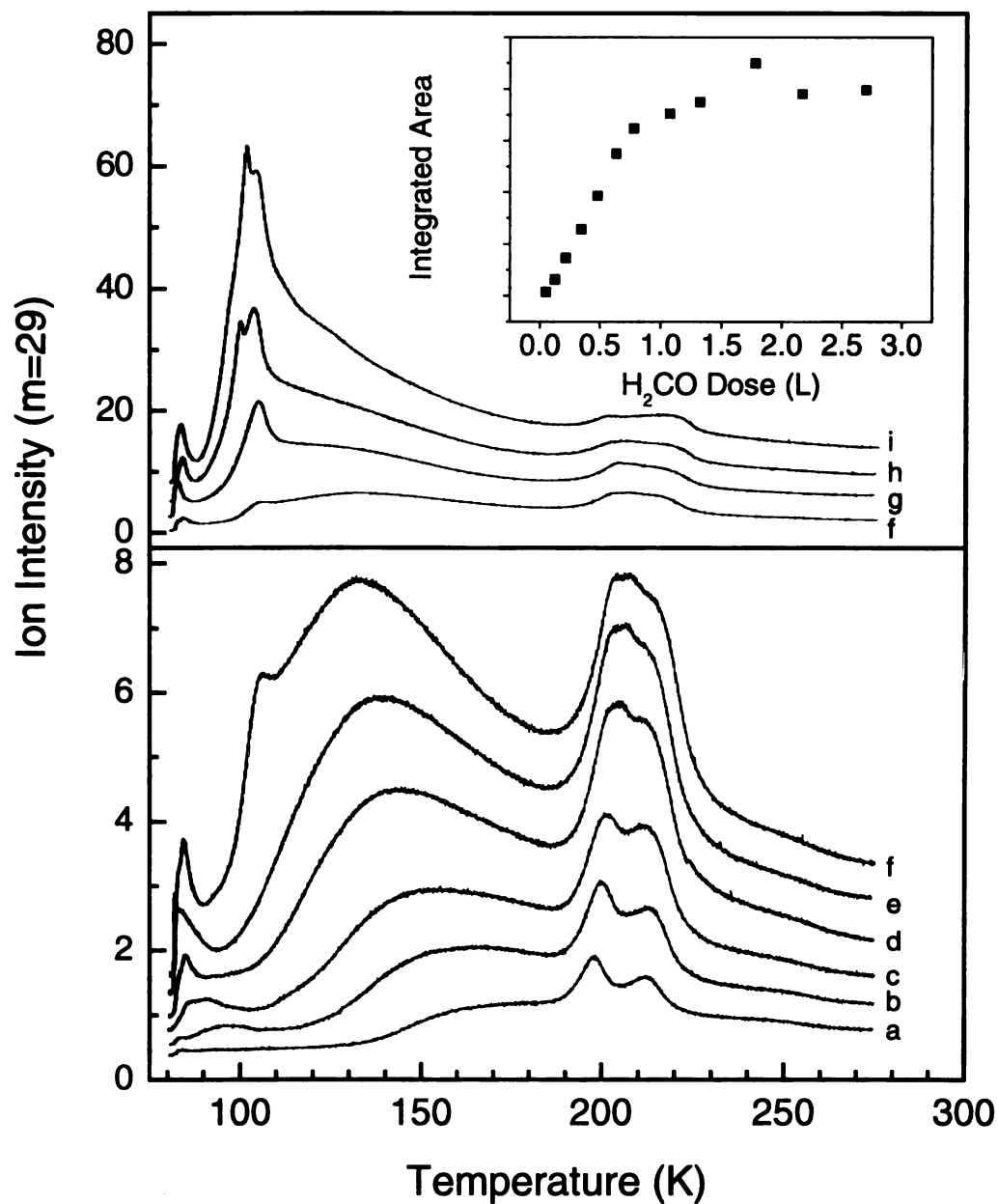


Figure 3.1 Mass 29 thermal desorption spectra for increasing doses of H<sub>2</sub>CO on Cu(100). All exposures were made at 85 K. The inset shows the total integrated area for the features between 190 and 230 K as a function of exposure. Exposures are: a) 0.2 L, b) 0.3 L, c) 0.5 L, d) 0.6 L, e) 0.8 L, f) 1.1 L, g) 1.8 L, h) 2.2 L, i) 2.7 L.



( $m=28$ ,  $\text{CO}^+$ ), formyl ( $m=29$ ,  $\text{HCO}^+$ ), formaldehyde ( $m=30$ ,  $\text{H}_2\text{CO}^+$ ) and  $^{13}\text{C}$ -formaldehyde ( $m=31$ ,  $\text{H}_2^{13}\text{CO}^+$ ). Each spectrum constituted a separate 1.0 L exposure. For masses 28, 29, 30 and 31, the relative abundances for each ion (20:100:48:1.3) between 190 K and 230 K were similar to those obtained from the mass spectrum of  $\text{H}_2\text{CO}(\text{g})$  (24:100:58:1.1).<sup>28</sup> This confirms that the identity of the species desorbing between 190 K and 230 K is molecular formaldehyde. We believe molecular  $\text{H}_2\text{CO}$  is generated as a result of depolymerization of a surface-bound polymer as will be discussed in detail below.

For  $m=28$ , three desorption peaks were observed. The two highest temperature peaks (approximately 200 K and 215 K) can be identified as fragment ions of molecular  $\text{H}_2\text{CO}$ , as described above. However, the 174 K peak was not observed at  $m=29$ , 30 or 31 and thus, is inconsistent with fragmentation of  $\text{H}_2\text{CO}$ . The similarity of the desorption temperature of this peak with that of a CO-exposed Cu(100) surface (data not shown) leads us to conclude that this feature is due to desorption of molecular CO. The  $m=2$  spectrum displays a peak at 178 K and a shoulder at ~200 K. The shoulder likely corresponds with cracking of the  $\text{H}_2\text{CO}$  and is associated with comparable peaks observed at  $m=29$ , 30 and 31. However, the peak at 178 K cannot be attributed to  $\text{H}_2\text{CO}$  cracking. This feature was likely due to recombinative desorption of adsorbed H atoms, which are known to adsorb on copper surfaces at 85 K.<sup>29-31</sup>

For the  $m=18$  TPD spectrum, peaks are observed at 197 K and 224 K, which are associated with desorption of water coadsorbed with the formaldehyde during the gas exposure. A scan of 1-100 amu during desorption showed no other desorbing species.

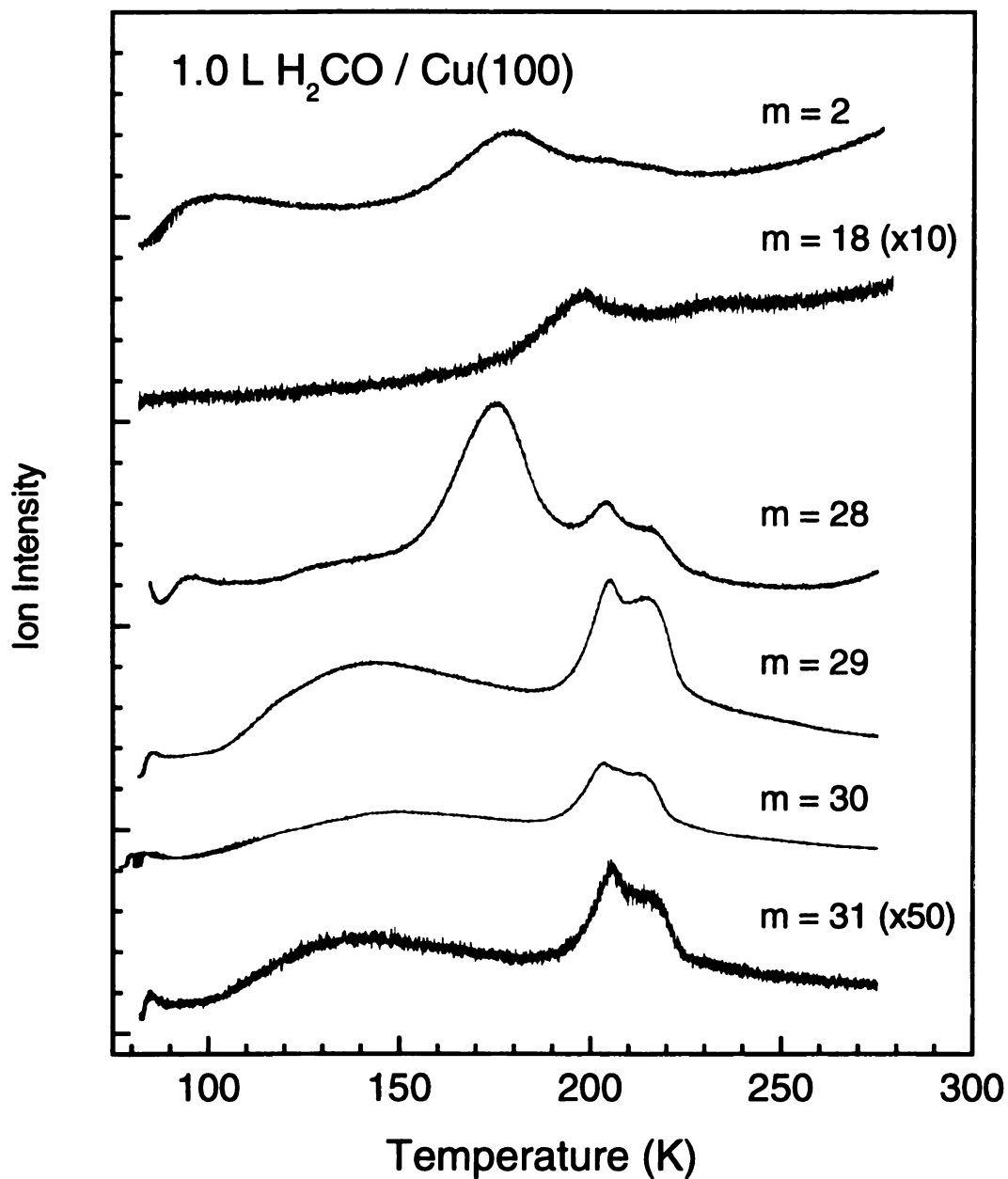


Figure 3.2 Thermal desorption spectra for masses 2 ( $\text{H}_2^+$ ), 18 ( $\text{H}_2\text{O}^+$ ), 28 ( $\text{CO}^+$ ), 29 ( $\text{HCO}^+$ ), 30 ( $\text{H}_2\text{CO}^+$ ), and 31 ( $\text{H}_2^{13}\text{CO}^+$ ) for a 1.0 L exposure of  $\text{H}_2\text{CO}$  on Cu(100). Each spectrum is a separate 1.0 L exposure. All exposures were made at 85 K. Spectra are offset for clarity.

*Electron Energy Loss Spectroscopy (EELS).* Figure 3.3 shows a series of EEL spectra for increasing exposures of H<sub>2</sub>CO on the 85 K Cu(100) surface. Immediately upon adsorption of H<sub>2</sub>CO on this surface, the EELS elastic beam intensity falls by more than two orders of magnitude (from  $>10^6$  Hz to  $\sim 10^4$  Hz), indicative of a significantly disordered adlayer. Table 3.1 summarizes the EELS results together with IR data obtained from gas-phase H<sub>2</sub>CO<sup>32</sup>, solid H<sub>2</sub>CO<sup>33</sup> and the polymer, POM.<sup>34</sup> Excellent agreement is obtained between our EELS data for the 0.5 L H<sub>2</sub>CO-dosed Cu(100) surface and the IR data for solid poly(oxymethylene). The losses at 338 cm<sup>-1</sup> and 2060 cm<sup>-1</sup> can be assigned to  $\nu(\text{Cu-CO})$  and  $\nu(\text{C}\equiv\text{O})$  for adsorbed CO. Importantly, the carbonyl loss due to  $\nu(\text{C=O})$  for H<sub>2</sub>CO is not observed, suggesting no molecular H<sub>2</sub>CO is present on the surface up to about 1.2 L. However, the possibility of H<sub>2</sub>CO adsorbed with the molecular axis parallel with the surface cannot be excluded. The only mode that would be active for dipole scattering in this geometry would be the out-of-plane deformation (B<sub>2</sub> character) which has an associated dipole moment oriented perpendicular to the surface. This mode should appear at  $\sim 1167$  cm<sup>-1</sup>, which is an area of the spectrum that is dominated by polymer loss features.

The presence of 1,3,5-trioxane, the cyclic trimer of H<sub>2</sub>CO, was eliminated based on EELS data taken for the adsorption of trioxane on Cu(100) at 85 K. Figure 3.4 is the comparison of EEL spectra of a 0.5 L exposure of H<sub>2</sub>CO (Figure 3.4a) with that of a 0.7 L exposure of trioxane (Figure 3.4b). Trioxane has been found to have complex adsorption

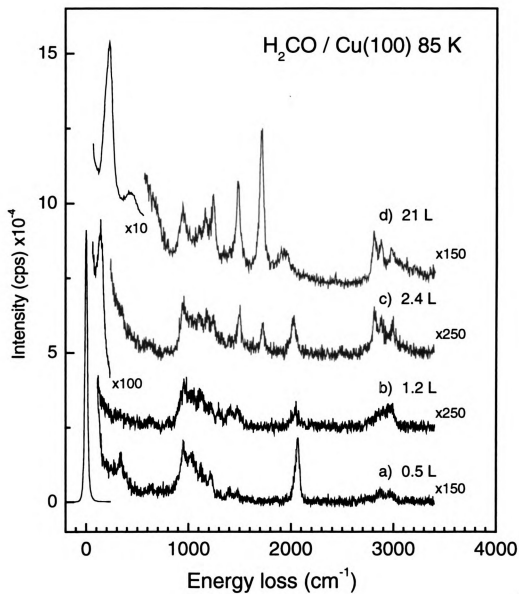


Figure 3.3 EEL spectra for increasing exposures of  $\text{H}_2\text{CO}$  on  $\text{Cu}(100)$  at 85 K. The sample was flashed to 300 K between exposures.

Table 3.1 Assignments of the vibrational bands (in  $\text{cm}^{-1}$ ) observed by EELS for 0.5 L and 21 L exposures of  $\text{H}_2\text{CO}$  on  $\text{Cu}(100)$  at 85 K. Also shown are IR data for solid poly(oxymethylene) (POM) and  $\text{H}_2\text{CO}$ .

Assignment	$\text{H}_2\text{CO Gas}^{32}$	$\text{H}_2\text{CO Solid}^{33}$	21 L $\text{H}_2\text{CO} /$ $\text{Cu}(100)$ 85 K	POM Solid <sup>34</sup>	0.5 L $\text{H}_2\text{CO} /$ $\text{Cu}(100)$ 85 K
lattice mode			228		
$\nu(\text{M-CO})$					338
overtone			423		
$\delta(\text{OCO})$				630	645
$\nu_s(\text{OCO})$			943	932	947
					1030
$\nu_{\text{as}}(\text{OCO})$			1107	1091	1121
$\delta_{\text{oop}}$			1170		
$\delta_{\text{ip}}(\text{H}_2\text{CO}), \tau(\text{CH}_2) / \tau(\text{CH}_2)$ (POM)	1167( $\nu_6$ )	1167	1235	1235/1286	1221
$w(\text{CH}_2)$	1249( $\nu_5$ )	1251		1434	1392
$\delta(\text{HCH})$	1500( $\nu_3$ )	1490	1483	1471	1472
$\nu(\text{C=O})$	1746( $\nu_2$ )	1711	1719		
$\nu(\text{C}\equiv\text{O})$			1931		2060
$\nu_s(\text{CH})$	2782( $\nu_1$ )	2831	2806		
$\nu_{\text{as}}(\text{CH})$	2843( $\nu_4$ )	2886	2874		
$\nu_s(\text{CH})$				2919	2873
$\nu_{\text{as}}(\text{CH})$				2979	2961
Fermi resonance ( $\nu_2 + \nu_5, \nu_4$ )		2996	2970		

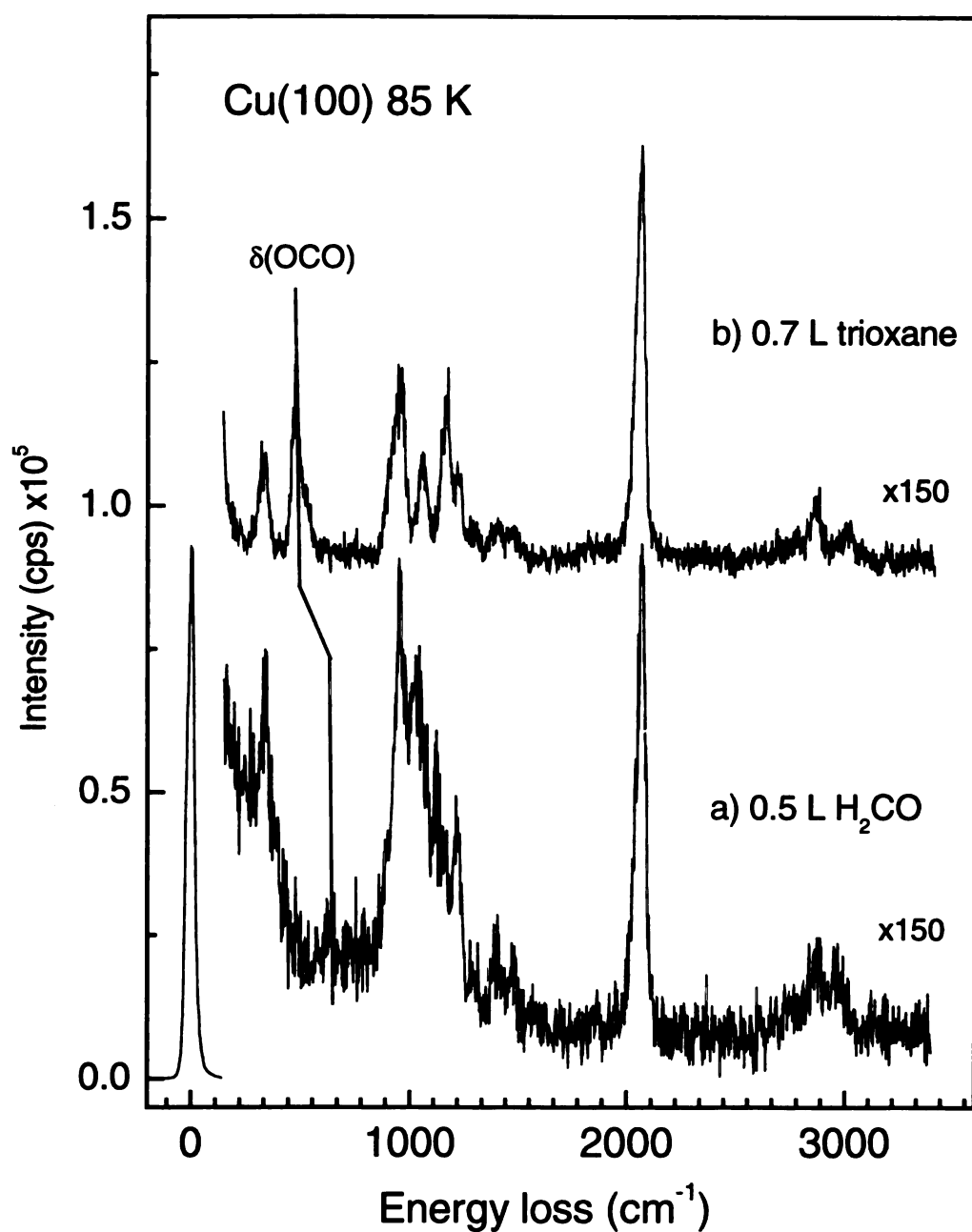


Figure 3.4 EEL spectra of a) 0.5 L exposure of  $\text{H}_2\text{CO}$  on  $\text{Cu}(100)$  and b) 0.7 L exposure of trioxane on  $\text{Cu}(100)$ . Both spectra were acquired at 85 K.

behavior on Cu(111) with monolayer coverage occurring at  $\sim 0.02$  ML and multilayers forming after saturation of the monolayer.<sup>35</sup> The EEL spectrum shown in Figure 3.4b likely corresponds to a multilayer coverage of trioxane on Cu(100) although absolute coverage was not calculated. The losses observed match well to those found for bulk crystalline trioxane as seen in Table 3.2. Also, the observation of losses corresponding

Table 3.2 Assignments of the vibrational bands (in  $\text{cm}^{-1}$ ) observed by EELS for 0.7 L exposure of trioxane on Cu(100) at 85 K. Also shown is IR data for solid trioxane.

Assignment	Symmetry <sup>a</sup>	Trioxane Solid <sup>36</sup>	0.7 L Trioxane / Cu(100)
$\nu(\text{M-CO})$			321
$\delta(\text{COC})$	$A_1$	469	470
$\delta(\text{OCO})$	E	521	526
$\nu_s(\text{COC}) / r(\text{CH}_2)$	$A_1 / E$	951 / 918	946
$\nu_s(\text{COC})$	E	1067	1049
$\nu_a(\text{COC})$	E	1152	1165
$r(\text{CH}_2)$	$A_1$	1222	1215
$t(\text{CH}_2)$	E	1313	1288
$w(\text{CH}_2)$	E	1419	1392
$\delta(\text{HCH})$	E	1483	1472
$\nu(\text{C}\equiv\text{O})$			2059
$\nu_s(\text{CH})$	E	2877	2853
$\nu_{as}(\text{CH})$	E	3031	3003

a) bulk symmetry,  $C_{3v}$

to E modes in bulk trioxane ( $C_{3v}$  symmetry) rules out an overlayer structure with the  $C_3$  axis parallel with the surface normal. Importantly, the loss observed at  $645 \text{ cm}^{-1}$  in Figure 3.4a, assigned to  $\delta(\text{OCO})$ , most closely matches the reported value for POM at  $630 \text{ cm}^{-1}$ . In the IR spectrum of solid 1,3,5-trioxane, this mode is split into two bands at  $744 \text{ cm}^{-1}$  and  $521 \text{ cm}^{-1}$ . For the EEL spectrum shown in Figure 3.4b, the  $744 \text{ cm}^{-1}$  loss was undetected due to its inherently low intensity.<sup>36</sup>

On increasing the H<sub>2</sub>CO exposure to 2.4 L (Figure 3.3c), some recovery of the elastic beam intensity was noted (approximately an order of magnitude), indicating that the second layer is somewhat more ordered than the first (polymer) layer. The appearance of an intense loss at 141 cm<sup>-1</sup> has been previously observed for H<sub>2</sub>CO on a number of surfaces and has been attributed to lattice (phonon) modes of crystalline H<sub>2</sub>CO(s).<sup>11-13,18,37,38</sup> At 2.4 L exposure, the loss at 1483 cm<sup>-1</sup> significantly increased in intensity and a new loss at 1719 cm<sup>-1</sup> appeared. These losses are attributed to molecular H<sub>2</sub>CO and agree with IR data taken on crystalline H<sub>2</sub>CO films at 80 K.<sup>32</sup> The losses at 1184 cm<sup>-1</sup> and 1240 cm<sup>-1</sup> also gained intensity and are assigned to the out-of-plane and in-plane bending modes of H<sub>2</sub>CO respectively. The ν(C-H) region showed three distinct losses which can be assigned to ν<sub>s</sub>(C-H) and ν<sub>as</sub>(C-H) of H<sub>2</sub>CO and to a Fermi resonance between ν<sub>2</sub>+ν<sub>5</sub> and ν<sub>4</sub>. This Fermi resonance has previously been observed in the IR spectrum of crystalline H<sub>2</sub>CO.<sup>32,33</sup> The loss due to adsorbed CO, ν(C≡O), has red-shifted to 2020 cm<sup>-1</sup> and gained intensity relative to 1.2 L, but the loss due to ν(Cu-CO) was still not detected at ~340 cm<sup>-1</sup>. We assume the modest red-shifting of the ν(C≡O) mode is due to intermolecular coupling between adsorbed H<sub>2</sub>CO polymer and CO.

At the largest H<sub>2</sub>CO exposure studied, 21 L, the losses due to molecularly adsorbed multilayer H<sub>2</sub>CO were observed clearly. The lattice mode has gained intensity and blue-shifted by 87 cm<sup>-1</sup> to 228 cm<sup>-1</sup> relative to the 2.4 L exposure. A loss at 423 cm<sup>-1</sup> appeared and is tentatively assigned to an overtone of the 228 cm<sup>-1</sup> lattice mode. The peak at 943 cm<sup>-1</sup>, for which there is no corresponding mode in molecular H<sub>2</sub>CO, is



assigned to the  $\nu_s(\text{OCO})$  mode of polymer formed during acquisition of the EELS spectrum. Previous studies of  $\text{H}_2\text{CO}$  adsorption on  $\text{Ag}(111)$  have shown that polymerization of molecular formaldehyde can be initiated by low-energy electrons and that even exposure to the low fluxes of electrons encountered in EELS can initiate polymerization of multilayers of  $\text{H}_2\text{CO}$ .<sup>25,39</sup>

Figure 3.5 shows a series of EELS spectra taken as a function of annealing temperature for a 6.3 L exposure (multilayer) of  $\text{H}_2\text{CO}$  on  $\text{Cu}(100)$ . The surface was dosed at 85 K, momentarily heated to the indicated temperature and immediately cooled to 85 K prior to data acquisition. Figure 3.5a shows the “as exposed” spectrum taken immediately after 6.3 L of  $\text{H}_2\text{CO}$  on the 85 K  $\text{Cu}(100)$  surface. As expected, it displayed losses characteristic of both molecular  $\text{H}_2\text{CO}$  and POM. In particular, the  $\nu(\text{C=O})$  of  $\text{H}_2\text{CO}$  at  $1720\text{ cm}^{-1}$  and the  $\nu_s(\text{OCO})$  of POM at  $950\text{ cm}^{-1}$  are observed. The  $\nu(\text{C}\equiv\text{O})$  loss due to adsorbed CO at  $2011\text{ cm}^{-1}$ , is observed but it is significantly red-shifted relative to CO adsorption on the bare  $\text{Cu}(100)$  surface.<sup>40</sup> However, at this exposure, the loss due to  $\nu(\text{Cu-CO})$  at  $\sim 340\text{ cm}^{-1}$  was not observed.

Figure 3.5b shows the EELS spectrum obtained after annealing the 6.3 L exposed surface to 120 K. In contrast to the unannealed (85 K) spectrum (Figure 3.5a), the loss due to  $\nu(\text{C=O})$  of multilayer  $\text{H}_2\text{CO}$  was not observed and the losses due to POM were narrower and more intense (in particular the losses assigned to  $\nu(\text{OCO})$  of POM), even though the full width at half-maximum (FWHM) of the elastic peaks for the two spectra were similar. We attribute this observation to increased ordering of the POM induced by

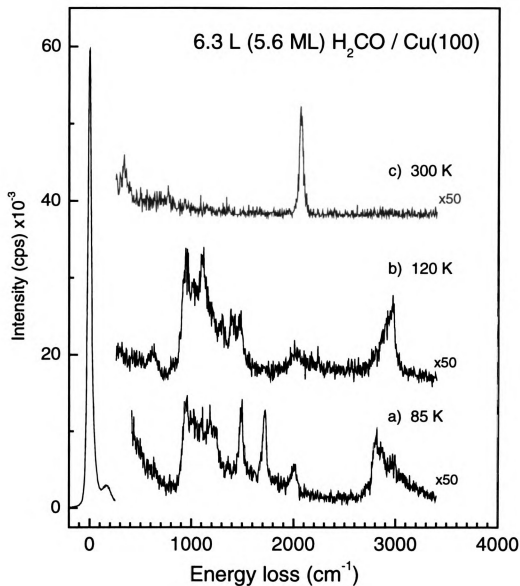


Figure 3.5 EEL spectra as a function of annealing temperature for a 6.3 L exposure of  $\text{H}_2\text{CO}$  on  $\text{Cu}(100)$ . The “as dosed” spectrum is shown in a) while b) and c) were annealed to the indicated temperature. All spectra were recorded at 85 K. The shoulder at  $\sim 200 \text{ cm}^{-1}$  on the elastic peak is the lattice mode associated with the spectrum shown in a). This peak is absent in b) and c).

heating to 120 K. The  $\nu(\text{C}\equiv\text{O})$  loss at  $2007\text{ cm}^{-1}$  has lost intensity and the loss due to  $\nu(\text{Cu-CO})$  was not observed.

Annealing the sample to 300 K, as shown in Figure 3.5c, resulted in complete decomposition/desorption of the polymer as evidenced by the absence of any losses due to POM. The only losses observed are due to CO readsorbed during cooling of the sample following annealing.

*X-ray Photoelectron Spectroscopy (XPS).* The adsorption of  $\text{H}_2\text{CO}$  was also studied using XPS. Figure 3.6 shows the C (1s) and O (1s) regions for increasing exposures of  $\text{H}_2\text{CO}$  on Cu(100) surface at 85 K. At low exposures ( $<1\text{ L}$ ), a peak is observed in the C (1s) spectrum at a binding energy (BE) of 288.2 eV. With increasing exposure, this peak shifted to higher binding energy (288.8 eV for 5.4 L  $\text{H}_2\text{CO}$ ). Indeed, our measured C (1s) binding energy for the adsorbed polymer is similar to that measured by Pireaux et al.<sup>41</sup> for bulk poly(oxymethylene) of 287.8 eV, suggesting that the polymer-surface interaction is weak. Similar behavior was observed for the O (1s) region; a peak was observed initially at 533.1 eV at 0.1 L which shifted to 533.8 eV at 5.4 L. These XPS binding energies are attributed to POM at  $<1\text{ L}$  exposure and, at higher exposures, to a mixture of POM and molecular  $\text{H}_2\text{CO}$ .

As mentioned above, absolute coverages of formaldehyde on Cu(100) were obtained using XPS by standardization with a known adsorbate system. Figure 3.7 displays the calculated coverage as a function of exposure for the adsorption of  $\text{H}_2\text{CO}$  on Cu(100) at 85 K. From the inset of Figure 3.1, TPD data indicate saturation of the polymer desorption features occurred at 0.87 L. Using the standardized XPS intensity ratios calculated above, this exposure corresponds to an absolute coverage of  $0.69 (\pm 0.14)$

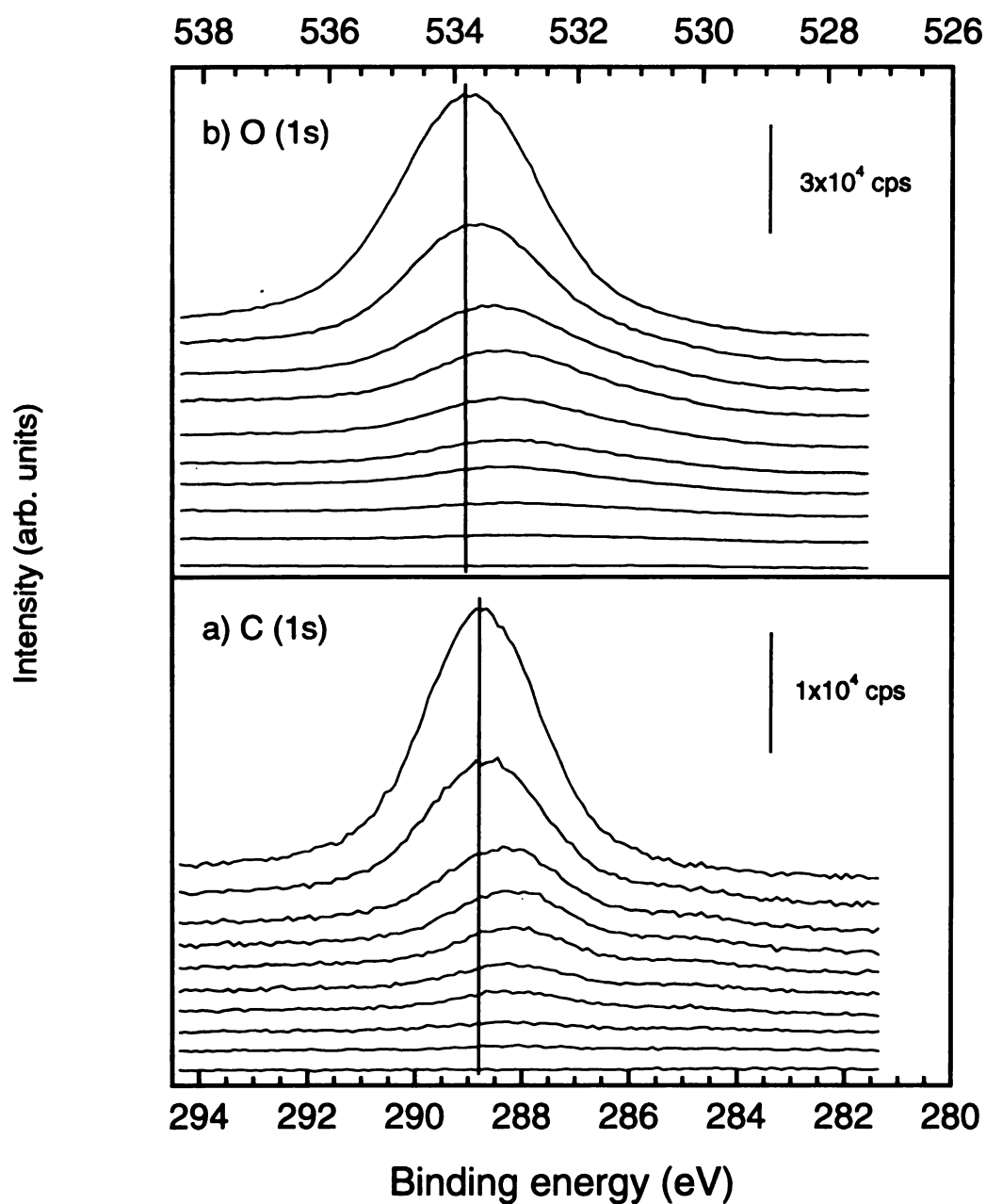


**Figure 3.6** XP spectra of a) C (1s) and b) O (1s) for increasing exposures of H<sub>2</sub>CO on Cu(100) at 85 K. The sample was flashed to 300 K between exposures. Exposures were 0, 0.1, 0.2, 0.4, 0.5, 0.7, 0.9, 1.2, 2.1, 5.4, L. Vertical lines are drawn at 288.8 eV and 533.8 eV for the C (1s) and O (1s) regions, respectively.

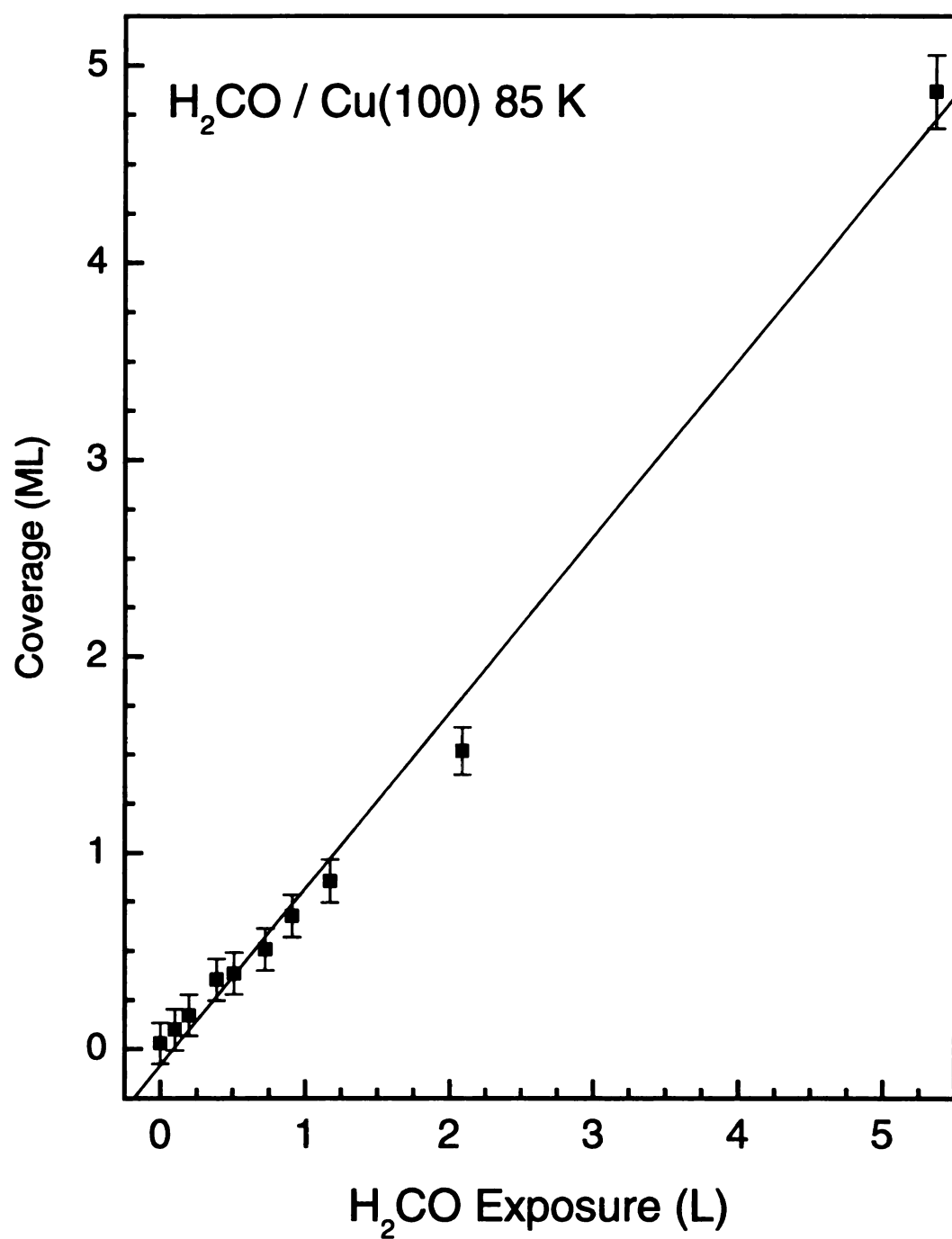


Figure 3.7 Calculated coverage as a function of exposure for the adsorption of H<sub>2</sub>CO on Cu(100) at 85 K based on XPS C(1s) peak areas. Equation of linear fit is  $y=0.898*x-0.082$ .

ML (0.69 formaldehyde molecules per surface atom) or equivalent to  $1.06 (\pm 0.22) \times 10^{15}$  formaldehyde molecules/cm<sup>2</sup>.

*Depolymerization Energetics.* The adsorption and reactions of formaldehyde on the Cu(100) surface described here can be compared with previous studies of formaldehyde on clean group IB metals. On Au(110)<sup>42</sup> and Ag(111),<sup>24</sup> formaldehyde adsorbs non-reactively and desorbs as molecular H<sub>2</sub>CO at approximately 160 K and 110 K, respectively. In the case of Ag(111), UV or low energy electron irradiation induces polymerization, with depolymerization occurring at 210 K producing molecular H<sub>2</sub>CO.

In contrast, on the 90 K Cu(110) surface, H<sub>2</sub>CO was found to adsorb reactively to form POM.<sup>18</sup> Desorption peaks were observed at 110 K and 225 K and attributed to multilayer H<sub>2</sub>CO desorption and decomposition of the polymer, respectively. Interestingly, the depolymerization temperatures noted in our work for Cu(100) are similar to the polymer formed *spontaneously* on the copper (110) surface and through *photopolymerization* on the silver (111) surface (~200-230 K), implying that the polymer produced is similar in these cases.

In contrast to the previous studies of H<sub>2</sub>CO adsorption on Cu(110) and Ag(111), in which a single peak due to depolymerization was observed in TPD spectra, we observe *two* distinct peaks. These features originate from POM. The most likely explanation for the appearance of two depolymerization features in our TPD data for Cu(100) is a difference in depolymerization kinetics and/or energetics. Expansion of the temperature region in which the depolymerization features are observed (180-240 K) (shown in Figure 3.8) reveals that the lower temperature peaks share a common leading edge and a shift to a higher peak desorption temperature with increasing H<sub>2</sub>CO exposure. For a true

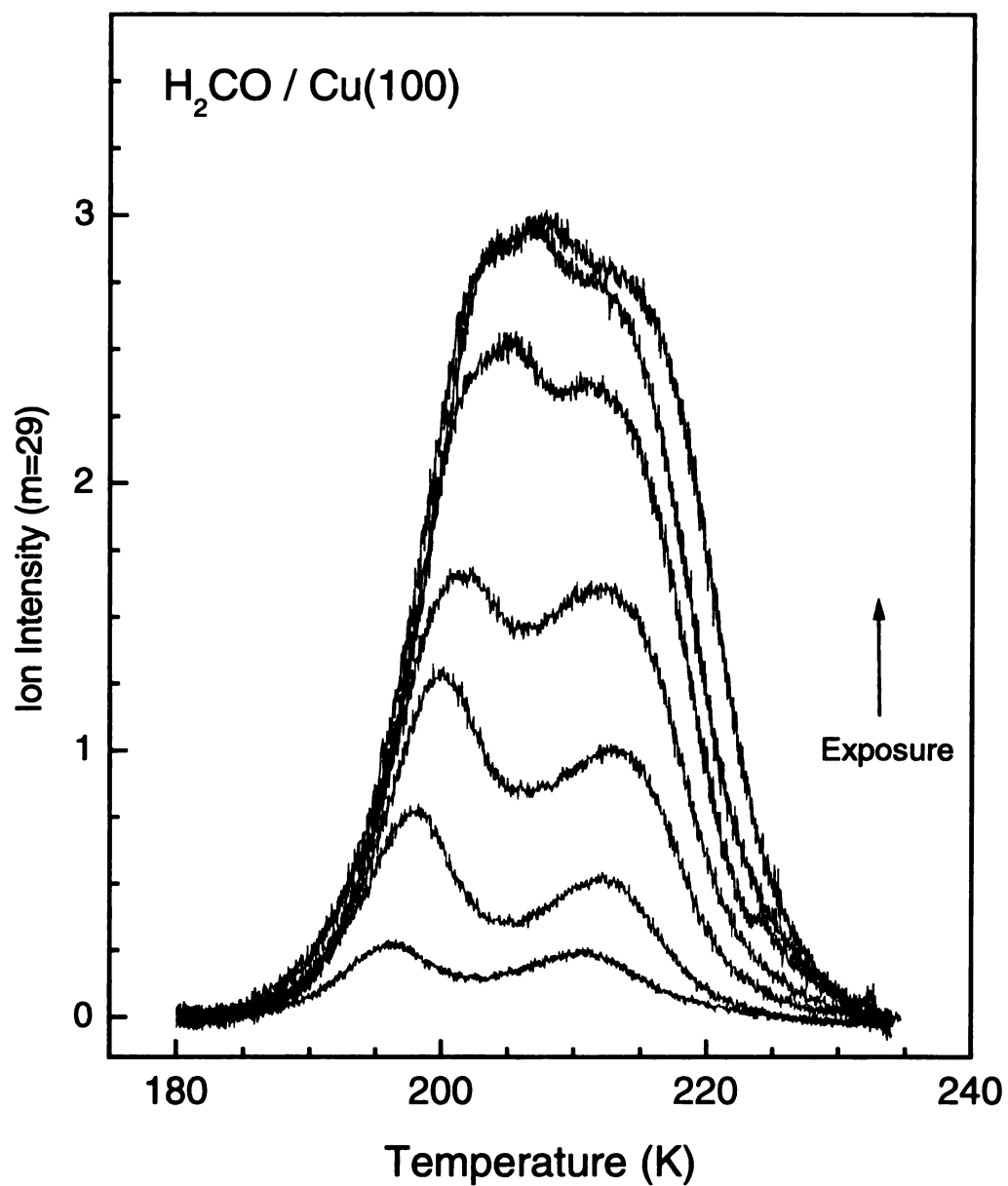


Figure 3.8 Enlarged view of the polymer features from the TPD spectra shown in fig. 1. A constant background was subtracted from each spectrum. Exposures ranged from 0.1 L to 1.1 L.

desorption process, these are the characteristics of zero-order desorption kinetics.<sup>43</sup> However, for the experiments presented here the measured desorption rate of formaldehyde is not reflective of the desorption kinetics associated with molecular  $\text{H}_2\text{CO}$ , but rather with decomposition of the polymer to produce molecular  $\text{H}_2\text{CO}$  which promptly desorbs. Hence, the zero-order desorption kinetics observed are representative of the poly(oxymethylene) depolymerization mechanism. Thus, standard TPD data analyses yield activation energies that are relevant to the rate of depolymerization. The higher temperature TPD feature shows a constant peak desorption temperature, which is indicative of a first-order desorption process.

We can estimate the activation energy and pre-exponential factors for depolymerization by subjecting the zero-order desorption feature to a leading edge analysis<sup>43</sup> (plots of  $\ln(\text{rate})$  vs.  $T^{-1}$ ) while the activation energy for the first-order feature was calculated by the Redhead method assuming a pre-exponential of  $10^{13} \text{ s}^{-1}$ .<sup>44</sup> These analyses yielded activation energies of  $75 (\pm 10)$  and  $53.9 (\pm 0.5) \text{ kJ/mol}$  for the zero- and first-order desorption features, respectively. These depolymerization energies fall within the broad range of 42-113 kJ/mol quoted for POM from various bulk studies.<sup>45</sup> The difference in activation energy is less important than the observation of two different kinetic orders for depolymerization and will be discussed in detail in Chapter 4.

The most reasonable explanation for the appearance of multiple desorption peaks for polymer decomposition is the presence of different polymer species that depolymerize by a similar pathway. The possibility of a single polymer species decomposing via two competing pathways can be immediately discounted because such a situation would be



expected to produce a single desorption feature; the fastest and/or lowest barrier process will always dominate.

*Possible Polymer Species.* An obvious choice for two different polymer species would be polymer adsorbed at distinct sites such as terrace sites versus defect or step-edge sites. The appearance of two desorption peaks in the monolayer TPD data (Figure 3.1) of approximately equal intensity implies that the surface concentrations of defects and/or edge sites would be approximately equal to the concentration of terrace sites. We estimate the density of step-edges for a Cu(100) surface cut to within  $0.5^\circ$  (supplier's specification) at  $\sim 1\%$ . Furthermore, excellent surface order is suggested by the high EELS elastic peak intensity ( $>10^6$  Hz) of the clean Cu(100) surface, and  $<20\%$  loss in instrumental resolution relative to the "straight-through" geometry. For these reasons, we believe defect sites and/or step-edges are not responsible for the two polymer desorption peaks.

It is possible conformational differences could give rise to the two polymer TPD peaks. In the crystalline state POM forms helices belonging to either the  $D(10\pi/9)$  or  $D(\pi)$  point group in the trigonal (t-POM) and orthorhombic (o-POM) crystal structures, respectively.<sup>46,47</sup> Both point groups are isomorphous with  $D_n$  and have an associated dynamic dipole oriented parallel ( $A_2$ ) or perpendicular (E) to the helical chain axis.<sup>34</sup> This is shown in Figure 3.9a for orthorhombic POM. Adsorption of these helices with the primary rotation axis (z-axis in Figure 3.9a) parallel to a surface would reduce the symmetry to  $C_1$ . As a consequence of the metal-surface selection rule, the original  $A_2$  modes, polarized within the surface plane, would be strictly screened and thus unobservable for dipole scattering in EELS. The E modes would still have some

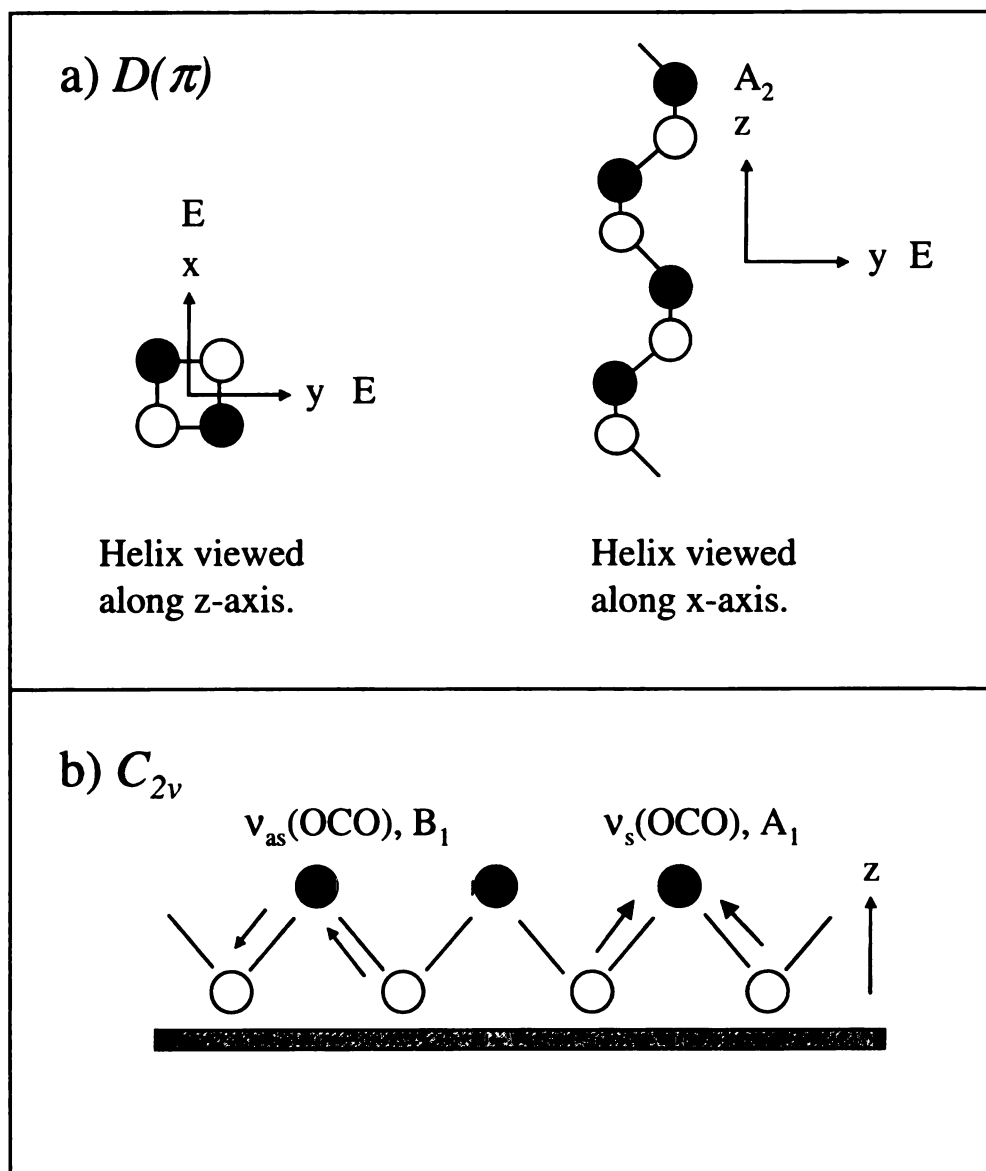


Figure 3.9 Comparison of symmetry for a) orthorhombic (helical) and b) planar POM. The Cartesian coordinates (x,y,z) and representations ( $A_2$ , E,  $B_1$ ,  $A_1$ ) for a) correspond to the helix in free space while for b) the substrate is considered. The filled circles are methylene units ( $CH_2$ ).

component of their dipoles oriented perpendicular to the surface depending on rotational orientation. Thus, for dipole scattering, the observed features in our EELS spectra must originate from what were E modes of the polymer. Similar arguments have been made for the thermal polymerization of acetaldehyde adsorbed on O/Ag(111).<sup>19</sup>

Another chain conformation the polymer could adopt is a planar zigzag bound to the surface through the O atoms (the planar conformation has never been observed experimentally in the solid) as shown in Figure 3.9b. Assuming the  $C_{2v}$  symmetry of the planar conformation is retained upon adsorption, the  $\nu_{as}(OCO)$  mode should be (strictly) screened in this conformation but observable for helical conformations. While the coexistence of the helical and planar forms cannot be ruled out on the basis of our EELS data, the observation of  $\nu_{as}(OCO)$  does eliminate the possibility that *only* the zigzag form was present on the surface. We expect the vibrational frequencies for the planar and helical conformations of the surface-bound POM to be very similar and therefore indistinguishable by EELS. Small morphology-dependent frequency shifts have been observed between orthorhombic POM and trigonal POM.<sup>48</sup> The largest difference observed by this study was  $37\text{ cm}^{-1}$  between the o-POM ( $596\text{ cm}^{-1}$ ) and t-POM ( $633\text{ cm}^{-1}$ )  $\delta(OCO)$  mode. The vibrational frequency of the  $\delta(OCO)$  mode observed in our EELS data ( $631\text{ cm}^{-1}$ ) implies that the crystal habit present on the Cu(100) surface is trigonal. Interestingly, we have preliminary evidence that this mode red shifts to approximately  $599\text{ cm}^{-1}$  upon annealing the polymer monolayer to 190 K, perhaps suggesting a transformation to the orthorhombic form (data not shown).

The surface density of formaldehyde molecules in the polymer monolayer, provides additional insight into the conformation of POM on the Cu(100) surface. It will

be recalled that the calculated density, based on standardized XPS measurements, was  $1.06 \times 10^{15} \text{ cm}^{-2}$ . For crystalline orthorhombic poly(oxymethylene), there are two possible planes that can be projected onto the surface to produce chain directions parallel to the surface plane (saturation of the polymer TPD features discounts polymer chain growth perpendicular to the surface plane). The **bc** plane has a calculated average monomer density of  $7.35 \times 10^{14} \text{ cm}^{-2}$ , while the **ac** plane has a calculated average monomer density of  $1.18 \times 10^{15} \text{ cm}^{-2}$ . For trigonal poly(oxymethylene), the **ac** plane has an average monomer density of  $1.16 \times 10^{15} \text{ cm}^{-2}$ . Thus, it can be seen the **ac** plane of both o-POM and t-POM produce surface monomer densities close to that calculated by the standardized XPS data for saturation of the polymer layer. Although agreement between these surface densities is good, and suggests that the polymer monolayer covers the surface completely, it should be stressed that we have already inferred that the layer is probably highly disordered and should not be considered crystalline.

The existence of a decomposition route that does not produce molecular  $\text{H}_2\text{CO}$  is evident by the desorption of CO and  $\text{H}_2$  prior to the depolymerization of POM. A common origin for these two species is indicated by the coincident desorption temperatures. Leading edge analysis of these second order desorption peaks yielded an activation energy of  $49 (\pm 8) \text{ kJ/mol}$  and a pre-exponential factor of  $1 \times 10^{15 \pm 1} \text{ molecules}^{-1} \cdot \text{cm}^2 \cdot \text{s}^{-1}$ . The ratio of desorption in the  $\text{H}_2 + \text{CO}$  versus  $\text{H}_2\text{CO}$  channels showed a maximum at  $\sim 0.04$  at 0.66 ML (95 % of saturation of the polymer monolayer). The intensity ratio for the  $m=28$  peak at 178 K and the  $m=2$  peak at 177 K, corrected for ionization probability and fragmentation, is approximately 1.15, very close to the expected decomposition ratio for a species containing equal proportions of  $\text{H}_2$  and CO.

We have already mentioned the possibility of the existence of  $\text{H}_2\text{CO}$  species bound to the surface with the molecular axis parallel to the surface plane; this adsorption geometry may give rise to the  $\text{H}_2$  and CO desorption products observed at 178 K in TPD. Therefore, the observation of  $\text{H}_2$  and CO desorption at 177 K must be due to decomposition of a third, as yet unidentified, species. This species may arise at step edge or defect site as these would be expected to be more reactive than terrace sites on the Cu(100) surface.

### 3.3 Conclusions

The adsorption of formaldehyde ( $\text{H}_2\text{CO}$ ) on the Cu(100) surface has been studied. At 85 K,  $\text{H}_2\text{CO}$  polymerizes spontaneously to form a monolayer of poly(oxymethylene) (POM) up to a saturation coverage of 0.69 ML ( $1.06 \times 10^{15} \text{ cm}^{-2}$ ). This surface density suggests that the POM chain directions are parallel to the surface plane. No molecularly adsorbed  $\text{H}_2\text{CO}$  was observed in EEL spectra prior to saturation. Further exposure of the polymer-covered Cu(100) surface resulted in multilayers of  $\text{H}_2\text{CO}$ , with EELS loss features characteristic of crystalline  $\text{H}_2\text{CO}$ . These multilayers are susceptible to polymerization by the low-energy electron beam during EELS data acquisition.

Temperature-programmed desorption spectra indicate there is one decomposition route available to the adsorbed polymer species: decomposition to molecular  $\text{H}_2\text{CO}$ . The route producing  $\text{H}_2\text{CO}$  is observed as two desorption features at approximately 200 and 215 K which show zero- and first-order depolymerization kinetics respectively. The observation of two orders can be possibly explained by the presence of two types of polymer existing in different conformations. We believe differences due to adsorption at

defect and/or step edges do not account for the appearance of two desorption features for route (ii). The observation of CO and H<sub>2</sub> desorption indicates a third species is present that is probably due to dissociation of H<sub>2</sub>CO at step edges and defect sites. Electron energy loss spectroscopy data indicate no other species besides an adsorbed polymer first layer and molecular H<sub>2</sub>CO multilayers on top of the polymer layer, are present on the 85 K Cu(100) surface.

### 3.4 References

- (1) Ejaz, M.; Yamamoto, S.; Ohno, K.; Tsujii, Y.; Fukuda, T. *Macromolecules* **1998**, *31*, 5934.
- (2) Shirai, E.; Urai, Y.; Itoh, K. *J. Phys. Chem. B* **1998**, *19*, 3765.
- (3) Ford, J. F.; Vickers, T.; Mann, C.; Schlenoff, J. *Langmuir* **1996**, *12*, 1944.
- (4) Sun, F.; Castner, D.; Grainger, D. *Langmuir* **1993**, *9*, 3200.
- (5) Kim, T.; Chan, K.; Crooks, R. *J. Am. Chem. Soc.* **1997**, *119*, 189.
- (6) Chan, K.; Kim, T.; Schoer, J.; Crooks, R. *J. Am. Chem. Soc.* **1995**, *117*, 5875.
- (7) Balasubramanian, K.; Cammarata, V. *Langmuir* **1996**, *12*, 2035.
- (8) Batchelder, D.; Evans, S.; Freeman, T.; Haussling, L.; Ringsdorf, H.; Wolf, H. *J. Am. Chem. Soc.* **1994**, *116*, 1050.
- (9) Bent, B. E. *Chem. Rev.* **1996**, *96*, 1361.
- (10) Somorjai, G. *Introduction to Surface Chemistry and Catalysis*; Wiley and Sons: New York, 1994.
- (11) Stuve, E.; Madix, R.; Sexton, B. *Surf. Sci.* **1982**, *119*, 279.
- (12) Richter, L.; Ho, W. *J. Chem. Phys.* **1985**, *83*, 2165.
- (13) Henderson, M.; Mitchell, G.; White, J. *Surf. Sci.* **1987**, *188*, 206.

- (14) Davis, J.; Barteau, M. *J. Am. Chem. Soc.* **1989**, *111*, 1782.
- (15) Houtman, C.; Barteau, M. *Surf. Sci.* **1991**, *248*, 57.
- (16) Davis, J.; Barteau, M. *Surf. Sci.* **1992**, *268*, 11.
- (17) Truong, C.; Wu, M.; Goodman, D. W. *J. Am. Chem. Soc.* **1993**, *115*, 3647.
- (18) Sexton, B.; Hughes, A.; Avery, N. *Surf. Sci.* **1985**, *155*, 366.
- (19) Sim, W.; Gardner, P.; King, D. *J. Am. Chem. Soc.* **1996**, *118*, 9953.
- (20) Wells, S.; Giergel, J.; Land, T.; Linquist, J.; Hemminger, J. *Surf. Sci.* **1991**, *257*, 129.
- (21) Tsai, W.; Boeri, F.; Clarson, S.; Montaudou, G. *J. Raman Spectrosc.* **1990**, *21*, 311.
- (22) Cheng, L.; Bocarsly, A.; Bernasek, S.; Ramanarayanan, T. *Surf. Sci.* **1997**, *374*, 357.
- (23) Land, T.; Hemminger, J. *Surf. Sci.* **1992**, *268*, 179.
- (24) Fleck, L.; Feehery, W.; Plummer, E.; Ying, Z.; Dai, H. *J. Phys. Chem.* **1991**, *95*, 8428.
- (25) Fleck, L.; Kim, J.; Dai, H.-L. *Surf. Sci.* **1996**, *356*, L417.
- (26) Carlo, S.; Grassian, V. *Langmuir* **1997**, *13*, 2307.
- (27) The large, broad desorption feature between 100 and 180 K was observed during evaluation of our experimental arrangement using a known system (CO/Cu(100)). This system generally shows no broad features in this temperature range and the appearance of features in this temperature range in our experiments was thus attributed to desorption from the sample mount. In subsequent experiments performed using directed dosing, these features were absent.

- (28) *NIST Chemistry WebBook, NIST Standard Reference Database Number 69*; Mallard, W., Linstrom, P., Eds.; National Institutes of Standards and Technology: Gaithersburg, MD, 1998; pp (<http://webbook.nist.gov>).
- (29) Chorkendorff, I.; Rasmussen, P. *Surf. Sci.* **1991**, *248*, 35.
- (30) Kammler, T.; Kuppers, J. *J. Chem. Phys.* **1999**, *111*, 8115.
- (31) Adsorbed hydrogen was assumed to arise from dissociation of molecular hydrogen and/or formaldehyde at the filaments of the ion gauge and/or QMS.
- (32) Khoshkoo, H.; Hemple, S.; Nixon, E. *Spectrochim. Acta A* **1974**, *30*, 863.
- (33) Weng, S.; Anderson, A.; Torrie, B. *J. Raman Spectrosc.* **1989**, *20*, 789.
- (34) Tadokoro, H.; Kobayashi, M.; Kawaguchi, Y.; Koybayashi, A.; Murahashi, S. *J. Chem. Phys.* **1963**, *38*, 703.
- (35) Hofmann, M.; Wegner, H.; Glenz, A.; Woll, C.; Grunze, M. *J. Vac. Sci. Technol. A* **1994**, *12*, 2063.
- (36) Kobayashi, M.; Iwamoto, R.; Tadokoro, H. *J. Chem. Phys.* **1966**, *44*, 922.
- (37) Anton, A.; Parmeter, J.; Weinberg, W. *J. Am. Chem. Soc.* **1986**, *108*, 1823.
- (38) Fleck, L.; Ying, Z.; Feehery, M.; Dai, H.-L. *Surf. Sci.* **1993**, *296*, 400.
- (39) Fleck, L. E. Ph.D. Thesis, University of Pennsylvania, 1994.
- (40) Sexton, B. *Chem. Phys. Lett.* **1979**, *63*, 451.
- (41) Pireaux, J.; Riga, J.; Boulanger, P.; Snauwaert, P.; Novis, Y.; Chtaib, M.; Gregoire, C.; Fally, F.; Beelen, E.; Caudano, R.; Verbist, J. *J. Electron Spectrosc. Relat. Phenom.* **1990**, *52*, 423.
- (42) Outka, D.; Madix, R. *Surf. Sci.* **1987**, *179*, 361.
- (43) de Jong, A.; Niemantsverdriet, J. *Surf. Sci.* **1990**, *233*, 355.
- (44) Redhead, P. A. *Vacuum* **1962**, *12*, 203.



- (45) Muck, K. In *Polymer Handbook*; Brandrup, J., Immergut, E., Grulke, E., Abe, A., Bloch, D., Eds.; Wiley & Sons: New York, 1999; Vol. 4; pp V/97.
- (46) Helical symmetry is specified by the nomenclature  $X(2m\pi/n)$  where X is the point group (C or D), m is the number of turns of the chain per unit cell and n is the number of monomer units per chain per unit cell).
- (47) Tadokoro, H. In *Macromolecular Reviews*; Peterlin, A., Goodman, M., Okamura, S., Zimm, B., Mark, H., Eds.; Interscience: New York, 1967; Vol. 1; pp 119.
- (48) Kobayashi, M.; Sakashita, M. *J. Chem. Phys.* **1992**, *96*, 748.

## Chapter 4 Evidence for Two Chain Length Distributions in the Thermal Polymerization of Formaldehyde on Cu(100)

### Abstract

The polymer species formed from the spontaneous polymerization of formaldehyde ( $\text{H}_2\text{CO}$ ) on clean Cu(100) at 85 K were studied using electron energy loss spectroscopy (EELS) and temperature-programmed desorption (TPD). Formaldehyde forms poly(oxymethylene) (POM) with differing chain lengths; the long ( $\alpha$ ) and short ( $\beta$ ) chain species depolymerize to give two features in TPD at approximately 207 and 219 K, respectively. The complex desorption kinetics observed for the  $\alpha$ -POM species were successfully modeled using equations based on the ratio of the average number of monomers unzipped from the chain per initiation event to the length of the polymer chain. Losses were observed in EEL spectra of the short chain species at  $\sim 290$ ,  $\sim 1020$  and  $\sim 1120 \text{ cm}^{-1}$  that can be assigned to the  $\nu(\text{Cu-O})$ ,  $\nu(\text{C-O})$  and  $\rho(\text{CH}_3)$  modes of oxygen and methoxy endgroups, respectively. Pre-adsorbed methanol increases the proportion of short chain POM species by increasing the probability of termination for the  $\beta$  species. Lower thermal stability for adsorbed POM was observed compared to bulk POM and is believed to be related to the stability of the surface bound oxygen endgroup.

H<sub>2</sub>OPO<sub>4</sub>

de-

PO<sub>4</sub>

zer

22

de-

In

of

Po

Py

SC

or

hi

de

no

de

th

## 4.1 Introduction

In Chapter 3, investigations of the spontaneous polymerization of formaldehyde ( $\text{H}_2\text{CO}$ ) on clean  $\text{Cu}(100)$  at 85 K were reported.<sup>1</sup> The formation of two types of poly(oxymethylene) (POM,  $-(\text{CH}_2\text{O})_n-$ ) was observed by temperature-programmed desorption (TPD) as two separate features corresponding to the depolymerization of the POM to produce  $\text{H}_2\text{CO}(\text{g})$ . The lower temperature feature ( $\sim 209$  K) exhibited apparent zero-order desorption/depolymerization kinetics while the higher temperature feature ( $\sim 220$  K) exhibited first-order desorption/depolymerization kinetics.<sup>2</sup> We ascribed the two depolymerization routes to conformational differences between the two adsorbed species. In contrast, bulk POM is known to be stable up to at least 350 K depending on the degree of polymerization and type of endgroups.<sup>3</sup>

The lower stability of the film is believed to be related to the endgroups of the polymer and has been observed previously. For example, bulk polyimide made from pyromellitic dianhydride (PMDA) and oxydianiline (ODA) is stable at temperatures up to  $500^\circ\text{C}$ .<sup>4,5</sup> However, polyimide films made from reactive adsorption of PMDA and ODA on  $\text{Cu}(110)$  decompose at  $\sim 280^\circ\text{C}$ .<sup>6,7</sup> The thermal stability of the film was shown to be limited by the reactivity of the carboxylate endgroups bound to the surface, but the decomposition pathway and the influence of the substrate on the endgroup stability has not been thoroughly studied.

In other studies on the thermal polymerization of  $\text{H}_2\text{CO}$  on  $\text{Cu}(110)$ , a single depolymerization feature was observed at 225 K.<sup>8</sup> Additionally, POM formed through the photopolymerization of  $\text{H}_2\text{CO}$  adsorbed on  $\text{Ag}(111)$  depolymerized at 210 K.<sup>9</sup>

Unfortunately, no studies were performed to determine the kinetics of depolymerization on either surface. Regardless, the similarity of depolymerization temperatures observed for these two surfaces and the Cu(100) surface suggests the POM species formed on each surface are similar.

While Chapter 3 dealt with identifying the products formed from the adsorption of  $\text{H}_2\text{CO}$  on Cu(100) at 85 K, the present chapter addresses the origin of the observed depolymerization processes and the nature of the endgroups of the POM polymer. The reduced thermal stability of the POM film formed is also considered. The reaction of adsorbed methanol ( $\text{CH}_3\text{OH}$ ) with  $\text{H}_2\text{CO}$  on Cu(100) at 85 K was used to probe the reaction mechanisms of the polymerization process and help in the identification of the POM endgroups.

## 4.2 Results and Discussion

*Isolation of POM species.* The adsorption of  $\text{H}_2\text{CO}$  on clean Cu(100) at 85 K resulted in the formation of two POM species. Temperature-programmed desorption was used to investigate whether the two types of POM observed to form on the Cu(100) surface could be isolated through annealing. Figure 4.1 shows  $m=29$  ( $\text{HCO}^+$ ) TPD spectra over the temperature range where depolymerization of POM occurs. Figure 4.1a shows TPD data obtained from a POM-saturated Cu(100) surface (1 ML, equivalent to a fractional coverage,  $\theta$ , of 0.69  $\text{H}_2\text{CO}$  molecules/Cu atom).<sup>1</sup> Two features were visible: the  $\alpha$ -POM species with a peak desorption temperature of  $\sim 207$  K and the  $\beta$ -POM species at  $\sim 219$  K.<sup>2</sup> Figure 4.1b shows the TPD data obtained after one monolayer of

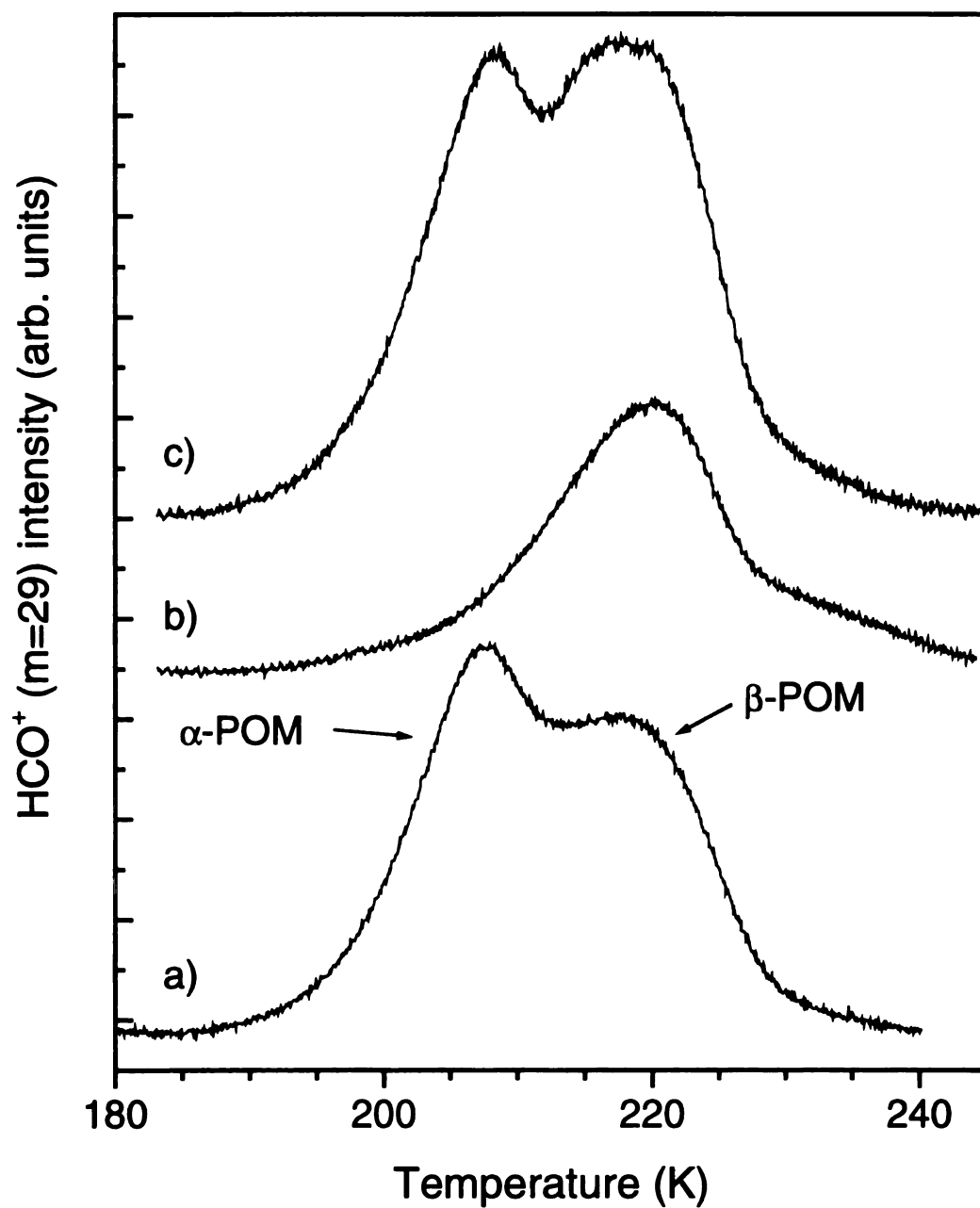


Figure 4.1 Mass 29 ( $\text{HCO}^+$ ) TPD spectra for (a) 1 ML  $\text{H}_2\text{CO}$  on Cu(100), (b) 1 ML  $\text{H}_2\text{CO}$  after annealing to 209 K and cooling to 85 K prior to TPD and (c) 1 ML  $\text{H}_2\text{CO}$  annealed to 209 K and dosed with  $\text{H}_2\text{CO}$  to re-saturate the surface. A constant linear background was subtracted from each spectrum.

POM was briefly annealed (2-3 seconds) to 209 K and then cooled to 85 K prior to the TPD experiment. Annealing to this temperature, the approximate peak desorption temperature for the  $\alpha$  species, resulted in the complete loss of the  $\alpha$  species. Due to the similarity of peak desorption temperatures for the  $\alpha$  and  $\beta$  POM, annealing also resulted in the loss of  $\sim 11\%$  of the  $\beta$  species (based on fits discussed below). Additionally, a TPD spectrum identical to Figure 4.1b was produced if the  $\beta$  species-covered surface was allowed to remain at 85 K for up to 10 minutes.

Figure 4.1c shows the TPD data obtained after a monolayer of POM was annealed to 209 K, cooled to 85 K, and then exposed to  $\text{H}_2\text{CO}$  to re-saturate the surface with POM. The data appear qualitatively similar to that shown in Figure 4.1a. The TPD results of Figure 4.1 suggest immediately that the  $\alpha$  species can be depopulated and repopulated by an annealing and re-dosing procedure and the  $\beta$  species does not convert to the  $\alpha$  species during the TPD experiment. Importantly, the higher temperature  $\beta$  species can be isolated through annealing.

*Depolymerization kinetics.* Equations can be derived to model the kinetics of the depolymerization process for a monodisperse polymer. For bulk POM, there are two limiting cases for depolymerization initiated at chain ends.<sup>3,10,11</sup> In the first case, once initiated, the POM chain fully depolymerizes to monomer and is first-order with respect to the mass of the polymer,  $W$  (proportional to coverage in our experiments). The rate of monomer ( $M$ ) evolution, with respect to time ( $t$ ), is equal to the rate of radical ( $R$ ) production

$$\frac{dM}{dt} = Z \frac{d[R]}{dt} \quad (4.1)$$

where  $Z$  is multiple of the degree of polymerization,  $D_p$  ( $Z=bD_p$  where  $b=1$  for a monodisperse sample). The rate of radical formation is

$$\frac{dR}{dt} = k_i[n] \quad (4.2)$$

where  $k_i$  is the rate constant for terminal initiation and  $[n]$  is the concentration of polymer chains. Combining equations (4.1) and (4.2), and using equation (4.3)

$$[n] = \frac{W}{M_m D_p} \quad (4.3)$$

where  $M_m$  is the molecular weight of the monomeric unit, results in equation (4.4)

$$\frac{dM}{dt} = k_i \frac{W}{M_m} \quad (4.4)$$

The equation can be transformed into the rate of monomer evolution with respect to temperature ( $T$ ) by use of the heating rate  $\beta$  ( $dT/dt$ ), resulting in equation (4.5).

$$\frac{dM}{dT} = k_i \frac{W}{\beta M_m} \quad (4.5)$$

The rate of monomer evolution is independent of  $D_p$  if the kinetic chain length  $KL$  (number of monomer units “unzipped” per initiation event) is equal to the degree of polymerization  $D_p$  (chain length).

In the second case, following initiation, unimolecular termination competes with depolymerization and only a small number of monomers are unzipped prior to termination ( $KL < D_p$ ). The rate of monomer evolution, as a function of time, can be related to the radical concentration by

$$\frac{dM}{dt} = k_d[R] \quad (4.6)$$



where  $k_d$  is the rate constant of depolymerization. The rate of radical production is dependent on the rate of initiation,  $k_i$ , and the rate of termination,  $k_t$  such that

$$\frac{dR}{dt} = k_i[n] - k_t[R]. \quad (4.7)$$

Assuming steady state conditions for equation (4.7), using equation (4.3) and the heating rate, equation (4.6) becomes

$$\frac{dM}{dT} = \frac{k_i k_d W}{\beta k_t M_m D_p}. \quad (4.8)$$

If the number of chains remains constant throughout the depolymerization (number of chains =  $W/D_p$ ), this process is zero-order with respect to the mass of polymer. This condition would be met only during the initial stages of depolymerization as short sections of each chain are removed and both  $W$  and  $D_p$  decrease at the same rate. However, following prolonged depolymerization, the kinetic chain length ( $KL = k_d/k_t$ ) eventually becomes comparable to  $D_p$ . At this stage, the total number of chains on the surface begins to decrease, the ratio  $W/D_p$  is no longer constant, equation (4.8) becomes first-order with respect to the mass of polymer and thus is identical to equation (4.5). Consequently, depolymerization should initially exhibit zero-order behavior (as described by equation (4.8)) but become first-order (as described by equation (4.5)) during the later stages of depolymerization. The temperature at which the apparent order changes will depend on the kinetic chain length and initial degree of polymerization and occurs when  $KL = D_p$ .

Equations (4.5) and (4.8) were used to fit TPD data both as a function of heating rate and increasing coverage. Both coverage and heating rate data were fit to increase the

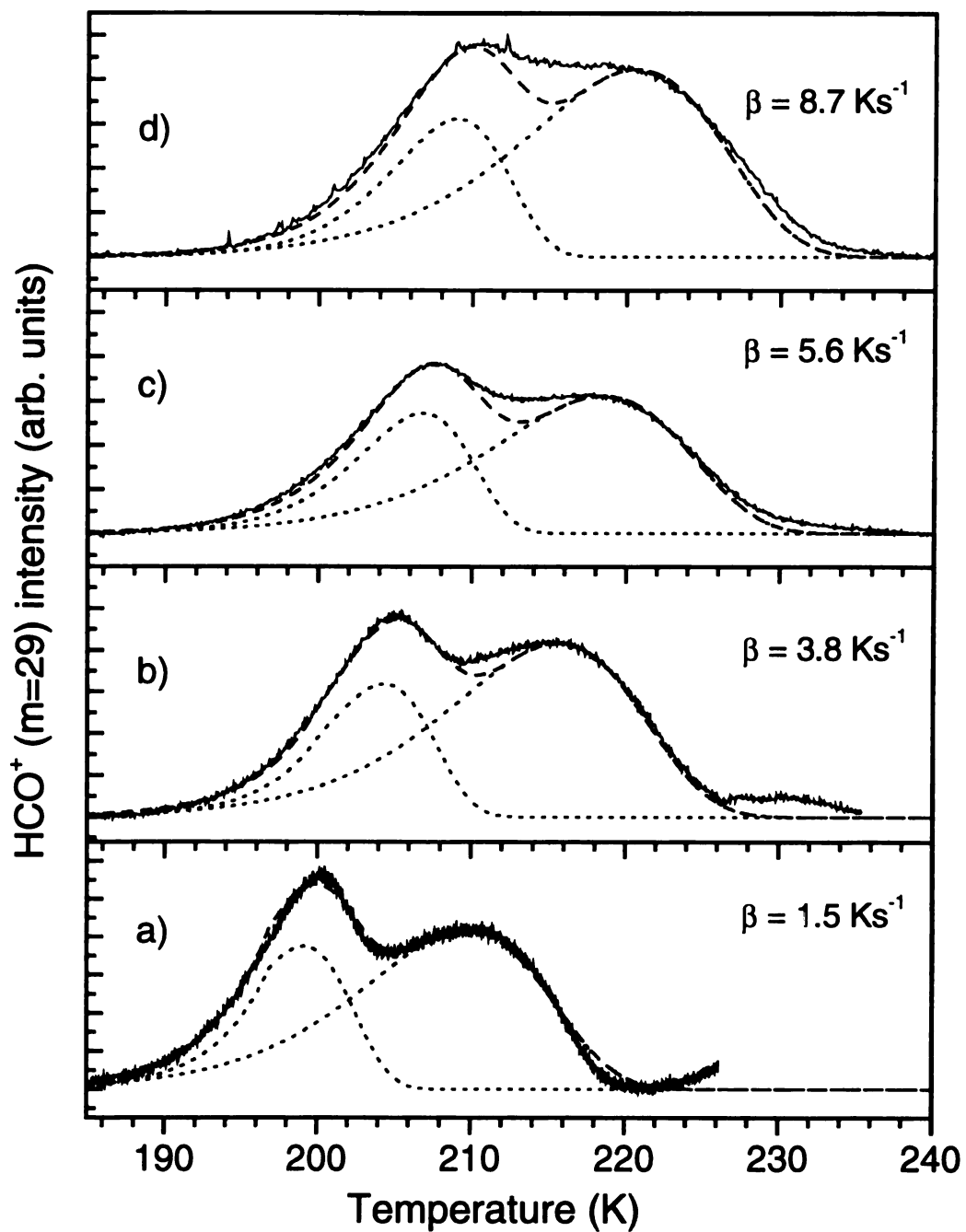


Figure 4.2 Mass 29 ( $\text{HCO}^+$ ) TPD spectra for a 1 ML coverage of  $\text{H}_2\text{CO}$  on  $\text{Cu}(100)$  exposed at 85 K as a function of heating rate ( $\beta$ ). The heating rates were (a)  $1.5 \text{ Ks}^{-1}$ , (b)  $3.8 \text{ Ks}^{-1}$ , (c)  $5.6 \text{ Ks}^{-1}$  and (d)  $8.7 \text{ Ks}^{-1}$ . The solid line (—) is the raw data, the dotted lines ( $\cdots$ ) are the fits to equations (4.5) and (4.8) and the dashed line (---) is the sum of the fits.

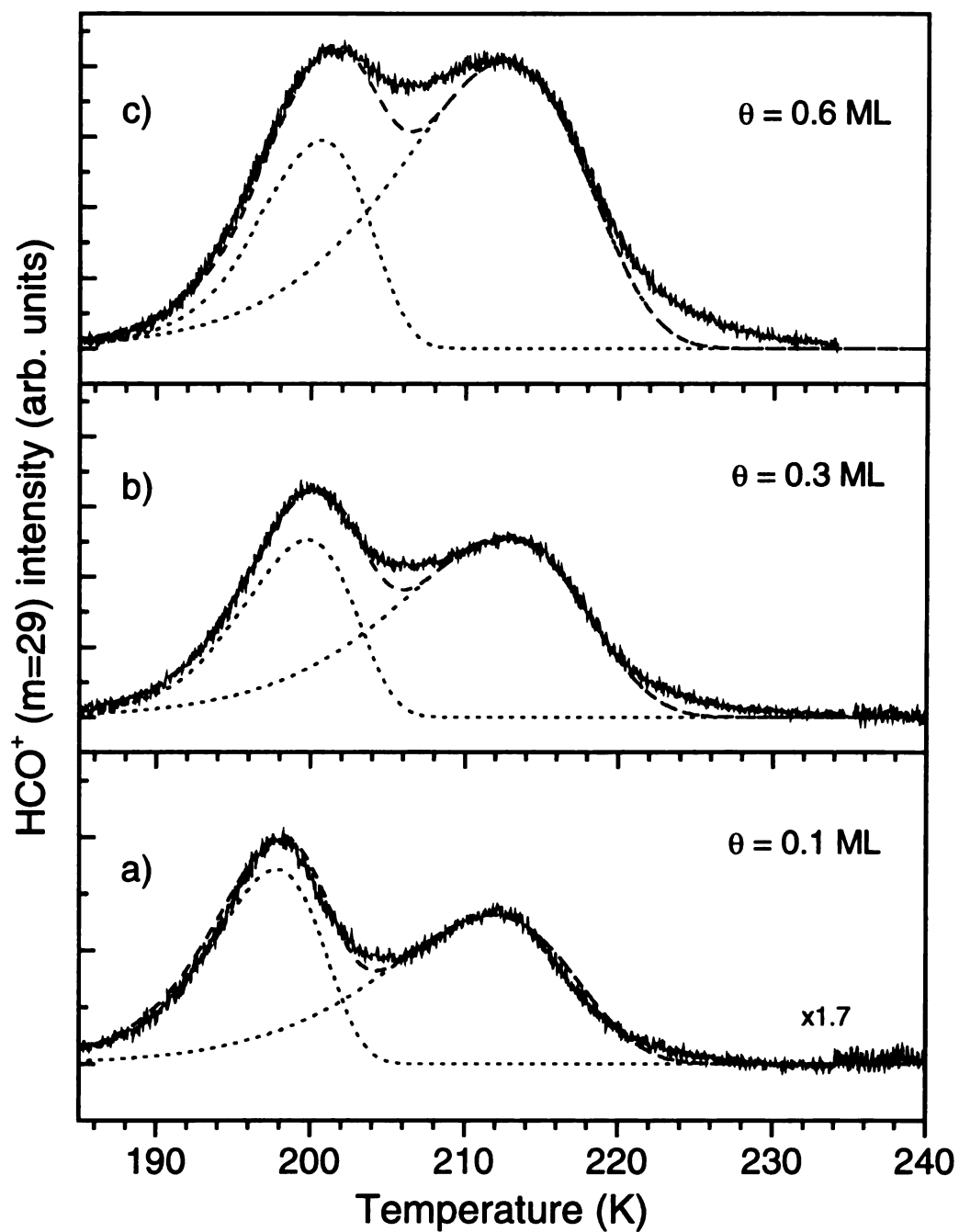


Figure 4.3 Mass 29 ( $\text{HCO}^+$ ) TPD spectra for increasing coverages ( $\theta$ ) of  $\text{H}_2\text{CO}$  on  $\text{Cu}(100)$  exposed at 85 K. The coverages were (a) 0.1 ML, (b) 0.3 ML and (c) 0.6 ML. The solid line (—) is the raw data, the dotted lines ( $\cdots$ ) are the fits to equations (4.5) and (4.8) and the dashed line (----) is the sum of the fits.

reliability of the fit parameters. Equation (4.5) alone produced a satisfactory fit to the higher temperature  $\beta$ -POM peak as shown in Figures 4.2 and 4.3. Since common leading edges were observed for the  $\alpha$ -POM species as a function of coverage, equation (4.8) was used to fit the TPD data for  $\alpha$ -POM. However, such an approach failed to accurately reproduce the majority of the  $\alpha$  peak shape, particularly near the peak maximum. As such, a combination of equation (4.5) and (4.8) was used to fit the  $\alpha$ -POM species and values for  $k_i$  and  $KL/Dp$  determined. The rate constant  $k_i$  was assumed to be of an Arrhenius form and preexponential and energetic terms extracted from the coverage and heating rate fits. Similar values cannot be determined uniquely for  $k_d$  and  $k_t$ , only the ratio  $KL/Dp$ , assumed to be temperature independent in our model. The effect of varying  $KL/Dp$  is illustrated in the simulated TPD spectra of Figure 4.4. When  $KL/Dp \geq 1$  the rate of monomer evolution follows first-order kinetics and when  $KL/Dp \ll 1$  the kinetics approach zero-order. At intermediate values (approximately  $0.1 < KL/Dp < 1$ ), the shapes of the leading and trailing edges are sensitive to the ratio  $KL/Dp$ .

Figure 4.2 shows TPD data for a saturation coverage of POM on Cu(100) collected at different heating rates along with the individual fits to the  $\alpha$ - and  $\beta$ -POM TPD peaks and the sum of the fits. For both species, the maximum depolymerization rate shifted to higher temperature and the separation between the features decreased as the heating rate increased. Figure 4.3 shows TPD data as a function of increasing initial coverage along with the individual fits as described above. For both Figures 4.2 and 4.3, the TPD data can be modeled reasonably accurately. Discrepancies between the fit and experimental data could arise from the effects of polydispersity present in the  $\alpha$  and

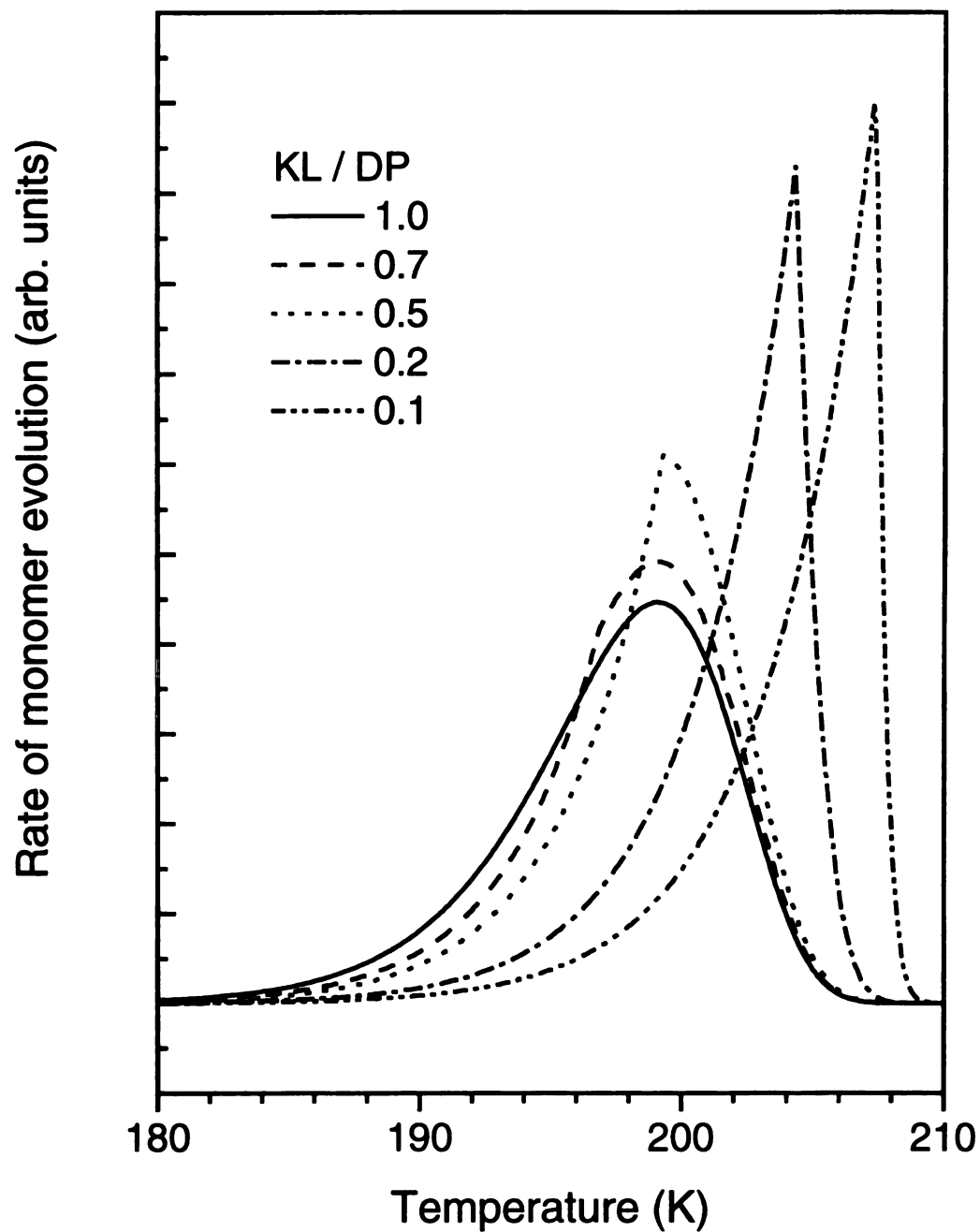


Figure 4.4 Simulated TPD spectra showing the effect of varying KL/Dp. The following constant parameters were used for all spectra:  $E = 90 \text{ kJmol}^{-1}$ ,  $\nu = 1 \times 10^{22} \text{ s}^{-1}$ , and  $\beta = 5.6 \text{ Ks}^{-1}$ .

$\beta$  species, variations in KL with temperature or non-infinite pumping efficiency for  $\text{H}_2\text{CO}$ . The fit parameters are summarized in Table 4.1.

The preexponential and energetic terms for the  $\alpha$ -POM species represent values for the ratio  $k_i \times k_d/k_t$  whereas the terms for  $\beta$ -POM are for  $k_i$  only. The ratio  $\text{KL}/\text{Dp}$  was varied to improve the accuracy of the fit, especially in the leading edge of the  $\alpha$ -peak. For the data shown in Figure 4.2, a constant value of  $\text{KL}/\text{Dp}=0.7$  was found to best fit the data for the  $\alpha$ -peak. In contrast,  $\text{KL}/\text{Dp}$  for the coverage dependant data shown in Figure 4.3 decreased from 1.0 (strict first order) at 0.1 ML to 0.8 at 0.6 ML. This immediately implies the degree of polymerization for the  $\alpha$ -peak increased as a function of coverage and the number of chains ( $\text{W}/\text{Dp}$ ) does not change up to the saturation coverage. A fixed number of chains could arise during polymerization initiated at a small number of surface sites such as defects or step edges.

Table 4.1 Results of the fits to equations (4.5) and (4.8) for the data shown in Figures 4.2 and 4.3.

	$\alpha$ -POM	$\beta$ -POM
E (kJ/mol)	91 ( $\pm 2$ ) <sup>a</sup>	60.1 ( $\pm 0.7$ )
$\nu$	9 ( $\pm 1$ ) $\times 10^{21}$	9 ( $\pm 1$ ) $\times 10^{12}$

a) Average values from Figures 4.2 and 4.3.

Errors represent  $1\sigma$ .

The results of the fits also suggest that, if the same depolymerization mechanisms are operative for both  $\alpha$ - and  $\beta$ -POM, the  $\alpha$ -species must be associated with long chain POM molecules (since  $\text{KL} < \text{Dp}$ ) while the  $\beta$ -species is associated with short chain POM

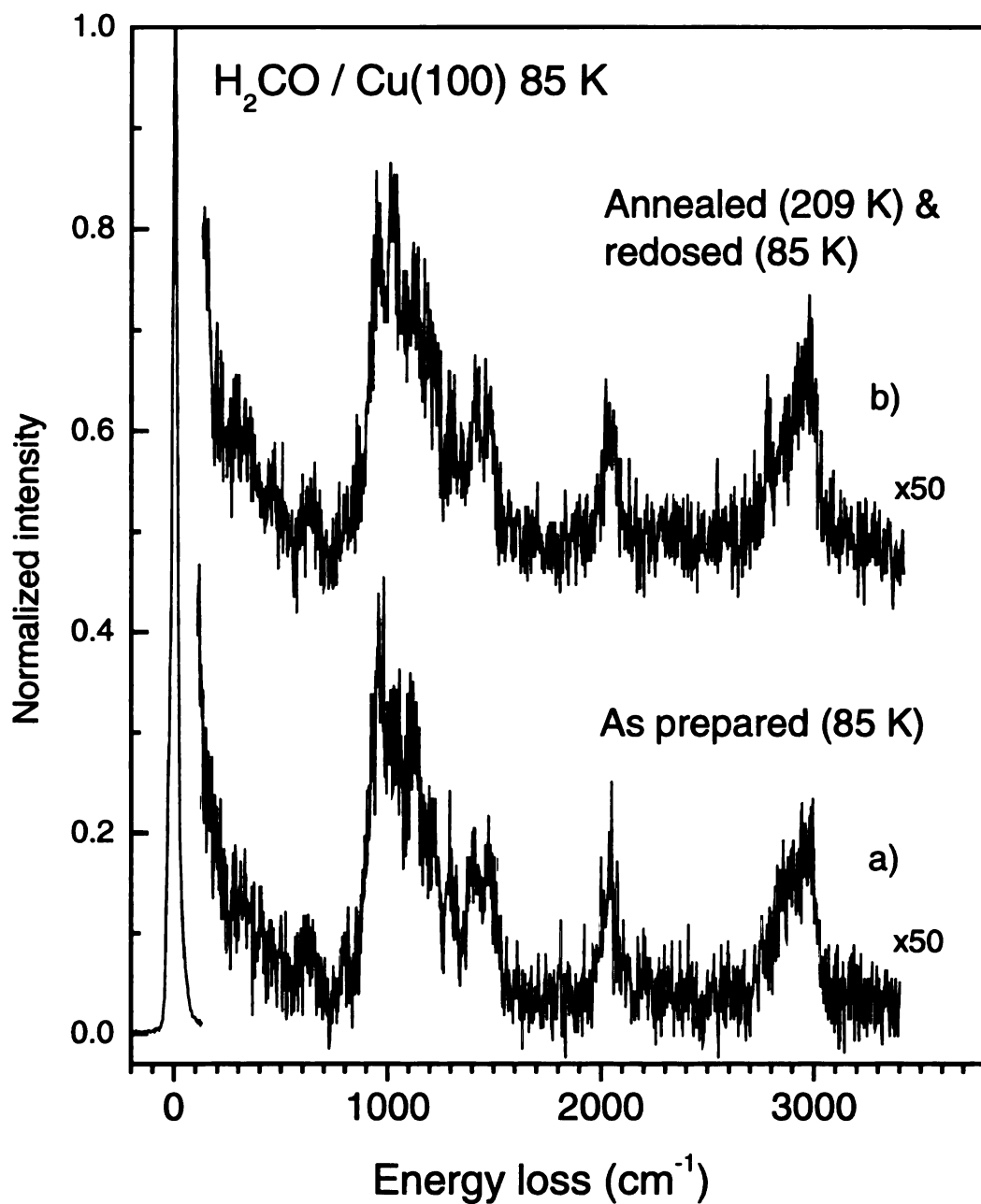


Figure 4.5 Electron energy loss spectra of (a) 1 ML  $\text{H}_2\text{CO}$  on  $\text{Cu}(100)$  exposed at 85 K and (b) 1 ML  $\text{H}_2\text{CO}$  annealed to 209 K and dosed with  $\text{H}_2\text{CO}$  to re-saturate the surface.

molecules ( $KL/Dp \geq 1$ ).

*Vibrational analysis.* The EEL spectra of the POM layer formed from the exposure of  $H_2CO$  at 85 K and that formed through the annealing (209 K) and re-dosing procedure were compared. Figure 4.5a shows the spectrum of the POM formed through exposure of  $H_2CO$  at 85 K. All features can be attributed to POM and closely match with both IR data from solid POM<sup>12,13</sup> and EELS data from POM formed on Cu(110)<sup>8</sup> and Ag(111).<sup>9</sup> Adventitious carbon monoxide (CO) was responsible for the loss observed at  $2050\text{ cm}^{-1}$  ( $\nu(C\equiv O)$ ). Figure 4.5b shows the EEL spectrum formed through the process described for Figure 4.1c: saturation of the surface with POM, annealing to 209 K to remove the  $\alpha$  species, and re-dosing  $H_2CO$  to 1 ML total coverage. Within our experimental resolution and signal-to-noise ratio (S/N), the spectrum appears to be identical to that shown in Figure 4.5a. The EELS data are consistent with the conclusion that the  $\alpha$  and  $\beta$  layers formed through the two different procedures (dosing  $H_2CO$  at 85 K versus annealing and re-dosing) are identical.

Electron energy loss spectroscopy was used to investigate the  $\beta$  species further. Figure 4.6 shows EEL spectra for separate monolayer coverages of POM prepared at 85 K followed by brief annealing to the temperature indicated. Figure 4.6a shows the EEL spectrum for a POM layer that has been annealed to 140 K. All loss features, except those at  $800$ ,  $1020$ , and  $1120\text{ cm}^{-1}$ , can be assigned to POM or adsorbed CO. Results for Figure 4.6a are summarized in Table 4.2, along with IR data for solid POM. All EEL spectra for monolayer POM acquired for annealing temperatures between 85-190 K were similar to that shown in Figure 4.6a. In contrast, Figure 4.6b shows the spectrum



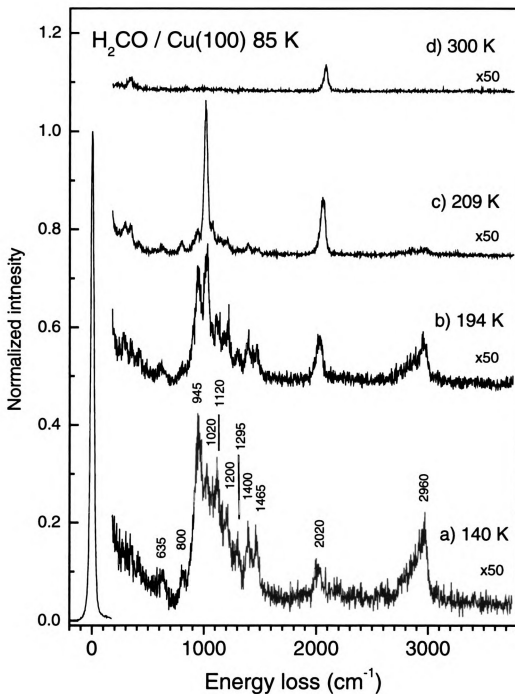


Figure 4.6 Electron energy loss spectra of 1 ML  $\text{H}_2\text{CO}$  on  $\text{Cu}(100)$  exposed at 85 K and annealed to (a) 140 K, (b) 194 K, (c) 209 K and (d) 300 K. Each spectrum is a separate 1 ML  $\text{H}_2\text{CO}$  dose.

Table 4.2 Assignments of the vibrational losses (in  $\text{cm}^{-1}$ ) observed by EELS for 1 ML coverages of  $\text{H}_2\text{CO}$  and  $\text{D}_2\text{CO}$  on  $\text{Cu}(100)$  at 85 K; also shown are IR data for solid poly(oxymethylene- $h_2$ ) (POM- $h_2$ ) and poly(oxymethylene- $d_2$ ) (POM- $d_2$ ).

Assignment	POM- $h_2$ solid <sup>12,13</sup>	POM- $d_2$ solid <sup>12,13</sup>	1 ML $\text{H}_2\text{CO}$ 140 K <sup>a</sup>	1 ML $\text{H}_2\text{CO}$ 140 K <sup>a</sup>	1 ML $\text{D}_2\text{CO}$ 140 K <sup>a</sup>	1 ML $\text{H}_2\text{CO}$ 209 K <sup>a</sup>	1 ML $\text{D}_2\text{CO}$ 209 K <sup>a</sup>
$\nu(\text{Cu-O})$					290	280	271
$\nu(\text{M-CO})$					350	337	340
$\delta(\text{COC})$	455	363				415	
$\delta(\text{OCO})$	630	618	635		600	620	603
			800		760	800	750
$\nu_s(\text{OCO})$	932	838	945		825	940	860
			1020		945	1020	980
$\nu_{as}(\text{OCO})$	1091	1128			1150	1070	1140
			1120			1120	
$\tau(\text{CH}_2) / (\text{CD}_2)$	1235	1156	1200			1190	1204
$\tau(\text{CH}_2) / (\text{CD}_2)$	1286	909	1295		905		
$w(\text{CH}_2) / (\text{CD}_2)$	1434	1078	1400			1390	
$\delta(\text{HCH}) /$ (DCD)	1471	1064	1465			1465	1068
$\nu(\text{C}\equiv\text{O})$			2020		2040	2050	2056
$\nu_s(\text{CH}) / (\text{CD})$	2919	2105			2105	2850	
$\nu_{as}(\text{CH}) / (\text{CD})$	2979	2235	2960		2240	2965	2236

a) anneal temperature

obtained after annealing to 194 K. The losses attributable to POM between 600 and 1500  $\text{cm}^{-1}$  decreased slightly in intensity while the losses at 800 and 1020  $\text{cm}^{-1}$  remained approximately unchanged. Also, the S/N has increased in Figure 4.6b suggesting a modest increase in order for the annealed surface.

After heating to 209 K to fully remove the  $\alpha$  species, the spectrum shown in Figure 4.6c was obtained. Based on TPD data shown Figure 4.1, this spectrum should be entirely due to the  $\beta$  species at a fractional coverage of  $\sim 0.4$ . A new loss appeared at 280  $\text{cm}^{-1}$ , which was tentatively assigned to  $\nu(\text{Cu-O})$  based on EELS studies of  $\text{O/Cu(100)}$ .<sup>14</sup> The detection of this mode was enhanced by the large S/N increase observed after annealing to 209 K, implying the  $\beta$  species was more ordered than the mixture the two species. While the losses were less intense, all modes except the strong losses at 800, 1020 and 1120  $\text{cm}^{-1}$ , were attributable to POM. The  $\nu(\text{CH})$  region showed two resolved losses at approximately 2850 and 2965  $\text{cm}^{-1}$ .

Annealing above 209 K resulted in the decrease of all mode intensities. Figure 4.6d shows the EEL spectrum obtained after annealing to 300 K. Complete depolymerization of both adsorbed polymer species occurred and a clean surface was recovered. The observed losses at 345 and 2087  $\text{cm}^{-1}$  were due to CO re-adsorbed during sample cooling to 85 K.

Electron energy loss spectroscopy, combined with the annealing studies, was also used to investigate the adsorption of formaldehyde- $d_2$  ( $\text{D}_2\text{CO}$ ) to determine the origin of the losses at 800, 1020, and 1120  $\text{cm}^{-1}$ . Figure 4.7 shows the adsorption of 1 ML of  $\text{H}_2\text{CO}$  ( $\text{D}_2\text{CO}$ ) at 85 K (mixture of  $\alpha$  and  $\beta$  species). All observed losses, except those

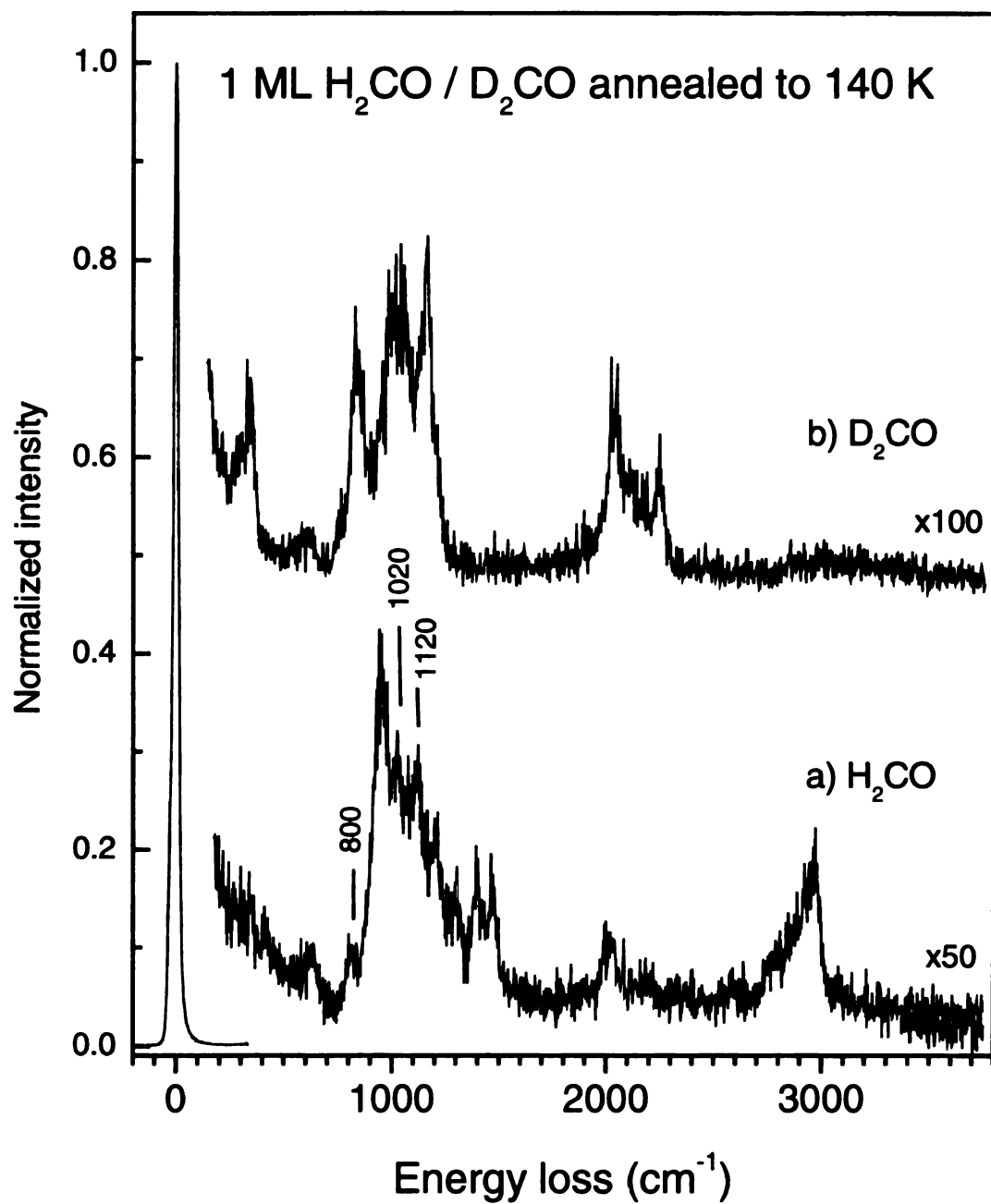


Figure 4.7 Electron energy loss spectra of (a) 1 ML  $\text{H}_2\text{CO}$  and (b) 1 ML  $\text{D}_2\text{CO}$  followed by a brief anneal to 140 K.

previously mentioned, can be assigned to POM (POM- $d_2$ ). The losses for Figure 4.7 are summarized in Table 4.2. The vibrational frequencies obtained following  $D_2CO$  adsorption (shown in Figure 4.7b) match well with IR data for solid POM-  $d_2$  and the expected isotope shifts were observed.<sup>12,13</sup> Importantly, the losses at 800 and 1020  $cm^{-1}$  (Figure 4.7a) were observed to shift to 760 and 945  $cm^{-1}$  upon isotopic substitution, corresponding to isotopic shifts ( $v(POM-h_2)/v(POM-d_2)$ ) of 1.07 and 1.08, respectively. These ratios are indicative of normal modes involving primarily carbon-oxygen motion in POM, although unambiguous assignment is difficult due to the large intramolecular coupling of modes observed for solid POM.

The identification of the loss for POM- $h_2$  observed at 1120  $cm^{-1}$  is hampered by the coincident loss observed for POM- $d_2$  at 1150  $cm^{-1}$ , assigned to  $\nu_{as}(OCO)$ . If the loss at 1120  $cm^{-1}$  for POM- $h_2$  involved pure carbon-hydrogen motion, isotopic substitution would shift this mode, assuming an isotopic ratio of 1.4, to  $\sim 816$   $cm^{-1}$ . For POM- $d_2$ , this region is dominated by a strong loss at 825  $cm^{-1}$  ( $\nu_s(OCO)$ ) thus obscuring the loss if present.

Figure 4.8 shows EEL spectra of 1 ML of  $H_2CO$  ( $D_2CO$ ) annealed to 209 K to fully remove the  $\alpha$  species and isolate the  $\beta$  species. The results for Figure 4.8 are summarized in Table 4.2. Figure 4.8a is similar to that shown in Figure 4.6c. Upon annealing to 209 K, POM- $d_2$  shows similar behavior to that seen for POM- $h_2$ . Namely, the losses attributable to POM- $d_2$  decreased in intensity while the losses at 750 and 980  $cm^{-1}$  (800 and 1020  $cm^{-1}$  in POM- $h_2$ ) remained relatively constant. As with POM- $h_2$ , the S/N increased upon annealing and the expected isotope shifts were observed. The broad

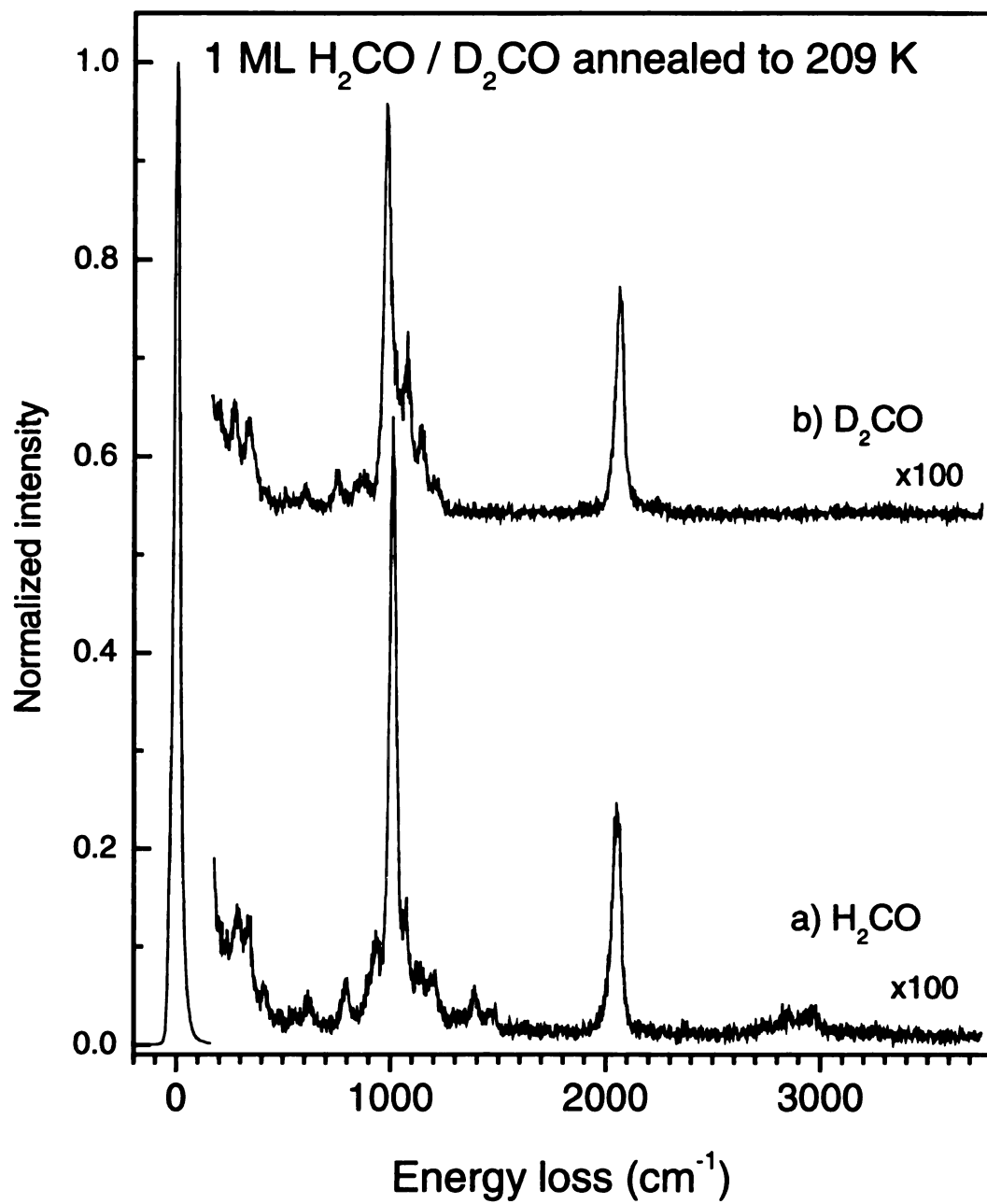


Figure 4.8 Electron energy loss spectra of (a) 1 ML  $\text{H}_2\text{CO}$  and (b) 1 ML  $\text{D}_2\text{CO}$  followed by a brief anneal to 209 K.

loss observed at  $860\text{ cm}^{-1}$  probably arises from overlap of two losses:  $\nu_s(\text{OCO})$  of POM- $d_2$  and the loss at  $\sim 816\text{ cm}^{-1}$  (red-shifted from  $1120\text{ cm}^{-1}$  for POM- $h_2$ ), as was previously discussed. A loss at  $271\text{ cm}^{-1}$  was tentatively assigned to  $\nu(\text{Cu-O})$ . The isotope shift of 1.08 observed upon deuteration suggests the loss is neither primarily derived from hydrogen (deuterium)-carbon motion nor strictly  $\nu(\text{Cu-O})$  for an isolated oxygen atom. It probably arises from isotopic substitution on an atom adjacent to an oxygen atom bound to the surface. The origin of this loss as well as the other unassigned losses at 800, 1020 and  $1120\text{ cm}^{-1}$  will be discussed below.

A possible conformation of the  $\beta$ -POM species can be proposed based on the EELS data in Figure 4.8. The observation of the  $\nu_{as}(\text{OCO})$  mode for both POM- $h_2$  and POM- $d_2$ , coupled with the surface selection rule, eliminates the planar zigzag conformation for the  $\beta$ -POM species. The most probable conformation is helical, as observed in bulk POM, and as proposed for poly(acetaldehyde) on O/Ag(111).<sup>15,16</sup>

*Endgroup identification.* The EEL spectrum shown in Figure 4.8a corresponds to the  $\beta$  species. If the chains are short enough, as suggested by the TPD fits, the concentration of endgroups for the  $\beta$  species may be sufficiently large to be visible in EELS spectra. Endgroups might be responsible for losses at 290, 800, 1020, and  $1120\text{ cm}^{-1}$  for the  $\beta$  species which cannot be ascribed to bulk POM.

Likely endgroups for POM on Cu(100) include -OH, -OCH<sub>3</sub>, and -O-Cu. The identity of the endgroups can be elucidated by comparison of the vibrational spectra of small molecules containing these functionalities adsorbed on Cu(100). For example, for monolayer methanol adsorbed on clean Cu(100), losses are observed at 610-810, 1020,

1130, 1450, 2850, 2945 and 3290  $\text{cm}^{-1}$  that can be assigned to  $\delta(\text{OH})$ ,  $\nu(\text{CO})$ ,  $\rho(\text{CH}_3)$ ,  $\delta(\text{CH}_3)$ ,  $\nu(\text{CH})$  and  $\nu(\text{OH})$ , respectively.<sup>17,18</sup> Methoxide shows a similar spectrum, except for the lack of modes due to the hydroxyl group, and an additional loss at 295  $\text{cm}^{-1}$  that can be attributed to  $\nu(\text{Cu-O})$ .<sup>17-19</sup> The losses at 280, 1020 and 1120  $\text{cm}^{-1}$ , for our POM- $h_2$  ( $\alpha$  and  $\beta$ ), closely match with  $\nu(\text{Cu-O})$ ,  $\nu(\text{CO})$  and  $\rho(\text{CH}_3)$ , respectively of adsorbed methanol or methoxide. Unfortunately, while all expected modes for methanol/methoxide are observed in our EELS data, they are either poorly resolved or overlap with features due to the POM backbone modes. Definitive assignment of the endgroups is also hampered by the poor S/N seen for the mixed POM overlayer.

Upon annealing to 209 K to remove the  $\alpha$  species, the losses due to the POM backbone lose intensity. This observation is consistent with the loss of longer POM chains while the shorter chains, having fewer monomer units per chain, show less intense POM losses relative to those of the endgroups. The losses at 1020 and 1120  $\text{cm}^{-1}$ , for the adsorbed POM- $h_2$  shown in Figure 4.8a, do not shift with annealing. While consistent with the  $\nu(\text{Cu-O})$  of an isolated methoxide species, the mode at 280  $\text{cm}^{-1}$  ( $\beta$  species) is, instead, assigned to a POM species bound to the surface through a terminal oxygen atom. Deuteration shifts this loss to 271  $\text{cm}^{-1}$  indicating it is not an isolated oxygen atom but is likely due to the attachment of an O atom to an adjacent  $\text{CH}_2$  ( $\text{CD}_2$ ) group within the POM chain.

For POM- $d_2$  shown in Figure 4.8b, the loss assigned to  $\nu_s(\text{OCO})$  at 860  $\text{cm}^{-1}$  is probably comprised of two losses: the  $\nu_s(\text{OCO})$  of POM-  $d_2$  and the  $\rho(\text{CD}_3)$ , accounting for the apparent broadening. Based on the observed isotope shifts and the close match of



the losses with those of a methoxide species, we conclude the  $\beta$  species is short chain length POM with one end bound to the surface through an oxygen atom and the other end terminated with a methoxide group, written as  $-\text{O}_a-(\text{CH}_2\text{O})_n-\text{CH}_3$ , where  $\text{O}_a$  is the oxygen atom of the POM chain bound to the surface. The number of monomer units involved in the  $\alpha$  and  $\beta$  species is unknown and under further investigation. The mechanism of formation of the  $\beta$  species will be discussed below.

The loss observed at  $800\text{ cm}^{-1}$ , for POM- $h_2$  shown in Figures 4.7a and 4.8a, is more difficult to assign. Comparing the frequency with reasonable candidates, it matches best with the  $\delta(\text{OCO})$  mode of adsorbed formate observed at  $758$  and  $780\text{ cm}^{-1}$  on Cu(100)<sup>20,21</sup> and Cu(110),<sup>22,23</sup> respectively. Two characteristic losses for adsorbed formate/formic acid have been observed at  $\sim 1360$  and  $\sim 1070\text{ cm}^{-1}$  that can be assigned to  $\nu_s(\text{OCO})$ <sup>20,21</sup> and  $\pi(\text{CH})$ ,<sup>23</sup> respectively. Although we observed losses at similar frequencies, the shifts upon deuteration do not match those expected for formate. The origin of  $800\text{ cm}^{-1}$  loss could arise either from the bending motion,  $\delta(\text{O}_a\text{CO})$ , or a  $150\text{ cm}^{-1}$  red-shifted  $\nu(\text{O}_a\text{CO})$  mode of solid POM- $h_2$  caused by anchoring one of the oxygen atoms to the surface.

The presence of isolated formate, methoxide and methanol on the Cu(100) surface can be eliminated by comparing the adsorption and desorption behavior of formic acid and methanol. Methanol exposed to clean Cu(100) has been found to adsorb molecularly and desorb at  $179\text{ K}$ .<sup>17,18</sup> Methoxide is formed following methanol exposure to preoxidized Cu(100) at  $\sim 120\text{ K}$  and is stable up to  $400\text{ K}$ .<sup>17</sup> Likewise, formic acid adsorbed on Cu(100) deprotonates to form formate. This formate species decomposes to

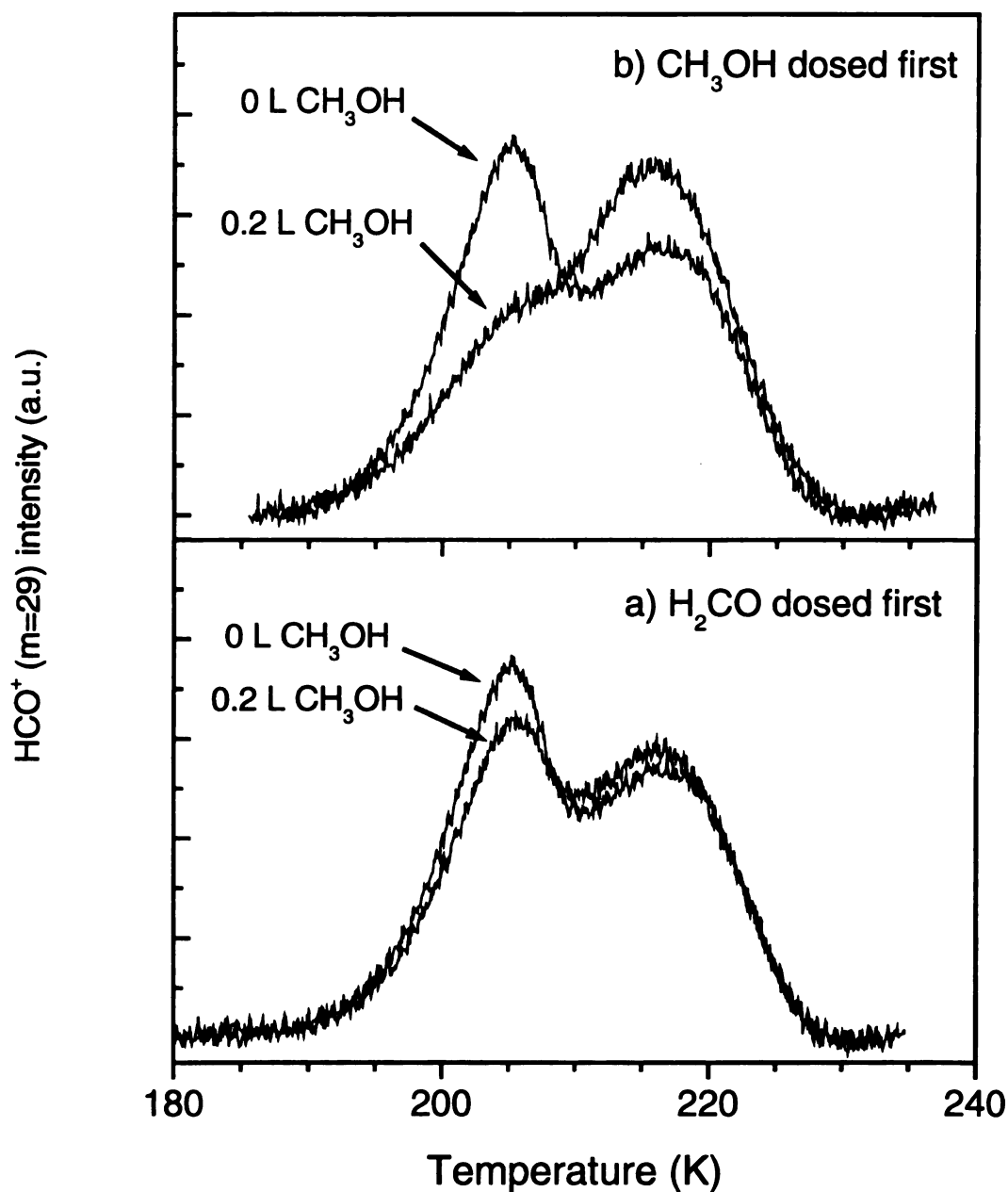


Figure 4.9 Mass 29 ( $\text{HCO}^+$ ) TPD spectra after the adsorption of (a) 0.2 L methanol ( $\text{CH}_3\text{OH}$ ) on the Cu(100) surface pre-covered with 0.6 ML  $\text{H}_2\text{CO}$  and (b) 0.6 ML  $\text{H}_2\text{CO}$  on the Cu(100) surface pre-covered with 0.2 L  $\text{CH}_3\text{OH}$ . The “0 L  $\text{CH}_3\text{OH}$ ” spectrum is the same for both (a) and (b).

CO<sub>2</sub> and H<sub>2</sub> at 420 K.<sup>20,21</sup> In the present work, a clean surface was generated upon annealing to 300 K indicating no isolated methoxide or formate species were formed. Thus, isolated methoxide, methanol and formate can be eliminated as the cause of the losses observed at 290, 800, 1020 and 1120 cm<sup>-1</sup> for the data shown in Figure 4.8a.

*Reaction of CH<sub>3</sub>OH and H<sub>2</sub>CO.* Since formaldehyde is known to react with methanol to form compounds of the type, CH<sub>3</sub>O-(CH<sub>2</sub>O)<sub>n</sub>-H,<sup>3</sup> and our EELS data is generally consistent with such a species, the reaction of H<sub>2</sub>CO with CH<sub>3</sub>OH adsorbed on Cu(100) was investigated. Figure 4.9 shows TPD data obtained following the reaction of H<sub>2</sub>CO with CH<sub>3</sub>OH on Cu(100) at 85 K. Figure 4.9a displays the TPD data obtained before and after exposing a POM-covered surface to CH<sub>3</sub>OH. Upon exposure to CH<sub>3</sub>OH, little change in the TPD was observed. In contrast, when H<sub>2</sub>CO was exposed to a surface pre-covered with methanol, a dramatic change was observed in the TPD data as shown in Figure 4.9b. The proportion of the α species decreased while the β species increased. In both cases, neither a change in peak position nor width was evident. These data suggest that the POM-covered surface is non-reactive towards CH<sub>3</sub>OH but the presence of pre-adsorbed CH<sub>3</sub>OH during H<sub>2</sub>CO exposure appears to decrease the formation of long chain POM species (α). It is possible that CH<sub>3</sub>OH is controlling the preferential formation of the β species indirectly, for example by site blocking. However, since no CH<sub>3</sub>OH was observed to desorb from the surface after the exposure sequence shown in Figure 4.9b, we discount this indirect role. Most likely, CH<sub>3</sub>OH terminates the polymerization to form increased quantities of short chain POM species of the type -O<sub>a</sub>-(CH<sub>2</sub>O)<sub>n</sub>-CH<sub>3</sub>, as previously discussed.

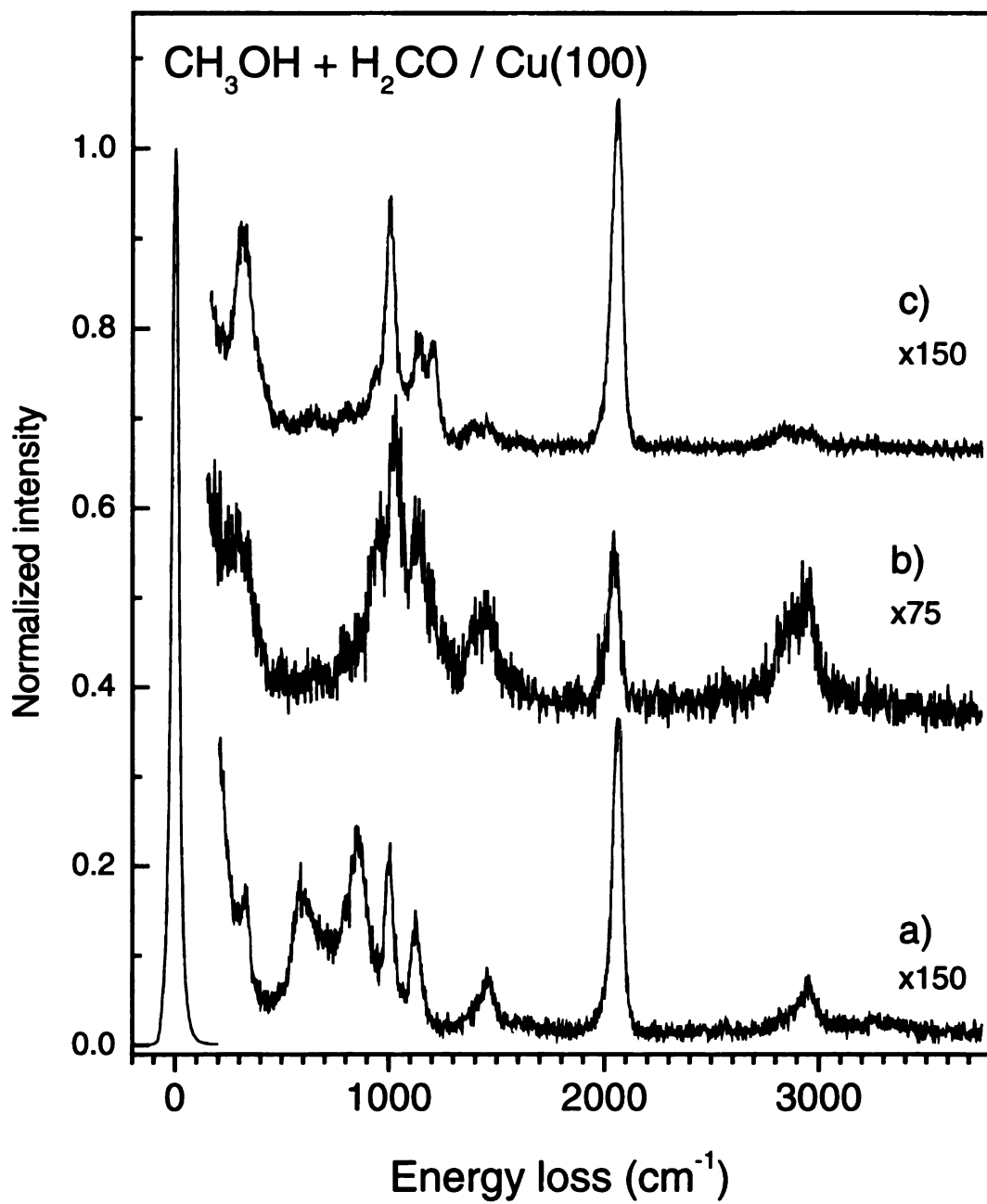


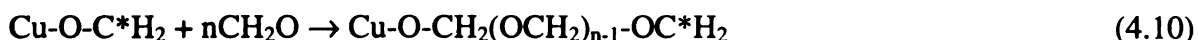
Figure 4.10 Electron energy loss spectra of (a) 0.2 L  $\text{CH}_3\text{OH}$ , (b) 0.6 ML  $\text{H}_2\text{CO}$  dosed onto the  $\text{Cu}(100)$  surface pre-covered with 0.2 L  $\text{CH}_3\text{OH}$  and (c) the spectrum in (b) annealed to 209 K.

Electron energy loss spectroscopy was used to confirm that CH<sub>3</sub>OH was incorporated into the  $\beta$ -POM species. Figure 4.10a shows the EELS spectrum of 0.2 L CH<sub>3</sub>OH (~0.15 of saturation) adsorbed on Cu(100) at 85 K. The position and intensities of the observed losses match well with previous investigations for molecularly adsorbed methanol.<sup>17,18</sup> Exposing this CH<sub>3</sub>OH-covered surface to 0.4 ML H<sub>2</sub>CO results in the spectrum shown in Figure 4.10b. New losses are evident that can be assigned to POM and the resulting spectrum is similar to that shown in Figure 4.5a. Importantly, losses due to  $\delta(\text{OH})$  are absent indicating CH<sub>3</sub>OH has been deprotonated, although the detection of  $\nu(\text{OH})$  is hampered by its small dipole scattering cross section.<sup>24</sup> Also, the losses at 290, 1020 and 1120 cm<sup>-1</sup>, discussed previously, are evident in Figure 4.10b confirming these losses arise from the methoxide endgroup of the POM species.

Annealing the overlayer shown in Figure 4.10b to 209 K results in the EEL spectrum in Figure 4.10c. Again, the data appear similar to that seen for POM formed in the absence of CH<sub>3</sub>OH (Figure 4.5a). The loss at 800 cm<sup>-1</sup> was still observed, along with those due to the methoxide endgroup and POM. Interestingly, the losses due to  $\rho(\text{CH}_3)$  (from the endgroup) and  $r(\text{CH}_2)$  (from POM) are more intense than those seen in Figure 8a. Additionally, the loss due to  $\nu(\text{Cu-O}_a)$  at the chain end, observed at ~ 300 cm<sup>-1</sup>, is also more intense. This is consistent with an increased number of chains, and thus chain ends, due to CH<sub>3</sub>OH reacting with the growing chain and effectively terminating the polymerization.

A reaction scheme for the formation of the  $\beta$  species can be proposed based on the similarities of the species formed with and without CH<sub>3</sub>OH during the adsorption and

polymerization of H<sub>2</sub>CO. The most likely initiation reaction is that the copper surface acts as a weak Lewis acid towards the oxygen of H<sub>2</sub>CO upon adsorption.<sup>25</sup> Solution phase H<sub>2</sub>CO is known to polymerize in the presence of Lewis acids,<sup>3</sup> and many oxygen containing molecules (alcohols,<sup>17</sup> ethers,<sup>26</sup> acetaldehyde,<sup>27</sup> and formic acid<sup>20,22,23</sup>) are known to interact with copper surfaces through the oxygen lone pairs. We speculate that for H<sub>2</sub>CO on Cu(100), propagation proceeds by reaction of H<sub>2</sub>CO molecules with an activated carbon atom adjacent to the surface bound oxygen. The growing chain is expected to have a lower mobility on the surface than the monomer: H<sub>2</sub>CO has been calculated to have a small binding energy of ~0.1 eV on Cu(111) and hence will be highly mobile at 85 K.<sup>28</sup> The polymerization likely terminates by abstracting a hydrogen atom from the surface, known to adsorb on copper surfaces at 85 K.<sup>29-31</sup> This series of reactions can be written as



where C\* is the growing chain end. The initiation and termination reactions are consistent with the EELS losses observed at 290, 1020 and 1120 cm<sup>-1</sup> that are assigned to  $\nu(\text{Cu-O})$ ,  $\nu(\text{CO})$  and  $\rho(\text{CH}_3)$ , respectively.

The reactions occurring when CH<sub>3</sub>OH is present during polymerization are similar to those shown above. The initiation and propagation steps shown in (4.9) and

(4.10) are identical but, instead of termination by a hydrogen atom, nucleophilic attack by CH<sub>3</sub>OH on the growing chain end occurs, followed by loss of a proton to the surface. This terminates the polymerization and forms the methoxy endgroup. This reaction can be written as



The reactions that lead to the longer chain species ( $\alpha$  species) are unknown at this time. A full description is limited by the poor S/N observed when both species are present and the inability to isolate the  $\alpha$  species from the  $\beta$ . While the  $\alpha$  species contains  $\sim 1/3$  of the H<sub>2</sub>CO molecules present within the POM overlayer (at 1 ML total coverage), it is possible few chains of the longer species exist, thus lowering the likelihood that the losses from the endgroups would be observed in EELS.

### 4.3 Conclusions

Formaldehyde polymerizes spontaneously on the 85 K Cu(100) surface forming long chain ( $\alpha$ ) and shorter chain ( $\beta$ ) poly(oxymethylene) (POM) species. Equations describing the kinetics of depolymerization suggest the number of chains of the  $\alpha$  species is constant for increasing coverage and determined at low coverages by a fixed number of surface initiation sites. However, the equations alone cannot explain the presence of two species based solely on differences in D<sub>p</sub>; for equal number of monomer units, the longer chain species should depolymerize at a higher temperature. As discussed in Chapter 3,

conformational differences are most likely the cause of the two depolymerization features observed in TPD.

Upon annealing to 209 K to fully depolymerize and remove the  $\alpha$  species, losses are observed attributable to the endgroups of the helical  $\beta$  species. Losses observed at 1020 and 1120  $\text{cm}^{-1}$  can be assigned to  $\nu(\text{CO})$  and  $\rho(\text{CH}_3)$ , respectively, of a methoxy endgroup while a loss at 290  $\text{cm}^{-1}$  is indicative of the end of the POM chain bound directly to the surface through an oxygen atom. This species can be written as  $-\text{O}_\text{s}-(\text{CH}_2\text{O})_n-\text{CH}_3$ . A loss at 800  $\text{cm}^{-1}$  is believed to arise from a mode associated with the surface-bound oxygen. Compared to bulk POM, the lower thermal stability observed for monolayer  $\beta$ -POM on Cu(100) most likely results from the chain being bound to the surface through the oxygen atom, resulting in a lower barrier to initiation of depolymerization. Methoxide endgroups are known to increase thermal stability in POM.<sup>3</sup> The weakening of the POM backbone due to interaction with the surface and its influence on the thermal depolymerization is minimal, based on the similarities of the vibrational frequencies for the adsorbed and bulk POM.

Pre-adsorbed methanol was found to terminate the polymerization and favor the formation of the  $\beta$ -POM species. The thermal stability and EEL spectra of the POM overlayer formed upon reaction with  $\text{CH}_3\text{OH}$  was similar to that of  $\beta$ -POM formed through the direct adsorption of  $\text{H}_2\text{CO}$ . However, the losses due to the endgroups were more intense than the POM layer formed by  $\text{H}_2\text{CO}$  adsorption alone, indicating the  $\beta$  species formed were shorter than those formed through the direct adsorption process. The ability to preferentially form a specific chain length polymer with a specific



endgroup may open the possibility to control both thin film order and morphology and tailor thermal stability based on the interaction of the endgroup with the surface.

#### 4.4 References

- (1) Bryden, T.; Garrett, S. *J. Phys. Chem. B.* **1999**, *103*, 10481.
- (2) The 2-3 K difference in absolute peak desorption maxima observed and reported in Chapter 4 and the previous chapter was ascribed to heating rate and thermocouple position variations.
- (3) Walker, J. F. *Formaldehyde*, 3rd. ed.; Reinhold Publishing Corp.: New York, 1964.
- (4) Kambe, H. In *Aspects of Degradation and Stabilization of Polymers*; Jellinek, H., Ed.; Elsevier: Amsterdam, 1978; pp 393.
- (5) Feger, C.; Franke, H. In *Polyimides: Fundamentals and Applications*; Ghosh, M., Mittal, K., Eds.; Marcel Dekker: New York, 1996; pp 759.
- (6) Haq, S.; Richardson, N. *J. Phys. Chem. B.* **1999**, *103*, 5256.
- (7) Plank, R.; DiNardo, J.; Vohs, J. *Phys. Rev. B.* **1997**, *55*, 10241.
- (8) Sexton, B.; Hughes, A.; Avery, N. *Surf. Sci.* **1985**, *155*, 366.
- (9) Fleck, L.; Feehery, W.; Plummer, E.; Ying, Z.; Dai, H. *J. Phys. Chem.* **1991**, *95*, 8428.
- (10) Reich, L.; Stivala, S. *Elements of Polymer Degradation*; McGraw-Hill: New York, 1971.
- (11) Jellinek, H. H. G. In *Aspects of Degradation and Stabilization of Polymers*; Jellinek, H. H. G., Ed.; Elsevier: Amsterdam, 1978; pp 1.

- (12) Tadokoro, H.; Kobayashi, M.; Kawaguchi, Y.; Koybayashi, A.; Murahashi, S. *J. Chem. Phys.* **1963**, *38*, 703.
- (13) Matsuura, H.; Murata, H. *Bull. Chem. Soc. Jpn.* **1982**, *55*, 2835.
- (14) Sueyoshi, T.; Sasaki, T.; Iwasawa, Y. *J. Phys. Chem. B.* **1997**, *101*, 4648-4655.
- (15) Tadokoro, H. In *Macromolecular Reviews*; Peterlin, A., Goodman, M., Okamura, S., Zimm, B., Mark, H., Eds.; Interscience: New York, 1967; Vol. 1; pp 119.
- (16) Sim, W.; Gardner, P.; King, D. *J. Am. Chem. Soc.* **1996**, *118*, 9953.
- (17) Dai, Q.; Gellman, A. *J. Phys. Chem.* **1993**, *97*, 10783.
- (18) Ellis, T.; Wang, H. *Langmuir* **1994**, *10*, 4083.
- (19) Camplin, J. P.; McCash, E. M. *Surf. Sci.* **1996**, *360*, 229-241.
- (20) Dubois, L.; Ellis, T.; Zegarski, B.; Kevan, S. *Surf. Sci.* **1986**, *172*, 385.
- (21) Taylor, P.; Rasmussen, P.; Ovesen, C.; Stoltze, P.; Chorkendorff, I. *Surf. Sci.* **1992**, *261*, 191.
- (22) Bowker, M.; Haq, S.; Holroyd, R.; Parlett, P.; Poulston, S.; Richardson, N. *J. Chem. Soc., Faraday Trans.* **1996**, *92*, 4683-4686.
- (23) Hayden, B.; Prince, K.; Woodruff, D.; Bradshaw, A. *Surf. Sci.* **1983**, *133*, 589.
- (24) Ibach, H.; Mills, D. L. *Electron Energy Loss Spectroscopy and Surface Vibrations*; Academic Press: San Diego, 1982.
- (25) Fleck, L.; Howe, P.; Kim, J.; Dai, H. *J. Phys. Chem.* **1996**, *100*, 8011.
- (26) Meyers, J.; Street, S.; Thompson, S.; Gellman, A. *Langmuir* **1996**, *12*, 1511.
- (27) Lamont, C.; Stenzel, W.; Conrad, H.; Bradshaw, A. *J. Electron Spectrosc. Relat. Phenom.* **1993**, *64/65*, 287-296.
- (28) J. Greeley and M. Mavrikakis, to be published.

2

b

2

3

- (29) Adsorbed hydrogen was assumed to arise from dissociation of molecular hydrogen and/or formaldehyde at the filaments of the ion gauge and/or QMS.
- (30) Chorkendorff, I.; Rasmussen, P. *Surf. Sci.* **1991**, *248*, 35.
- (31) Kammler, T.; Kuppers, J. *J. Chem. Phys.* **1999**, *111*, 8115.

## Chapter 5 Photochemistry of Formaldehyde Adsorbed on CO-saturated Cu(100)

### Abstract

The photochemistry of formaldehyde ( $\text{H}_2\text{CO}$ ) adsorbed on CO-saturated Cu(100) at 85 K was studied using electron energy loss spectroscopy (EELS) and temperature-programmed desorption (TPD). Formaldehyde was weakly adsorbed on CO/Cu(100) and desorbed at 104 K, corresponding to a desorption energy of 18.2 ( $\pm 0.8$ ) kJ/mol. Irradiation of the  $\text{H}_2\text{CO}/\text{CO}/\text{Cu}(100)$  surface caused the molecularly adsorbed  $\text{H}_2\text{CO}$  to polymerize, forming poly(oxymethylene) (POM). Irradiation also caused the formation of ethylene glycol ( $\text{CH}_2\text{OH}$ )<sub>2</sub>. Losses observed at 870 and 3365  $\text{cm}^{-1}$ , after UV irradiation, were assigned to  $\nu(\text{CC})$  and  $\nu(\text{OH})$  modes, respectively, of ( $\text{CH}_2\text{OH}$ )<sub>2</sub> indicating ethylene glycol was formed promptly upon irradiation. The presence of ( $\text{CH}_2\text{OH}$ )<sub>2</sub> was confirmed by studying the adsorption of ( $\text{CH}_2\text{OH}$ )<sub>2</sub> on clean and oxygen-covered Cu(100). The formation of ethylene glycol was likely governed by geometric constraints present within the formaldehyde overlayer.

## 5.1 Introduction

Formaldehyde polymerizes spontaneously to form poly(oxymethylene) (POM), - $(\text{H}_2\text{CO})_n$ -, upon adsorption on a variety of clean and oxygenated surfaces: O/Ag(110),<sup>1</sup> Ni(110),<sup>2</sup> Pt(111),<sup>3</sup> Pd(111),<sup>4</sup> O/Rh(111),<sup>5</sup> O/Pd(111),<sup>6</sup> NiO(100),<sup>7</sup> Cu(110)<sup>8</sup> and Cu(100).<sup>9</sup> Although the polymer has been positively identified through a variety of techniques, in most cases little is known about the precise initiation, propagation or termination mechanisms that lead to the polymer. The morphology, crystallinity, conformation and chain length of the polymer produced are similarly poorly characterized. Recently, formaldehyde molecularly adsorbed on Ag(111) has been polymerized to POM using photons and electrons, offering the potential for precise temporal and spatial control of creation and deposition of polymer monolayers.<sup>10,11</sup> Such control also increases the prospects for understanding surface polymerization reactions at a more fundamental level.

We recently reported the facile thermal polymerization of formaldehyde on Cu(100) at 85 K.<sup>9</sup> The film appeared to be composed of two different types of polymer chain with different conformation and/or chain length as inferred from vibrational spectroscopy and thermal desorption/depolymerization measurements.<sup>12</sup> We turn our attention here to the photopolymerization of formaldehyde and the nature of the polymeric film produced. In this case we use carbon monoxide as a spacer layer to prevent direct interaction of the formaldehyde with the Cu(100) surface and thereby inhibit spontaneous polymerization.

Co-adsorbed carbon monoxide (CO) is known to influence the chemistry observed on surfaces. For example, co-adsorbed CO has been found to increase the

stability of ethynylidyne on Ru(001),<sup>13</sup> decrease the stability of the methyl hydrogen atoms of toluene on Ru(001),<sup>14</sup> perturb the decomposition pathway of methylamine on Ru(001)<sup>15</sup> and promote the decomposition of saturated hydrocarbons on Ni(755).<sup>16</sup> Carbon monoxide is weakly chemisorbed on Cu(100), desorbing molecularly at ~ 180 K.<sup>9</sup> This desorption temperature is some 20-40 K lower than the decomposition temperature of the POM polymer but about 80 K higher than the desorption temperature of the formaldehyde monomer on CO/Cu(100). Such a situation offers the possibility for forming patterned polymer films through photopolymerization, followed by desorption of monomer (from the unirradiated areas) and the CO spacer layer. In this way, it may be possible to selectively deposit intact polymer onto specific regions of the Cu surface in a controlled fashion.

## 5.2 Results and Discussion

*Photochemistry of H<sub>2</sub>CO/CO/Cu(100).* The adsorption and photochemistry of formaldehyde (H<sub>2</sub>CO) on CO-saturated Cu(100) (CO/Cu(100)) was investigated using temperature-programmed desorption. At 85 K, H<sub>2</sub>CO adsorbs molecularly and desorbs as a single peak at 104 K as shown in Figure 5.1a (0 min.). This feature does not saturate with increasing coverage and spectra for increasing coverages have coincident leading edges (data not shown), suggestive of zero-order desorption. An Arrhenius plot of ln(rate) vs. T<sup>-1</sup> indicated a desorption energy of 18.2 (±0.8) kJ/mol, confirming H<sub>2</sub>CO is physisorbed on CO/Cu(100). This desorption energy compares favorably to that seen

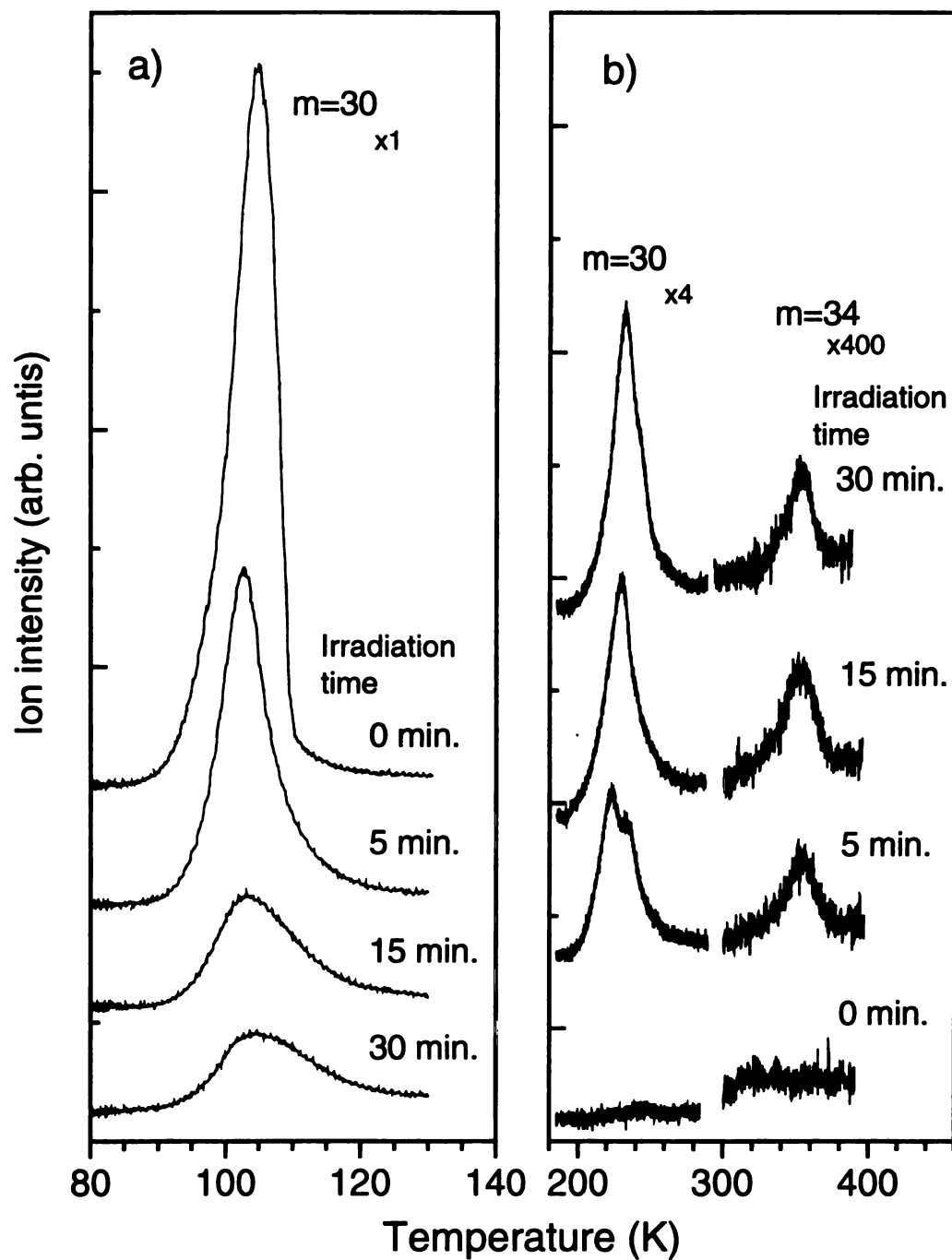


Figure 5.1 Temperature-programmed desorption spectra for (a)  $m=30$  ( $\text{H}_2\text{CO}^+$ ) and (b)  $m=30$  ( $\text{H}_2\text{CO}^+$ ) and  $m=34$  ( $\text{D}_2\text{COD}^+$ ) for a 1.1 ML coverage of  $\text{H}_2\text{CO}$  ( $\text{D}_2\text{CO}$ ) on CO-saturated Cu(100) as a function of UV irradiation time.  $\text{D}_2\text{CO}$  was used to reduce coincident mass fragment interferences.



for  $\text{H}_2\text{CO}$  physisorbed on  $\text{Ag}(111)$  of 25 kJ/mol.<sup>10</sup> Importantly, no desorption features were observed between 200-240 K where the polymer, formed through the thermal polymerization on the clean  $\text{Cu}(100)$  surface, was found to depolymerize.<sup>9</sup> This immediately suggests the CO-saturated surface is inert towards thermal polymerization at 85 K and the CO inhibits the polymerization possibly through a site-blocking mechanism. No other species were observed to desorb from the unirradiated surface except for the CO monolayer, which desorbs at  $\sim 180$  K for a saturation coverage.

Figure 5.1 also shows TPD spectra for a 1.1 ML  $\text{H}_2\text{CO}$  on  $\text{CO}/\text{Cu}(100)$  as a function of irradiation time. Irradiating the overlayer for 5 minutes caused a decrease in the molecularly adsorbed  $\text{H}_2\text{CO}$  intensity as observed in Figure 5.1a for  $m=30$  ( $\text{H}_2\text{CO}^+$ ). Continued irradiation caused this feature to decrease further. The peak desorption temperature was constant and the peak broadened slightly for increasing irradiation times. New features were observed for  $m=30$  after 5 minutes irradiation at  $\sim 220$  and  $\sim 235$  K as shown in Figure 5.1b. These two features increase in intensity, as a function of irradiation time, and merge into a large peak centered at  $\sim 230$  K with a small shoulder at  $\sim 240$  K. Measurement of other fragments associated with  $\text{H}_2\text{CO}$  ( $\text{HCO}^+$  and  $\text{H}_2^{13}\text{CO}^+$ ) resulted in identical TPD spectra for the features at 104 K and between 220-250 K and whose intensity ratios reflected that of the mass spectral fragmentation pattern for gas-phase  $\text{H}_2\text{CO}$ .<sup>17</sup> This confirms the features observed at 104 and between 220-250 K are due to molecular  $\text{H}_2\text{CO}$ . Importantly, comparison of pre- and post-irradiation TPD spectra for CO ( $m=28$ ), indicated no change in the desorption temperature or the coverage of the saturated CO layer.

Molecular formaldehyde has been observed to desorb ~ 205 and ~ 220 K due to the depolymerization of poly(oxymethylene) (POM) formed from the thermal reaction on clean Cu(100).<sup>9</sup> The desorption temperatures observed following irradiation in the current work were similar to those observed for the depolymerization of POM formed through the photopolymerization of H<sub>2</sub>CO on Ag(111).<sup>10</sup> This suggests the features observed between 220-250 K for m=30, as shown in Figure 5.1b, are due to the depolymerization of POM formed upon photopolymerization of H<sub>2</sub>CO adsorbed on CO/Cu(100). The presence of POM will be confirmed using EELS data as discussed below. The slight shift to higher depolymerization temperatures, observed in Figure 5.1b, could be related to changes in chain length or endgroup stability and is currently under investigation.

A desorption feature was observed for m=31 at 350 K that did not show any corresponding intensity at m=29 or 30 (data not shown). This feature is inconsistent with molecular H<sub>2</sub>CO. To remove interference from coincident mass fragments and help in the identification of this peak, the adsorption and photochemistry of D<sub>2</sub>CO on CO/Cu(100) was investigated. Identical TPD data to H<sub>2</sub>CO were obtained for D<sub>2</sub>CO for the features at 104 K and between 220-250 K after irradiation. The peak observed at 350 K for m=31 (H<sub>2</sub>CO) was detected at m=34 for D<sub>2</sub>CO, as shown in Figure 5.1b, indicating the fragment contains at least 3 protons.

A number of small molecules can be eliminated as the source of the 350 K desorption feature. The lack of intensity for m=29 excludes adsorbed alkoxides as the source of the 350 K feature. These species are known to desorb at temperatures  $\geq$  350 K on Cu(100),<sup>18</sup> however, at these temperatures, alkoxides undergo  $\beta$ -hydride elimination

to produce the corresponding aldehydes, all of which show  $m=29$  as the most abundant mass fragment in their mass spectrum.<sup>17</sup> Also, the lack of intensity at  $m=60$ , coupled with lack of intensity at  $m=29$ , eliminates the simplest dialdehyde, ethanedial ( $\text{CDO}$ )<sub>2</sub>, as the source of the feature at 350 K.

The most likely species that gives rise to the feature at 350 K is ethylene glycol. This is consistent with previous experiments on the adsorption of ethylene glycol on  $\text{O/Cu(110)}$ <sup>19</sup> and  $\text{O/Ag(110)}$ <sup>20</sup> where desorption features were observed at 390 and 365 K, respectively. In contrast to the present work, ethylene glycol was observed to undergo  $\beta$ -hydride elimination to produce ethanedial on both  $\text{O/Cu(110)}$  and  $\text{O/Ag(110)}$ . It is possible, without surface oxygen present, molecular desorption is favored over ethanedial generation for the ethylene glycol produced in the irradiation of  $\text{H}_2\text{CO}$  adsorbed on  $\text{CO/Cu(100)}$ . The presence of ethylene glycol will be confirmed by the EELS data discussed below.

The amount of ethylene glycol formed saturates after 15 minutes of irradiation, as shown in Figure 5.1b, and was calculated using both TPD and XPS data. Initially, 1.1 ML of  $\text{H}_2\text{CO}$  was adsorbed on  $\text{CO/Cu(100)}$ . After 15 minutes of irradiation, ~ 80 % of the original 1.1 ML  $\text{H}_2\text{CO}$  desorbed as monomer (0.45 ML) or formed polymer (0.43 ML), leaving ~ 20 % unaccounted for  $\text{H}_2\text{CO}$ . The lack of knowledge regarding the electron impact ionization cross-section of ethylene glycol prevented quantification using TPD. However, XPS analysis of a sample that had been irradiated for 15 minutes and then annealed to 270 K to remove monomer, polymer and CO, revealed a coverage of 0.17 ML of carbon, consistent with the remaining 20 %.

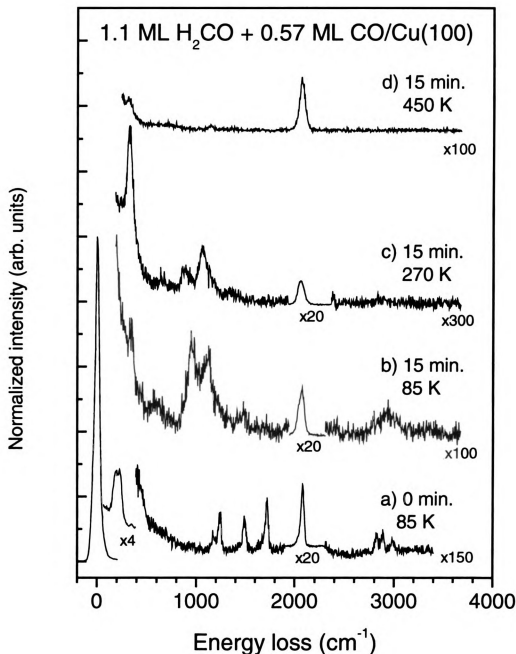


Figure 5.2 Electron energy loss spectra for a 1.1 ML coverage of  $\text{H}_2\text{CO}$  on  $\text{CO}$ -saturated  $\text{Cu}(100)$  for (a) 0 minutes irradiation at 85 K, (b) 15 minutes irradiation at 85 K, (c) 15 minutes irradiation followed by an anneal to 270 K and (d) 15 minutes irradiation followed by an anneal to 450 K. Each spectrum constituted a separate 1.1 ML coverage of  $\text{H}_2\text{CO}$ . The data were acquired at 85 K.

The adsorption and photochemistry of  $\text{H}_2\text{CO}$  on  $\text{CO}/\text{Cu}(100)$  was investigated using EELS. Figures 5.2a and 5.2b show EEL spectra for 1.1 ML  $\text{H}_2\text{CO}$  adsorbed on  $\text{CO}/\text{Cu}(100)$  after 0 and 15 minute irradiation. Figure 5.2a shows 1.1 ML  $\text{H}_2\text{CO}$  on  $\text{CO}/\text{Cu}(100)$  prior to irradiation. The losses observed at 350 and 2080  $\text{cm}^{-1}$  are due to  $\nu(\text{Cu-CO})$  and  $\nu(\text{CO})$ , respectively, of the adsorbed CO and are observed at these approximate energies for all the spectra shown in Figure 5.2. The other losses were assigned to molecular  $\text{H}_2\text{CO}$  and match well with IR data for crystalline formaldehyde.<sup>21</sup> The frequencies are only slightly shifted from the solid-phase data confirming  $\text{H}_2\text{CO}$  was weakly adsorbed on the  $\text{CO}/\text{Cu}(100)$  surface. The observation of lattice modes at 200 and 230  $\text{cm}^{-1}$  suggests the adsorbed  $\text{H}_2\text{CO}$  was well ordered. Also, the observation of all the modes of molecular  $\text{H}_2\text{CO}$  indicates the molecule was adsorbed with the C-O bond axis tilted from the surface normal. This geometry would render the  $B_1$  ( $\nu_4$ ,  $\nu_5$ ) and  $B_2$  ( $\nu_6$ ) modes within the  $C_{2v}$  point group, to which  $\text{H}_2\text{CO}$  belongs, visible according to the surface selection rule.<sup>22</sup> The data from Figure 5.2a is summarized in Table 5.1.

After 15 minutes of UV irradiation, the spectrum shown in Figure 5.2b was obtained. New modes appeared at 600, 950, 1120, 1480 and 2930  $\text{cm}^{-1}$  that can be assigned to the polymer, POM, and match well with both the IR data for solid POM<sup>23</sup> and POM formed through the photopolymerization of  $\text{H}_2\text{CO}$  adsorbed on  $\text{Ag}(111)$ .<sup>10</sup> The data from Figure 5.2b is summarized in Table 5.1. The observation of the mode at 600  $\text{cm}^{-1}$  is characteristic of the  $\delta(\text{OCO})$  mode of POM and eliminates trioxane (cyclic trimer of  $\text{H}_2\text{CO}$ ) as a photoproduct. The corresponding mode for trioxane is split into two bands which appear at 744 and 521  $\text{cm}^{-1}$ .<sup>24</sup>

Table 5.1 Assignments of the vibrational bands (in  $\text{cm}^{-1}$ ) observed for a 1.1 ML coverage of  $\text{H}_2\text{CO}$  on CO-saturated  $\text{Cu}(100)$  after 0 and 15 minutes UV irradiation. Also shown are IR data for solid  $\text{H}_2\text{CO}$  and POM along with EELS data for POM on  $\text{Ag}(111)$ .

Assignment	$\text{H}_2\text{CO}$ Solid <sup>21</sup>	POM Solid <sup>23</sup>	POM/ $\text{Ag}(111)$ <sup>10a</sup>	$\text{H}_2\text{CO}/\text{CO}/\text{Cu}(100)$ 0 min. irr.	$\text{H}_2\text{CO}/\text{CO}/\text{Cu}(100)$ 15 min. irr.
lattice mode				220	
lattice mode				230	
$\nu(\text{M}-\text{CO})$				350	340
$\delta(\text{OCO})$		630	600		600
					870
$\nu_s(\text{OCO})$		932	940		950
$\nu_{as}(\text{OCO})$		1091	1110		1120
$\delta_{oop}$	1167( $\nu_6$ )			1170	
$\delta_{ip}$	1251( $\nu_5$ )			1250	
$w(\text{CH}_2)$		1434			
$\delta(\text{HCH})$	1490( $\nu_3$ )	1471	1450	1490	1480
$\nu(\text{C}=\text{O})$	1711( $\nu_2$ )			1720	
$\nu(\text{C}\equiv\text{O})$				2080	2080
$\nu_s(\text{CH})$	2831( $\nu_1$ )			2820	
$\nu_{as}(\text{CH})$	2886( $\nu_4$ )			2890	
$\nu_s(\text{CH})$		2919	2935 <sup>nr</sup>		2930 <sup>nr</sup>
$\nu_{as}(\text{CH})$		2979	2935 <sup>nr</sup>		2930 <sup>nr</sup>
$(\nu_2+\nu_5, \nu_4)$	2996			2990	
$\nu(\text{OH})$					3370

a) POM from photopolymerized  $\text{H}_2\text{CO}$

nr = not resolved

Interestingly, the losses due to molecular  $\text{H}_2\text{CO}$ , in particular the loss at  $\sim 1720\text{ cm}^{-1}$  for  $\nu(\text{C}=\text{O})$ , were not observed even though, based on TPD measurements, it makes up  $\sim 40\%$  of the overlayer after 15 minutes of irradiation. The most probable explanation for the absence of these modes is a change of orientation, rendering the modes inactive according to the surface selection rule, coupled with the reduced signal-to-noise (S/N) observed in Figure 5.2b. The absence of the strong phonon losses seen in Figure 5.2a indicates the  $\text{H}_2\text{CO}$  present after irradiation was no longer well ordered.

The spectrum in Figure 5.2b appears qualitatively different than that seen for the thermal polymerization of  $\text{H}_2\text{CO}$  on clean  $\text{Cu}(100)$ .<sup>9</sup> The losses observed in the thermal polymerization at  $1220\text{ cm}^{-1}$  ( $\tau(\text{CH}_2)$ ),  $1390\text{ cm}^{-1}$  ( $w(\text{CH}_2)$ ), and  $1470\text{ cm}^{-1}$  ( $\delta(\text{HCH})$ ) are much more intense than those seen for the present work. As seen in Figure 5.2b, losses at  $1220\text{ cm}^{-1}$  and  $1390\text{ cm}^{-1}$  were not detected. Additionally, the loss observed at  $1030\text{ cm}^{-1}$  for the thermally polymerized POM was also absent. This loss has previously been identified as a mode ( $\nu(\text{CO})$ ) due to an endgroup of the POM chain.<sup>12</sup> The differences in intensity could be due to orientation effects and/or chain length dependence (the absence of the endgroup mode in the present work implies longer chains).

There are two losses in Figure 5.2b that cannot be assigned to POM. The small shoulder observed at  $870\text{ cm}^{-1}$  is in the correct range for a mode due to  $\nu(\text{C}-\text{C})$  while the broad loss centered at  $3365\text{ cm}^{-1}$  is probably due to  $\nu(\text{OH})$ . Adsorbed water could give rise to the loss at  $3365\text{ cm}^{-1}$ , however, this loss was not detected prior to irradiation as shown in Figure 5.2a. More likely, these two losses were due to the feature observed to desorb at  $350\text{ K}$  in the TPD data that was tentatively assigned to ethylene glycol.

Annealing the overlayer shown in Figure 5.2b to 270 K resulted in the spectrum shown in Figure 5.2c. This temperature was high enough to desorb the monomeric  $\text{H}_2\text{CO}$  (104 K), CO (180 K) and the POM (220-250 K) with the remaining losses due to the feature observed to desorb at 350 K. The broad loss at  $890\text{ cm}^{-1}$  matches well to that seen in Figure 5.2b suggesting the species desorbing at 350 K was formed upon irradiation and not during the temperature ramp for the TPD experiment. Another loss was observed at  $1070\text{ cm}^{-1}$  which most likely corresponded to a mode involving carbon-oxygen motion. The  $\nu(\text{OH})$  mode at  $3365\text{ cm}^{-1}$  was lost upon annealing and no  $\nu(\text{CH})$  modes were detected. The spectrum in Figure 5.2c matches well with that observed for deprotonated ethylene glycol on O/Ag(110) where losses were observed at 890 and  $1090\text{ cm}^{-1}$  corresponding to  $\nu(\text{CC})$  and  $\nu(\text{CO})$ , respectively.<sup>20</sup> Therefore, based on TPD and EELS data, the species observed to desorb at 350 K was identified as ethylene glycol.

Annealing the sample to 450 K resulted in the spectrum shown in Figure 5.2d. All losses due to molecular  $\text{H}_2\text{CO}$ , POM and ethylene glycol were absent; the species formed during irradiation had desorbed. The observed losses were due to CO re-adsorbed during sample cooling.

*Ethylene glycol on Cu(100) and O/Cu(100).* The adsorption of ethylene glycol  $(\text{CH}_2\text{OH})_2$  on clean and oxygen-covered Cu(100) was studied using TPD. Figure 5.3 shows  $m=31$  ( $\text{CH}_2\text{OH}^+$ ) spectra for three exposures of  $(\text{CH}_2\text{OH})_2$  on clean Cu(100). A single desorption feature was observed at 237 K for a 0.1 L exposure. For increasing exposures, this peak grew in intensity and the peak desorption temperature remained unchanged. Above 0.1 L, a new feature was observed at 220 K that neither saturated nor shifted with increasing exposures. Measurement of other mass fragments of ethylene



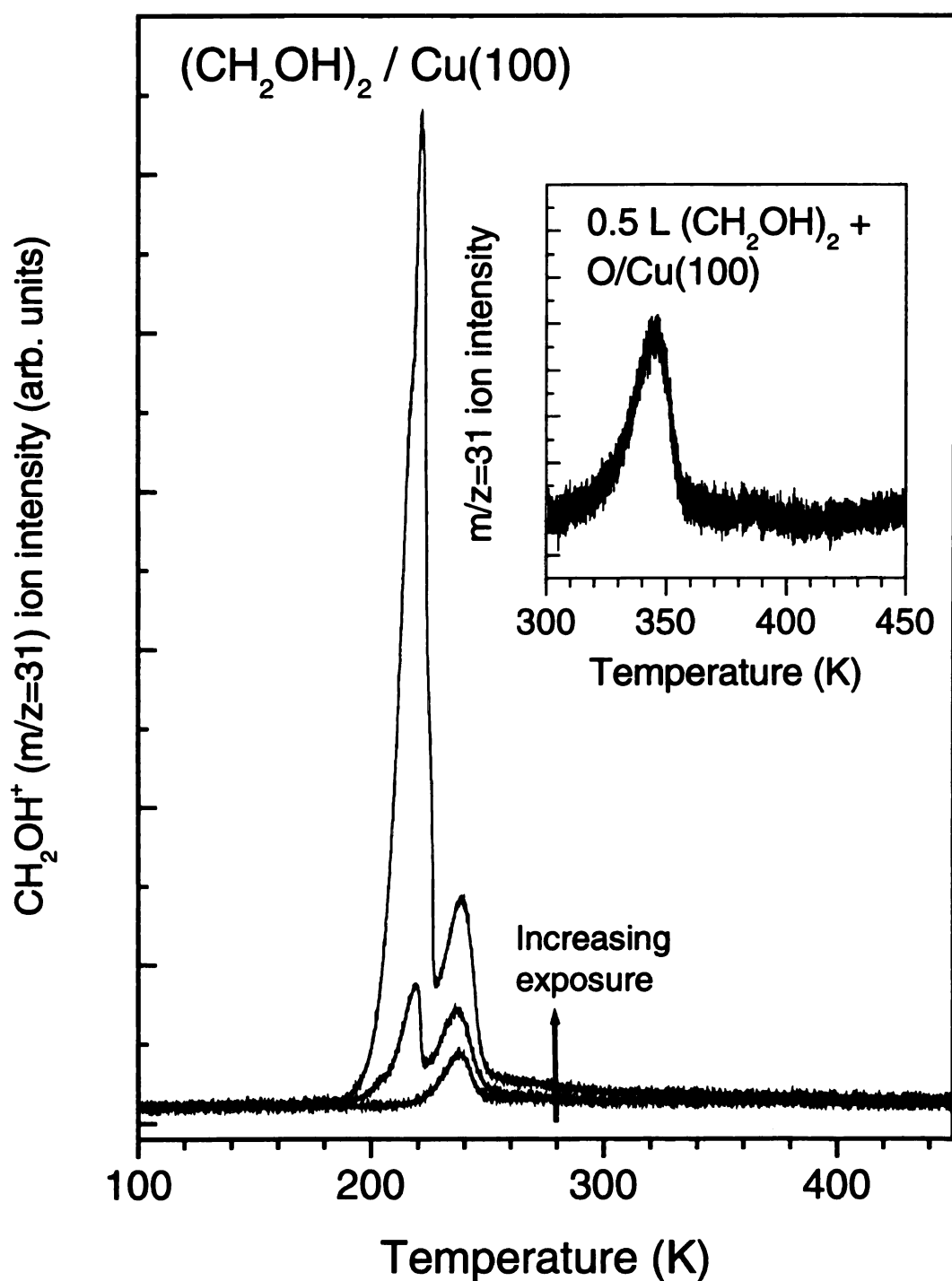


Figure 5.3 Temperature-programmed desorption spectra for  $m=31$  ( $\text{CH}_2\text{OH}^+$ ) following exposures of 0.1 L, 0.2 L and 0.5 L of ethylene glycol ( $\text{CH}_2\text{OH})_2$  on clean  $\text{Cu}(100)$ . The inset is the TPD spectrum obtained for a 0.5 L exposure on a  $\text{Cu}(100)$  pre-covered with 0.1 ML oxygen showing a new feature desorbing at 347 K.

glycol confirmed  $(\text{CH}_2\text{OH})_2$  adsorbed and desorbed molecularly. The features at 220 and 237 K are assigned to multi- and monolayer states, respectively. These temperatures match well with those seen for  $(\text{CH}_2\text{OH})_2$  adsorption on clean Ag(110) where multi- and monolayer states were found to desorb at 205 and 225 K, respectively.<sup>20</sup> Molecularly adsorbed  $(\text{CH}_2\text{OH})_2$  was found to desorb at  $\sim 220$  K from the Cu(110) surface,<sup>19</sup> consistent with the current results. Assuming first-order kinetics for the state at 237 K on Cu(100) and a preexponential factor of  $10^{13} \text{ s}^{-1}$ , a desorption energy of 59 kJ/mol was estimated. This value compares favorably to the 60 kJ/mol desorption energy found for the monolayer state on Ag(110).<sup>20</sup>

The inset of Figure 5.3 shows the  $m=31$  TPD spectrum of a 0.5 L exposure of  $(\text{CH}_2\text{OH})_2$  on a Cu(100) surface pre-covered with 0.1 ML oxygen. The desorption of the multi- and monolayer states were unaffected by the oxygen. A new feature was observed at 347 K which corresponds to desorption of  $(\text{CH}_2\text{OH})_2$  that had reacted with the adsorbed oxygen forming a dialkoxide species. It is known that alcohols, including ethylene glycol, adsorb molecularly on oxygen-covered copper and silver surfaces at temperatures  $< 120$  K.<sup>18-20</sup> Heating the sample above  $\sim 200$  K causes the alcohols to deprotonate by reaction with the adsorbed oxygen, desorbing as water and forming a surface-bound alkoxide species. These species are stable to temperatures  $\geq 350$  K where they desorb molecularly in competition with production of the corresponding aldehyde.

The result shown in the inset of Figure 5.3, showing desorption at 347 K, is consistent with previous experiments on O/Cu(110)<sup>19</sup> and O/Ag(110)<sup>20</sup> where this dialkoxide state was found to desorb at 395 and 365 K, respectively. Importantly, the temperature observed for the desorbing dialkoxide species matches closely with that for

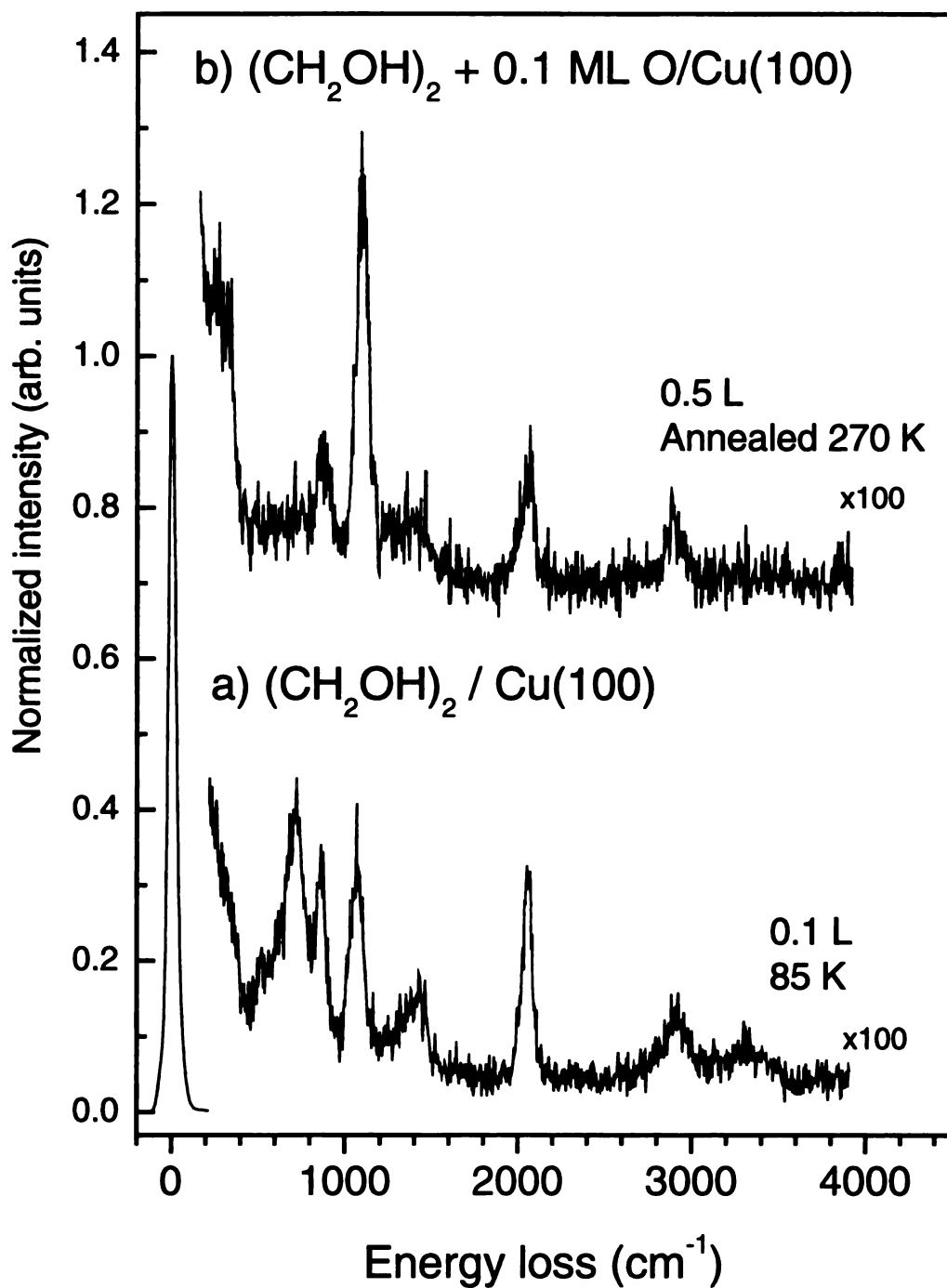


Figure 5.4 Electron energy loss spectra for (a) 0.1 L exposure of ethylene glycol (CH<sub>2</sub>OH)<sub>2</sub> on clean Cu(100) and (b) a 0.5 L exposure of (CH<sub>2</sub>OH)<sub>2</sub> on a Cu(100) pre-covered with 0.1 ML of oxygen followed by annealing to 270 K.

the feature observed to desorb at 350 K after 15 minutes of UV irradiation of 1.1 ML on CO/Cu(100), supporting the identification of this species as ethylene glycol.

The adsorption of (CH<sub>2</sub>OH)<sub>2</sub> on clean and O/Cu(100) was also studied using EELS. Figure 5.4a shows the EEL spectrum of a 0.1 L exposure (CH<sub>2</sub>OH)<sub>2</sub> on clean Cu(100) at 85 K. This exposure only populated the monolayer state as seen in Figure 5.3. The losses observed match well with liquid-phase IR data<sup>25</sup> for (CH<sub>2</sub>OH)<sub>2</sub> and that observed for (CH<sub>2</sub>OH)<sub>2</sub> adsorbed on clean Ag(110).<sup>20</sup> The loss observed at 2060 cm<sup>-1</sup> was due to adsorbed CO. The results of Figure 5.4 are summarized in Table 5.2. Noticeably absent from the monolayer spectrum was the loss due to  $\nu_{as}(\text{CO})$ . This indicates the (CH<sub>2</sub>OH)<sub>2</sub> was most likely bound to the surface via both oxygen atoms in a bidentate configuration with the O-H bonds parallel with the surface and the C-O bonds perpendicular to the surface. This geometry would have the effect of rendering inactive the  $\nu_{as}(\text{CO})$  mode as well as increasing the intensity of the mode due to  $\tau(\text{OH})$ . Similar arguments have been made for the monolayer spectrum of (CH<sub>2</sub>OH)<sub>2</sub> adsorbed on clean Ag(110).<sup>20</sup>

Annealing a 0.5 L dose of (CH<sub>2</sub>OH)<sub>2</sub> on a Cu(100) surface pre-covered with 0.1 ML of oxygen to 270 K resulted in the spectrum shown in Figure 5.4b. At this temperature the multi- and monolayer states have desorbed and a fraction of the total adsorbed (CH<sub>2</sub>OH)<sub>2</sub> has been deprotonated through reaction with the oxygen. X-ray photoelectron spectroscopic analysis indicates a coverage of 0.1 ML of (CH<sub>2</sub>OH)<sub>2</sub> remaining. The losses due to  $\tau(\text{OH})$  and  $\nu(\text{OH})$  at 700 and 3320 cm<sup>-1</sup>, respectively were absent in Figure 5.4b confirming deprotonation via reaction with the adsorbed oxygen.

Table 5.2 Assignments of the vibrational bands (in  $\text{cm}^{-1}$ ) for the species observed following 15 minutes UV irradiation and annealing to 270 K of a 1.1 ML coverage of  $\text{H}_2\text{CO}$  on CO-saturated  $\text{Cu}(100)$ . Also shown are IR data for liquid  $(\text{CH}_2\text{OH})_2$  along with EELS data for  $(\text{CH}_2\text{OH})_2$  on  $\text{O}/\text{Ag}(110)$  and  $(\text{CH}_2\text{OH})_2$  on  $\text{O}/\text{Cu}(100)$ .

Assignment	$(\text{CH}_2\text{OH})_2$ liquid <sup>25</sup>	$(\text{CH}_2\text{OH})_2/$ $\text{Cu}(100)^a$	$(\text{CH}_2\text{OH})_2+ \text{O}/\text{Ag}(110)$ <sup>20b</sup>	$(\text{CH}_2\text{OH})_2+ \text{O}/\text{Cu}(100)^c$	$\text{H}_2\text{CO}/\text{CO}/\text{Cu}(100)$ 15 min. irr. <sup>c</sup>	$(\text{CD}_2\text{OH})_2+ \text{O}/\text{Cu}(100)^c$	$\text{D}_2\text{CO}/\text{CO}/\text{Cu}(100)$ 15 min. irr. <sup>c</sup>
$\tau(\text{CC})$	360						
$\delta(\text{CCO})$	478	520					
$\tau(\text{OH})$	700	710	710				
$\nu(\text{CC})$	864	870 <sup>nr</sup>	850 <sup>nr</sup>	880 <sup>nr</sup>	890 <sup>nr</sup>	760	800
$\rho(\text{CH}_2)$	887	870 <sup>nr</sup>	850 <sup>nr</sup>	880 <sup>nr</sup>	890 <sup>nr</sup>		
$\nu_{\text{as}}(\text{CO})$	1038					1090 <sup>nr</sup>	1070 <sup>nr</sup>
$\nu_s(\text{CO})$	1087	1080	1090	1090	1070	1090 <sup>nr</sup>	1070 <sup>nr</sup>
$\tau(\text{CH}_2)$	1212						
$w(\text{CH}_2)$	1332						
$\delta(\text{COH})$	1405	1370	1410			980	970
$\delta(\text{HCH})$	1459	1440	1450				
$\nu(\text{C}\equiv\text{O})$		2070		2060	2050	1190	1180
$\nu_s(\text{CH})$	2875	2900 <sup>nr</sup>	2900 <sup>nr</sup>	2880 <sup>nr</sup>		2050	2070
$\nu_{\text{as}}(\text{CH})$	2935	2900 <sup>nr</sup>	2900 <sup>nr</sup>	2880 <sup>nr</sup>		2200 <sup>nr</sup>	
$\nu(\text{OH})$	3275	3320	3350			2200 <sup>nr</sup>	

a) Present work

b) Dialkoxide species

c) Present work, annealed 270 K

nr = not resolved

The losses remaining at 1090 and 2880  $\text{cm}^{-1}$  can be assigned to  $\nu_s(\text{CO})$  and  $\nu(\text{CH})$  modes, respectively, of the adsorbed alkoxide. The loss at 880  $\text{cm}^{-1}$  was comprised of two modes,  $\nu(\text{CC})$  and  $\rho(\text{CH}_2)$ . This assignment matches well with that for the alkoxide on O/Ag(110) where the corresponding modes were observed at 890, 1090 and 2860  $\text{cm}^{-1}$ , respectively.<sup>20</sup> In contrast to the work on O/Ag(110), the losses due to  $\omega(\text{CH}_2)$  (1340  $\text{cm}^{-1}$ ) and  $\delta(\text{HCH})$  (1450  $\text{cm}^{-1}$ ) were not positively identified on the O/Cu(100) surface although there appears to be a weak, broad loss in that range. This is probably due to the lower surface coverage used in the present work, which resulted in a lower S/N. Again, the absence of the  $\nu_{\text{as}}(\text{CO})$  mode indicates the alkoxide species was bound to the surface through the oxygen atoms in an upright configuration.

The results of Figure 5.4b can be compared with the EEL spectrum obtained for the species observed to desorb at 350 K after 15 minutes of UV irradiation of 1.1 ML  $\text{H}_2\text{CO}$  on CO/Cu(100). Figure 5.5a shows the spectrum of the species formed upon irradiation and is identical to that shown in Figure 5.2c. Figure 5.5b shows the EEL spectrum of the alkoxide species formed through the adsorption of  $(\text{CH}_2\text{OH})_2$  on O/Cu(100). Excellent agreement was observed between the spectra. The losses due to  $\nu(\text{CC})+\rho(\text{CH}_2)$  and  $\nu_s(\text{CO})$  were observed at 880 and 1090  $\text{cm}^{-1}$ , respectively for the adsorbed alkoxide and at 890 and 1070  $\text{cm}^{-1}$  for the species produced during the irradiation as shown in Figure 5.5a. These spectra confirm the species observed in Figure 5.5a as ethylene glycol.

The same experiments shown in Figure 5.5 were repeated with the deuterated species:  $\text{D}_2\text{CO}$  on CO/Cu(100) and  $(\text{CD}_2\text{OH})_2$  on O/Cu(100). The spectra obtained are shown in Figure 5.6. For the irradiation and subsequent annealing of  $\text{D}_2\text{CO}$  on

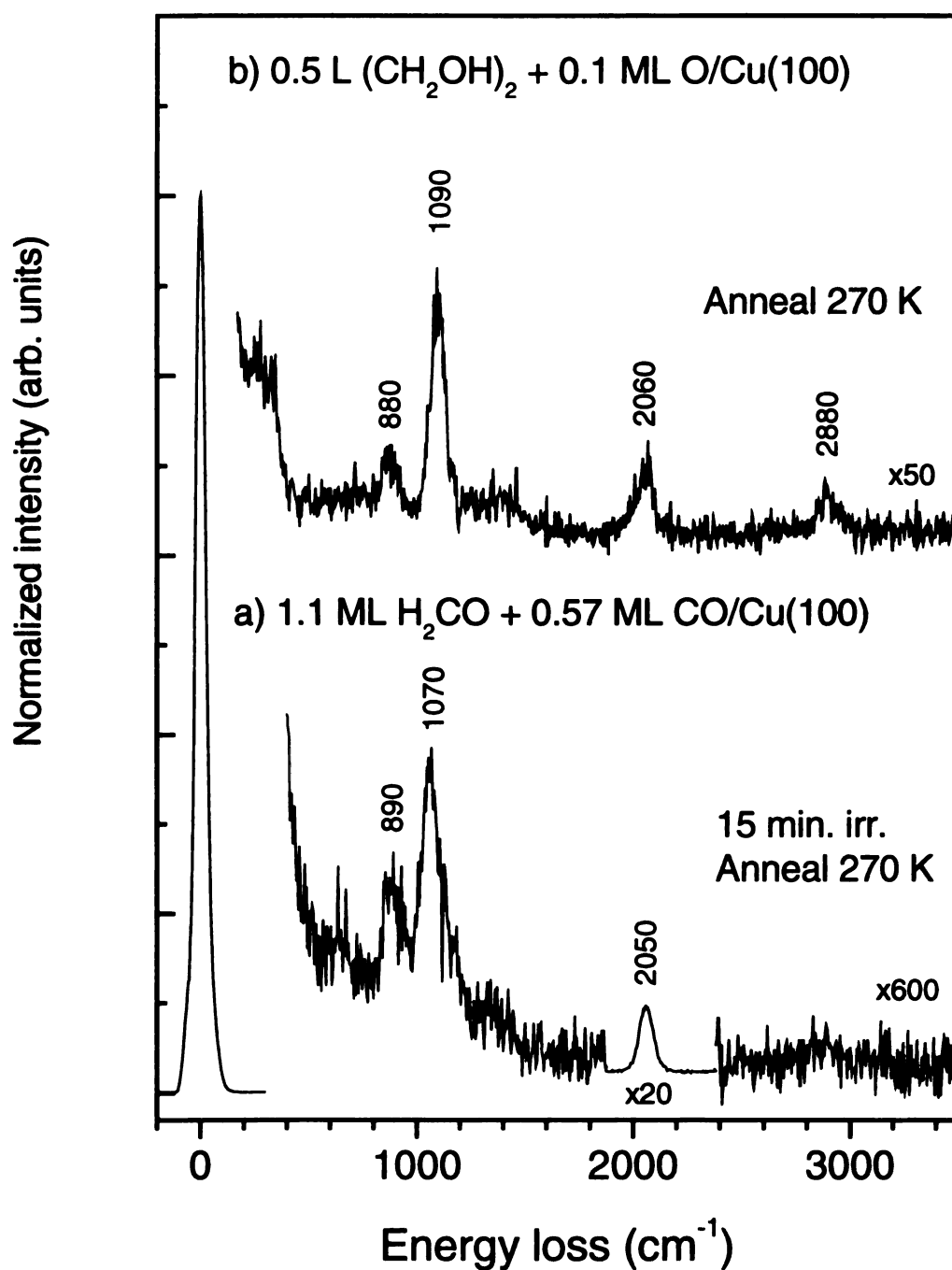


Figure 5.5 Electron energy loss spectra for (a) 1.1 ML coverage of H<sub>2</sub>CO on CO-saturated Cu(100) irradiated for 15 minutes followed by an anneal to 270 K and (b) a 0.5 L exposure of (CH<sub>2</sub>OH)<sub>2</sub> on a Cu(100) pre-covered with 0.1 ML of oxygen followed by an anneal to 270 K.

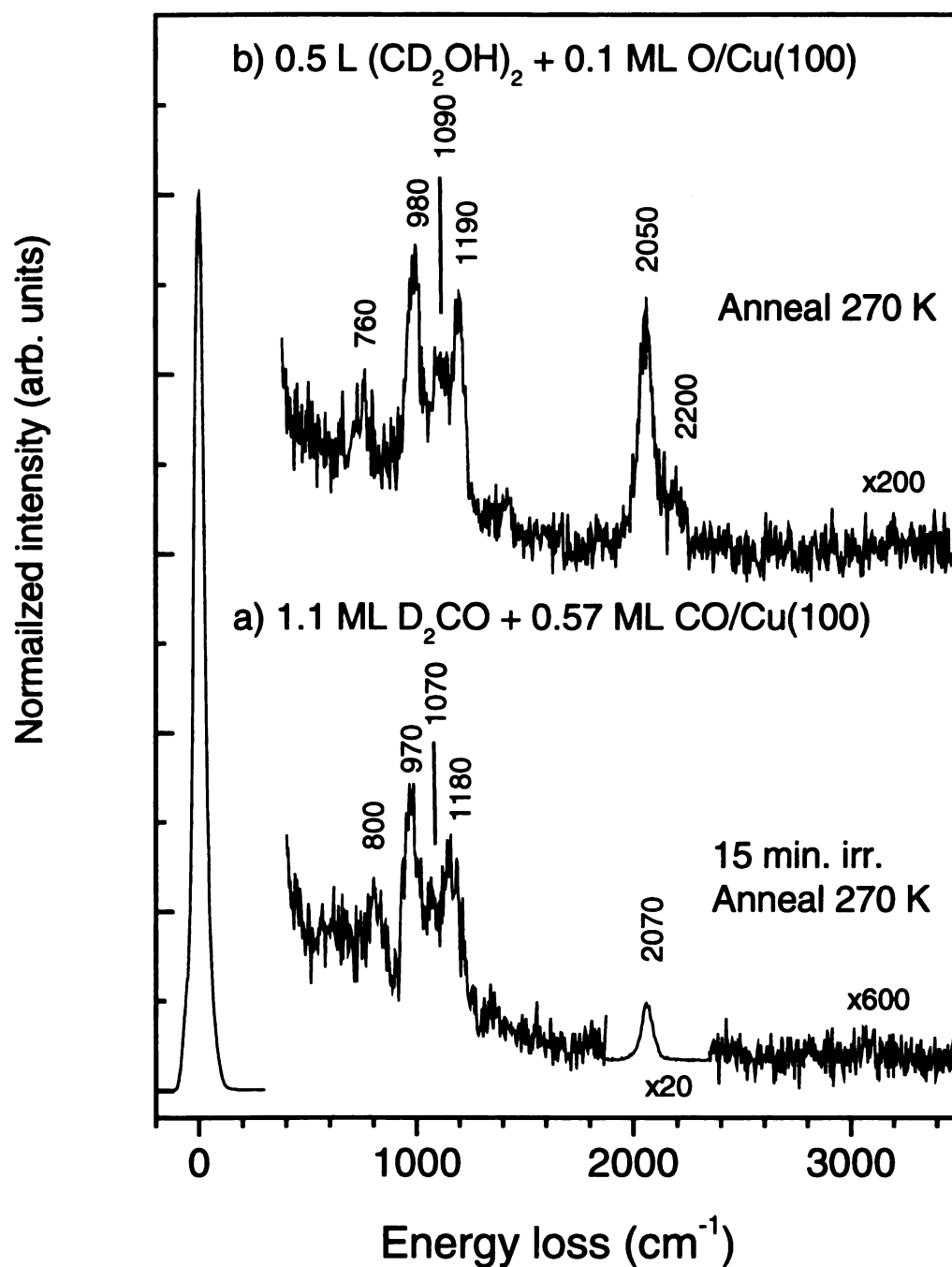


Figure 5.6 Electron energy loss spectra for (a) 1.1 ML coverage of D<sub>2</sub>CO on CO-saturated Cu(100) irradiated for 15 minutes followed by an anneal to 270 K and (b) a 0.5 L exposure of (CD<sub>2</sub>OH)<sub>2</sub> on a Cu(100) pre-covered with 0.1 ML of oxygen followed by an anneal to 270 K.



CO/Cu(100), as shown in Figure 5.6a, losses were observed at 800, 970, 1070, and 1180  $\text{cm}^{-1}$  that can be assigned, through comparison with Figure 5.6b, to  $\nu(\text{CC})$ ,  $\omega(\text{CH}_2)$ ,  $\nu_{\text{s,as}}(\text{CO})$  and  $\delta(\text{HCH})$ , respectively. Excellent agreement was again observed between the spectra. The results of Figure 5.5 and 5.6 are summarized in Table 5.2 along with liquid IR data of  $(\text{CH}_2\text{OH})_2$  and  $(\text{CH}_2\text{OH})_2$  adsorbed on O/Ag(110).

From the above TPD and EELS data, the results of the adsorption and photochemistry of  $\text{H}_2\text{CO}$  adsorbed on CO/Cu(100) can be now summarized. Formaldehyde physisorbed on the CO-saturated surface at 85 K desorbs molecularly at 104 K. Upon UV irradiation, POM was formed that was observed to depolymerize, and desorb as  $\text{H}_2\text{CO}$ , between 220 and 250 K. A second photoproduct was observed to desorb at 350 K that was identified as ethylene glycol. The formation of both POM and  $(\text{CH}_2\text{OH})_2$  will be discussed below.

*Formation of POM.* The polymerization of  $\text{H}_2\text{CO}$  could proceed via three photoexcitation mechanisms. A thermal mechanism is discounted based on the observation of an insignificant 2 K temperature rise upon irradiation. Gaseous  $\text{H}_2\text{CO}$  has a  $S_1 \leftarrow S_0$  ( $\pi^* \leftarrow n$ ) band origin at 3.49 eV<sup>26</sup> which is unlikely to be perturbed upon physisorption on CO/Cu(100). Ultraviolet irradiation, in the wavelength range used here, can dissociate  $\text{H}_2\text{CO}$  via two channels:  $\text{H}_2\text{CO} \rightarrow \text{H}_2 + \text{CO}$  (molecular) and  $\text{H}_2\text{CO} \rightarrow \text{H} + \text{HCO}$  (radical). The molecular channel has its threshold at 3.52 eV.<sup>26</sup> However, polymerization is not expected to be initiated by the molecular photoproducts and no  $\text{H}_2$ , which is not known to adsorb on Cu(100) at 85 K, was observed to evolve upon irradiation. The radical channel, whose threshold is at 3.73 eV,<sup>26</sup> may initiate the polymerization through reaction of the radical species with molecular  $\text{H}_2\text{CO}$ . However,

for experiments performed on amorphous  $\text{H}_2\text{CO}$  films deposited on CsI, no polymerization occurred upon irradiation with 4.0 eV photons.<sup>27</sup> For both channels, dissociation is expected to compete with electronic relaxation which is known to occur on metal surfaces on a time scale of  $\sim 10^{-13} - 10^{-14}$  s.<sup>28</sup> The effect of the CO spacer layer will be to decrease the relaxation rate.

The most probable excitation mechanism leading to POM is that proposed for  $\text{H}_2\text{CO}$  photopolymerization on  $\text{Ag}(111)$ .<sup>10,29,30</sup> In this mechanism, absorption of the UV irradiation by the substrate produces hot electrons, which then populate the  $\pi^*$  state of  $\text{H}_2\text{CO}$ , forming  $\text{H}_2\text{CO}^-$ . This radical anion then dissociates into products that can initiate the polymerization. In the gas-phase,  $\text{H}_2\text{CO}^-$  dissociates into  $\text{H}^- + \text{HCO}^{31}$  while on  $\text{Ag}(111)$ ,  $\text{H}_2\text{CO}^-$  was observed to dissociate into  $\text{CH}_2$  and  $\text{O}$ .<sup>29</sup> The dissociation products on  $\text{CO}/\text{Cu}(100)$  are not yet known. In contrast to the work on  $\text{Ag}(111)$ , where subvacuum electrons were produced upon irradiation, the photon energies used in the current work will produce both subvacuum and free photoelectrons. The work function of a CO-saturated  $\text{Cu}(100)$  surface was found to be 4.39 eV<sup>32</sup> and the majority of intensity from the lamp used in this work ( $\sim 80\%$ ) occurs between 5.5 and 4.9 eV, indicating most of the electrons produced will be free, low energy photoelectrons.

*Formation of Ethylene Glycol.* The formation of ethylene glycol can be explained based on the well known photochemistry of carbonyl compounds.<sup>33,34</sup> These molecules are known to be excellent hydrogen atom abstractors in their singlet  $^1(n\pi^*)$  and triplet  $^3(n\pi^*)$  electronically excited states, with the majority of chemistry occurring on the triplet surface. Formaldehyde, in its triplet state, can be thought of a biradical which abstracts a proton from another molecule to form a hydroxymethylene radical  $^{\bullet}\text{CH}_2\text{OH}$ .

22

23

24

25

26

27

28

29

30

31

32

For the UV irradiation of  $\text{H}_2\text{CO}$  on  $\text{CO}/\text{Cu}(100)$ , excited formaldehyde,  $\text{CH}_2\text{O}^*$  abstracts a proton from a neighboring  $\text{H}_2\text{CO}$  forming  $^*\text{CH}_2\text{OH}$  and  $^*\text{HCO}$ . The formyl radical can then initiate the polymerization of  $\text{H}_2\text{CO}$  to form POM. The hydroxymethylene radical can react in two ways:  $^*\text{CH}_2\text{OH}$  could couple to another  $^*\text{CH}_2\text{OH}$ , forming ethylene glycol  $(\text{CH}_2\text{OH})_2$  directly or it could react with another  $\text{CH}_2\text{O}$  to form  $^*\text{OCH}_2\text{CH}_2\text{OH}$ . This radical species could then abstract a hydrogen from another  $\text{H}_2\text{CO}$  to form  $(\text{CH}_2\text{OH})_2$  and another formyl radical.

The saturation of the formation of ethylene glycol after 15 minutes of irradiation may be due to geometric constraints. *Ab initio* results on hydrogen abstraction from methane by formaldehyde indicates only approach of the hydrogen within the molecular plane of  $\text{H}_2\text{CO}$  results in reaction and an upper limit on the barrier was estimated to be  $\sim 77$  kJ/mol.<sup>35,36</sup> This barrier was strongly dependent on  $\text{O}_{\text{H}_2\text{CO}}\text{-C}_{\text{CH}_4}$  separation with the distance equal to  $2.53$  Å at the transition state.<sup>35</sup> Once ethylene glycol is formed and POM polymerization initiated by the formyl radicals, the remaining electronically excited  $\text{H}_2\text{CO}$  may be in an unfavorable geometric position within the overlayer to abstract further hydrogens from either  $\text{H}_2\text{CO}$ , POM or ethylene glycol. Unfortunately, the structure of the physisorbed  $\text{H}_2\text{CO}$  on  $\text{CO}/\text{Cu}(100)$  is unknown at this time. However, the structure of crystalline formaldehyde does have pairs of  $\text{H}_2\text{CO}$  molecules that are oriented correctly for H-atom abstraction to occur.<sup>37</sup>

The formation of ethylene glycol through the reaction of electronically excited formaldehyde has not been observed in studies of solid phase  $\text{H}_2\text{CO}$ <sup>27,38</sup> nor in the photopolymerization of  $\text{H}_2\text{CO}$  on  $\text{Ag}(111)$ .<sup>10</sup> The presence of the CO spacer layer could influence the photochemistry by lengthening the lifetime of the excited formaldehyde

10

11

12

13

14

15

16

17

18

19

20

21

22

23

24

25

26

27

28

29

30

( $\text{H}_2\text{CO}^*$ ) by moving it away from the metallic surface or through the formation of a unique formaldehyde overlayer geometry that is favorable to the hydrogen abstraction reaction.

### 5.3 Conclusions

The presence of a saturation coverage of CO on Cu(100) inhibited the thermal polymerization of  $\text{H}_2\text{CO}$  which formed a weakly adsorbed overlayer on CO/Cu(100). Upon 30 minutes of UV irradiation,  $\text{H}_2\text{CO}$  formed POM (40 %) and ethylene glycol (20 %). The photopolymerized POM depolymerized at higher temperatures than those observed for POM formed from the thermal polymerization on clean Cu(100), suggesting a longer chain length or more thermally stable endgroup. Additionally, no losses due to endgroups were observed in EEL spectra taken after irradiation. The initiation of polymerization likely occurs via the radical anion  $\text{H}_2\text{CO}^-$  formed from electron capture of photoelectrons generated from irradiation of the CO/Cu(100) surface. The use of CO to block the thermal polymerization of  $\text{H}_2\text{CO}$  on Cu(100) and subsequent photopolymerization shows the potential for controlling polymer thin film formation for reactive monomer-substrate combinations by use of a co-adsorbate. The polymer film can be formed in a “controlled” fashion using photons and can then be deposited on the substrate after annealing to remove the co-adsorbate.

The formation of ethylene glycol from the irradiation of  $\text{H}_2\text{CO}$  adsorbed on CO/Cu(100) has not been observed previously in studies of solid phase  $\text{H}_2\text{CO}$  nor in the photopolymerization of  $\text{H}_2\text{CO}$  on surfaces. The formation likely occurs via electronically excited  $\text{H}_2\text{CO}$  which abstracts a proton from a neighboring  $\text{H}_2\text{CO}$  molecule forming a

hydroxymethylene radical  $\cdot\text{CH}_2\text{OH}$  which then reacts with other  $\cdot\text{CH}_2\text{OH}$  radicals or  $\text{H}_2\text{CO}$  ultimately forming  $(\text{CH}_2\text{OH})_2$ . The saturation of formation of ethylene glycol likely results from geometric constraints present within the overlayer.

## 5.4 References

- (1) Stuve, E.; Madix, R.; Sexton, B. *Surf. Sci.* **1982**, *119*, 279.
- (2) Richter, L.; Ho, W. *J. Chem. Phys.* **1985**, *83*, 2165.
- (3) Henderson, M.; Mitchell, G.; White, J. *Surf. Sci.* **1987**, *188*, 206.
- (4) Davis, J.; Barteau, M. *J. Am. Chem. Soc.* **1989**, *111*, 1782.
- (5) Houtman, C.; Barteau, M. *Surf. Sci.* **1991**, *248*, 57.
- (6) Davis, J.; Barteau, M. *Surf. Sci.* **1992**, *268*, 11.
- (7) Truong, C.; Wu, M.; Goodman, D. W. *J. Am. Chem. Soc.* **1993**, *115*, 3647.
- (8) Sexton, B.; Hughes, A.; Avery, N. *Surf. Sci.* **1985**, *155*, 366.
- (9) Bryden, T.; Garrett, S. *J. Phys. Chem. B.* **1999**, *103*, 10481.
- (10) Fleck, L.; Feehery, W.; Plummer, E.; Ying, Z.; Dai, H. *J. Phys. Chem.* **1991**, *95*, 8428.
- (11) Fleck, L.; Kim, J.; Dai, H.-L. *Surf. Sci.* **1996**, *356*, L417.
- (12) Bryden, T.; Garrett, S. *Langmuir*, in press.
- (13) Sasaki, T.; Kawada, F.; Aruga, T.; Iwasawa, Y. *Surf. Sci.* **1992**, *278*, 291.
- (14) Rauscher, H.; Menzel, D. *Surf. Sci.* **1995**, *342*, 155.
- (15) Sasaki, T.; Aruga, T.; Kuroda, H.; Iwasawa, Y. *Surf. Sci.* **1992**, *276*, 69.
- (16) Orita, H.; Kondoh, H.; Nozoye, H. *Chem. Phys. Lett.* **1994**, *228*, 385.

11

12

13

14

15

16

17

18

19

20

21

22

23

24

25

26

27

28

29

30

31

32

33

34

35

36



- (17) *NIST Chemistry WebBook, NIST Standard Reference Database Number 69*; Mallard, W., Linstrom, P., Eds.; National Institutes of Standards and Technology: Gaithersburg, MD, 1998; pp (<http://webbook.nist.gov>).
- (18) Dai, Q.; Gellman, A. *J. Phys. Chem.* **1993**, *97*, 10783.
- (19) Bowker, M.; Madix, R. *Surf. Sci.* **1982**, *116*, 549.
- (20) Capote, A.; Madix, R. *J. Am. Chem. Soc.* **1989**, *111*, 3570.
- (21) Khoshkoo, H.; Hemple, S.; Nixon, E. *Spectrochim. Acta A* **1974**, *30*, 863.
- (22) Ibach, H.; Mills, D. L. *Electron Energy Loss Spectroscopy and Surface Vibrations*; Academic Press: San Diego, 1982.
- (23) Tadokoro, H.; Kobayashi, M.; Kawaguchi, Y.; Koybayashi, A.; Murahashi, S. *J. Chem. Phys.* **1963**, *38*, 703.
- (24) Kobayashi, M.; Iwamoto, R.; Tadokoro, H. *J. Chem. Phys.* **1966**, *44*, 922.
- (25) Sawodny, W.; Niedenzu, K.; Dawson, J. *Spectrochim. Acta A* **1967**, *23A*, 799.
- (26) Moore, C.; Weissnar, J. *Ann. Rev. Phys. Chem.* **1983**, *34*, 525.
- (27) Mansueto, E.; Ju, C.; Wight, C. *J. Phys. Chem.* **1989**, *93*, 2143-2147.
- (28) Zhou, X.; Zhu, X.; White, J. *Surf. Sci. Rep.* **1991**, *13*, 73.
- (29) Fleck, L.; Howe, P.; Kim, J.; Dai, H. *J. Phys. Chem.* **1996**, *100*, 8011.
- (30) Fleck, L. E. Ph.D. Thesis, University of Pennsylvania, 1994.
- (31) Azria, R. Ph.D. Thesis, University of Orsay, 1972.
- (32) Dubois, L.; Zegarski, B. *Chem. Phys. Lett.* **1985**, *120*, 537.
- (33) Turro, N. In *Molecular Photochemistry*; W. A. Benjamin, Inc.: New York, 1965; **PP 137**.



- (34) Klessinger, M.; Michl, J. In *Excited States and Photochemistry of Organic Molecules*; VCH Publishers: New York, 1995; pp 395.
- (35) Severance, D.; Pandey, B.; Morrison, H. *J. Am. Chem. Soc.* **1987**, *109*, 3231.
- (36) Sumathi, K.; Chandra, A. *J. Photochem. Photobiol. A:Chem.* **1988**, *43*, 313.
- (37) Weng, S.; Torrie, B.; Powell, B. *Mol. Phys.* **1989**, *68*, 25.
- (38) Gol'danskii, V. *Ann. Rev. Phys. Chem.* **1976**, *27*, 85.

6.1.7

poly

cover

drac

stac

deco

mole

4777

depo

H<sub>2</sub>C

H<sub>2</sub>C

edge

obse

edge

no o

on to

be a

PO

## Chapter 6 Conclusions and Future Work

### 6.1 Thermal Reactions and Control of Stability

The work described in Chapter 3 has shown that at 85 K,  $\text{H}_2\text{CO}$  spontaneously polymerizes to form a monolayer of poly(oxymethylene) (POM) up to a saturation coverage of 0.69 ML ( $1.06 \times 10^{15} \text{ cm}^{-2}$ ). This surface density suggests that the POM chain directions are parallel to the surface plane and is consistent with the known crystal structures of POM.<sup>1</sup> However, the POM overlayer is probably not highly ordered.

Temperature-programmed desorption spectra indicate there is only one decomposition route available to the adsorbed polymer species: depolymerization to molecular  $\text{H}_2\text{CO}$ . The route producing  $\text{H}_2\text{CO}$  is observed as two desorption features at approximately 200 and 215 K which show apparent zero- and first-order depolymerization kinetics, respectively. This behavior has neither been observed for  $\text{H}_2\text{CO}$  adsorption Cu(110)<sup>2</sup> nor for the POM produced in the photopolymerization of  $\text{H}_2\text{CO}$  on Ag(111).<sup>3-6</sup> We believe differences due to adsorption at defect and/or step edges do not account for the appearance of two depolymerization features. The observation of CO and  $\text{H}_2$  desorption indicates  $\text{H}_2\text{CO}$  is probably dissociating at step edges and defect sites upon adsorption. Electron energy loss spectroscopy data indicate no other species besides an adsorbed polymer first layer and molecular  $\text{H}_2\text{CO}$  multilayers on top of the polymer layer, are present on the 85 K Cu(100) surface.

The observation of two features for the depolymerization of POM on Cu(100) can be ascribed to the formation of long chain ( $\alpha$ ) and short chain ( $\beta$ ) poly(oxymethylene) (POM) species as described in Chapter 4. Equations describing the kinetics of

de-  
con-  
Fu-  
inc-  
at  
de-  
sp-  
pro-  
the-  
P  
ac-  
C  
C  
at  
Si  
sp-  
fo  
o  
th  
m  
sp

depolymerization suggest the number of chains of the  $\alpha$  species is constant for increasing coverage and determined at low coverages by a fixed number of surface initiation sites. Future experiments should include increasing the number of defect sites, which may increase the proportion of  $\alpha$ -POM species produced upon adsorption of  $\text{H}_2\text{CO}$  if initiated at these sites. Chapter 4 has demonstrated that equations describing the bulk depolymerization process can be used to model the TPD spectra which should be applicable to future surface polymerization studies where multiple depolymerization processes are observed

Upon removal of the  $\alpha$  species by annealing, losses are observed attributable to the endgroups of the helical  $\beta$  species. Losses can be assigned to  $\nu(\text{Cu-O})$ ,  $\nu(\text{CO})$  and  $\rho(\text{CH}_3)$  of the end of the POM chain bound directly to the surface through an oxygen atom and to a methoxy endgroup. This species can be written as  $-\text{O}_a-(\text{CH}_2\text{O})_n-\text{CH}_3$ . Compared to bulk POM, the lower thermal stability observed for monolayer  $\beta$ -POM on  $\text{Cu}(100)$  most likely results from the chain being bound to the surface through the oxygen atom, resulting in a lower barrier to initiation of depolymerization. We believe, due to similarities in depolymerization temperature and product (molecular  $\text{H}_2\text{CO}$ ), the  $\alpha$ -POM species likely has similar endgroups to  $\beta$ -POM.

Pre-adsorbed methanol was found to terminate the polymerization and favor the formation of the  $\beta$ -POM species. The thermal stability and EEL spectra of the POM overlayer formed upon reaction with  $\text{CH}_3\text{OH}$  were similar to that of POM formed through the direct adsorption of  $\text{H}_2\text{CO}$ . However, the losses due to the endgroups were more intense than in the POM layer formed by  $\text{H}_2\text{CO}$  adsorption alone, indicating the  $\beta$  species formed were shorter than those formed through the direct adsorption process.

The experiments with the co-adsorbed methanol and  $D_2CO$  also lend support to the directly bound oxygen controlling the thermal stability of the POM species. For bulk POM, methoxy termination is known to be more stable than the hydroxy endgroup.<sup>7</sup> This indicates the oxygen bound end is likely responsible for the ~ 100 K lower stability observed for POM on Cu(100) as compared to bulk POM.

The ability to preferentially form a specific chain length polymer with a specific endgroup may open the possibility to control both thin film order and morphology and tailor thermal stability based on the interaction of the endgroup with the surface. Transforming the oxygen bound end into a methoxy terminus should increase the thermal stability dramatically. Poly(oxymethylene) dimethyl ethers are known to be stable to temperatures > 470 K, some 100 K higher than the dihydroxy terminated paraformaldehyde.<sup>7</sup> A potentially simple way to form a methoxy endgroup from the surface bound oxygen is through the reaction with methyl radicals ( $CH_3^\bullet$ ). The methyl radicals can be generated photochemically from co-adsorbed  $CH_3Br$ <sup>8</sup> or dosed from the gas phase as  $CH_3^\bullet$ , produced from the pyrolysis of azomethane.<sup>9</sup> Methyl radicals are known to be highly mobile, even at 85 K, on Cu(111)<sup>10</sup> and thus could react with the oxygen bound to the surface forming a methoxy endgroup. However, the  $CH_3^\bullet$  may also destroy the POM backbone chain through hydrogen abstraction reactions. As in the methanol experiments, the order of adsorption may influence the products greatly.

Acetoxy-terminated bulk POM is also known to be more thermally stable than the hydroxy-terminated form.<sup>7</sup> On the Cu(100) surface, acetoxy endgroups may be formed by pre-adsorbing acetic acid prior to adsorption of  $H_2CO$ . In a similar fashion to the formation of methoxy endgroups with pre-adsorbed methanol, described in Chapter 4,



action

meth-

and b

diva

poly-

6.21

int-

on C

(40

high

poly-

obse

intr-

elec

furni

disp

phya

intra-

obse

the c

acetoxy endgroups would thus be formed. In this case, as acetic acid is more acidic than methanol, the initiation and termination mechanisms for polymerization may be different and both endgroups may now be acetoxy. Further experiments with co-adsorbates may allow for a full elucidation of the propagation and termination events during the surface polymerization process.

## 6.2 Photochemical Reactions

*UV and X-ray Photons.* The presence of a saturation coverage of CO on Cu(100) inhibited the thermal polymerization of H<sub>2</sub>CO which formed a weakly adsorbed overlayer on CO/Cu(100). Upon irradiation for 30 minutes with UV photons, H<sub>2</sub>CO formed POM (40 %) and ethylene glycol (20 %). The photopolymerized POM depolymerized at higher temperatures than those observed for POM formed from the thermal polymerization on clean Cu(100). Additionally, no losses due to endgroups were observed in EEL spectra taken after irradiation, consistent with longer chains. The initiation of polymerization likely occurs via the radical anion H<sub>2</sub>CO<sup>-</sup> formed from electron capture of photoelectrons generated from irradiation of the CO/Cu(100) surface.

X-ray irradiation also caused polymerization of H<sub>2</sub>CO adsorbed on CO/Cu(100), further supporting a substrate mediated process. Figure 6.1 shows TPD spectra displaying the effect of irradiating 1.1 ML of H<sub>2</sub>CO on CO/Cu(100) with X-ray photons ( $h\nu=1486.6$  eV,  $\lambda=0.8$  nm). Figure 6.1a shows the m=29 (HCO<sup>+</sup>) TPD prior to irradiation and is identical to Figure 5.1a-b (0 min.). A single feature at 104 K is observed corresponding to molecularly adsorbed H<sub>2</sub>CO. Figure 6.1b shows irradiation of the overlayer for 84 s

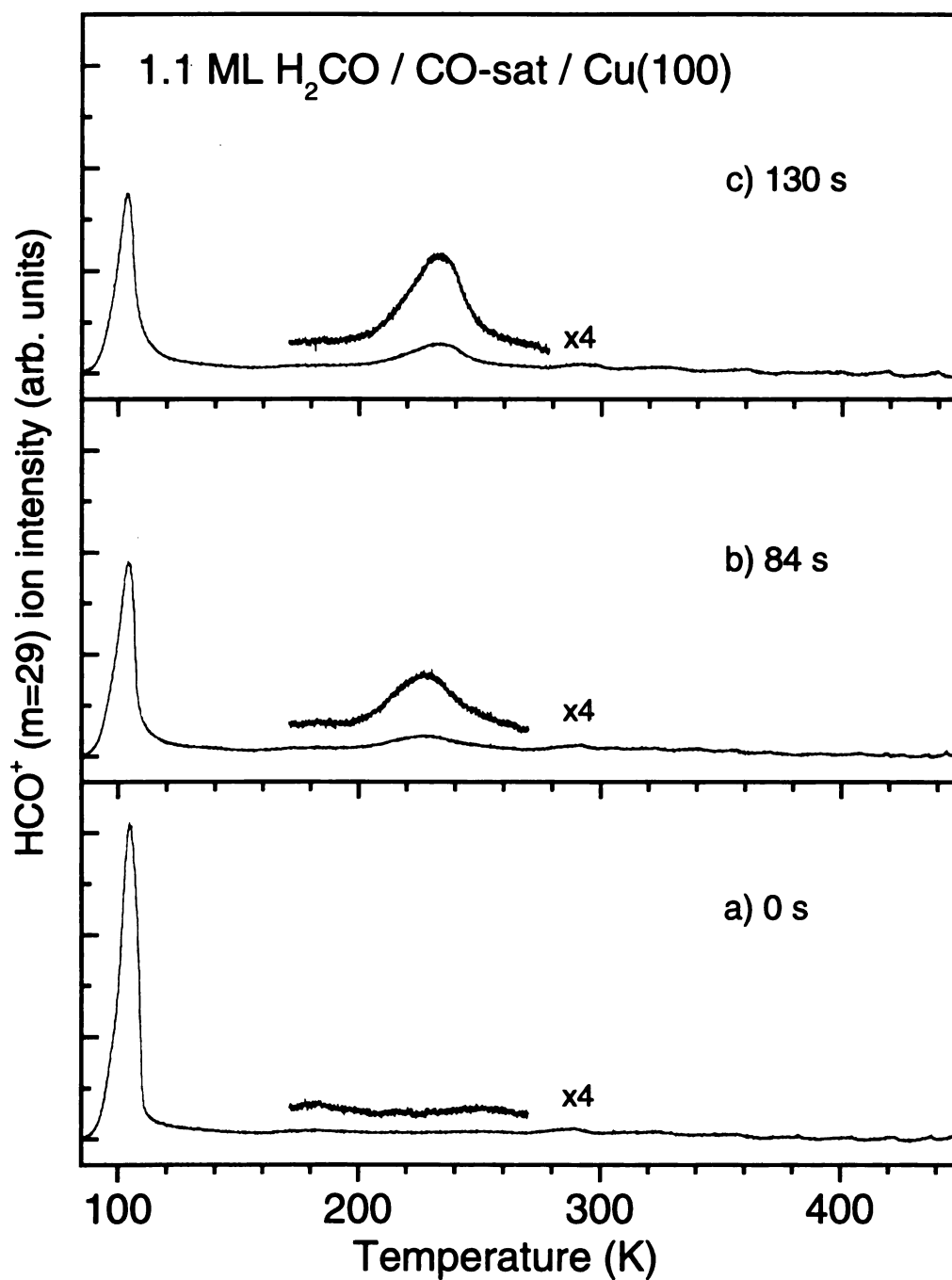


**Figure 6.1** Mass=29 ( $\text{HCO}^+$ ) TPD spectra showing the effect of X-ray irradiation on 1.1 ML  $\text{H}_2\text{CO}$  on CO/Cu(100). Irradiation times were a) 0, b) 84 and c) 130 seconds. The X-ray wavelength was the Al  $\text{K}\alpha$  ( $h\nu=1486.6$  eV) line and operated at 300 W (20 mA, 15 kV).

the

the

the

the

the

the

the

the

the

the

the

the

the

the

the

the

the

the

the

the

the

the

the

the

causes the feature at 104 K to decrease while a new feature is observed at 228 K that can be identified as  $\text{H}_2\text{CO}$  arising from the depolymerization of POM formed upon irradiation. Further irradiation causes a further decrease in the feature at 104 K, an increase in the  $\text{H}_2\text{CO}$  due to POM depolymerization and a shift to higher peak depolymerization maximum (233 K), as shown in Figure 6.1c. The large number of secondary electrons produced from the substrate upon X-ray irradiation<sup>11</sup> likely initiates the polymerization via the radical anion channel, although more work is necessary to elucidate the mechanisms of polymerization. The ability to form a polymer thin film using X-ray photons is advantageous in the field of lithography where feature sizes of < 100 nm are needed.<sup>12-14</sup>

*New Co-adsorbates.* While the use of CO is convenient, its desorption temperature (~ 180 K) prevents a determination of the "true" thermal stability of the POM formed in the irradiation of  $\text{H}_2\text{CO}$  adsorbed on CO/Cu(100) because, after the CO has desorbed, the POM then can interact with the substrate, lowering the depolymerization temperature as was discussed in Chapter 4. A more suitable co-adsorbate would be one that is stable on Cu(100) above the bulk POM depolymerization temperature of ~ 370 K. An excellent candidate for this is  $\text{CH}_3\text{O}(\text{ad})$  formed from the reaction of methanol on a oxygen covered Cu(100) surface. This species forms a c(2x2) overlayer ( $\theta_{\text{CH}_3\text{O}}=0.5$ ) similar to the CO/Cu(100) overlayer and is stable up to 400 K at which temperature  $\beta$ -hydride elimination occurs and  $\text{H}_2\text{CO}$  desorbs.<sup>15,16</sup> In this fashion, the stability of the POM may be deconvoluted from its interaction with the substrate. The  $\text{CH}_3\text{O}$  covered Cu(100) surface may also be prepared from methyl nitrite ( $\text{CH}_3\text{ONO}$ ), eliminating the need for the oxygen precoverage.<sup>17</sup>

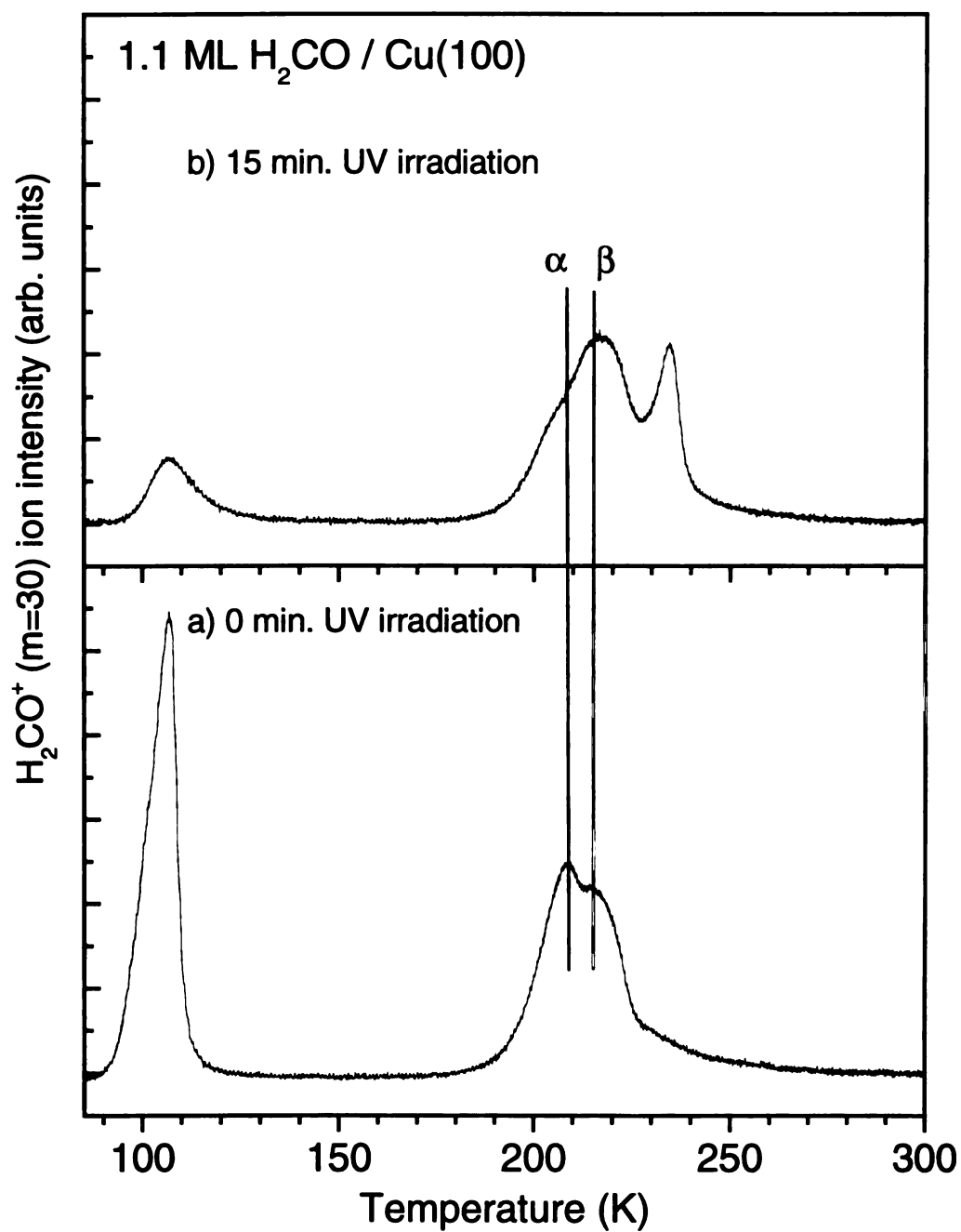


**Figure 6.2** Mass=30 ( $\text{H}_2\text{CO}^+$ ) TPD spectra for the UV irradiation of 1.1 ML  $\text{H}_2\text{CO}$  adsorbed on a surface that had been pre-covered with a saturation of poly(oxymethylene) (0.69 ML) for a) 0 minutes and b) 15 minutes UV irradiation.

Preliminary work has been done using another co-adsorbate system. Formaldehyde molecularly adsorbed on a POM saturated Cu(100) surface does polymerize upon UV irradiation. Figure 6.2 displays TPD spectra (a) prior to and (b) after 15 minutes of UV irradiation of a 1.1 ML coverage of molecularly adsorbed H<sub>2</sub>CO on a POM saturated Cu(100) surface. There are three features observed prior to irradiation which can be ascribed to desorption of physisorbed H<sub>2</sub>CO (105 K) and H<sub>2</sub>CO arising from depolymerization of the  $\alpha$  and  $\beta$ -POM species at  $\sim 210$  and  $\sim 215$  K, respectively. Fifteen minutes of UV irradiation causes both the physisorbed H<sub>2</sub>CO and  $\alpha$ -POM species to decrease and a new feature to appear at 234 K. The feature at 234 K is consistent with a new POM species and is similar to that observed for the photopolymerization of H<sub>2</sub>CO on CO/Cu(100), shown in Figure 5.1b, where a feature is observed at 235 K. The explanation for the decrease in  $\alpha$ -POM species, while little change in the  $\beta$ -POM species was observed, is still under investigation. However, the results shown in Figure 6.2b do suggest other co-adsorbate systems can be used to produce a more thermally stable POM thin film.

### 6.3 References

- (1) Tadokoro, H. In *Macromolecular Reviews*; Peterlin, A., Goodman, M., Okamura, S., Zimm, B., Mark, H., Eds.; Interscience: New York, 1967; Vol. 1; pp 119.
- (2) Sexton, B.; Hughes, A.; Avery, N. *Surf. Sci.* **1985**, *155*, 366.
- (3) Fleck, L.; Feehery, W.; Plummer, E.; Ying, Z.; Dai, H. *J. Phys. Chem.* **1991**, *95*, 8428.
- (4) Fleck, L.; Ying, Z.; Dai, H.-L. *J. Vac. Sci. Technol. A* **1993**, *11*, 1942.

- (5) Fleck, L.; Kim, J.; Dai, H.-L. *Surf. Sci.* **1996**, *356*, L417.
- (6) Fleck, L.; Howe, P.; Kim, J.; Dai, H. *J. Phys. Chem.* **1996**, *100*, 8011.
- (7) Walker, J. F. *Formaldehyde*, 3rd. ed.; Reinhold Publishing Corp.: New York, 1964.
- (8) Lamont, C.; Conrad, H.; Bradshaw, A. *Surf. Sci.* **1993**, *280*, 79.
- (9) Bent, B. E. *Chem. Rev.* **1996**, *96*, 1361.
- (10) Chan, Y.; Chuang, P.; Chuang, T. *J. Vac. Sci. Technol. A* **1998**, *16*, 1023.
- (11) Briggs, D.; Riviere, J. In *Practical Surface Analysis*; Briggs, D., Seah, M., Eds.; Wiley and Sons: New York, 1990; Vol. 1-Auger and X-ray Photoelectron Spectroscopy; pp 85.
- (12) Lawes, R. *Appl. Surf. Sci.* **2000**, *154-155*, 519.
- (13) Wallraff, G.; Hinsberg, W. *Chem. Rev.* **1999**, *99*, 1801.
- (14) Cerrina, F. *J. Phys. D: Appl. Phys.* **2000**, *33*, R103.
- (15) Dai, Q.; Gellman, A. *J. Phys. Chem.* **1993**, *97*, 10783.
- (16) Andersson, S.; Persson, M. *Phys. Rev. B.* **1981**, *24*, 3659.
- (17) Ihm, H.; Scheer, K.; Celio, H.; White, J. *Langmuir* **2001**, *17*, 786.



## APPENDICES

and

and

and

and

and

## Appendix A Mass Spectra

Prior to use in experiments, the molecules studied in this thesis were first analyzed for purity. This was accomplished by opening the molecular leak valve to introduce some of the gas-phase molecules into the UHV chamber. The mass spectrum was acquired after a steady state pressure (as measured by the ion gauge) was achieved within the chamber. Typical operating condition of the mass spectrometer were 1-50 amu mass range, 10 amu/s scan rate, and 1.7 kV electron multiplier voltage.

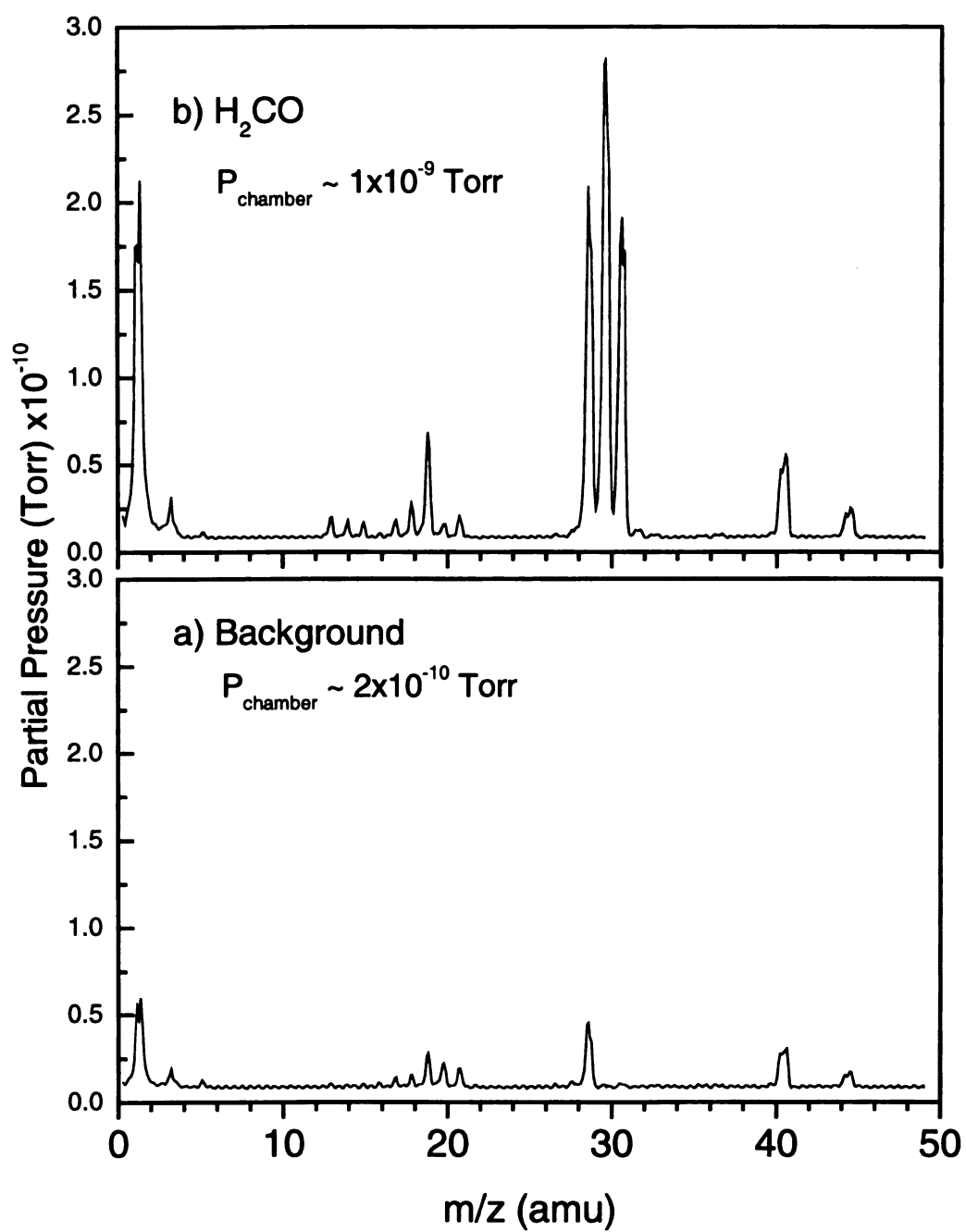


Figure A.1 Mass spectra of a) background vacuum prior to introduction of H<sub>2</sub>CO and b) after a pressure of  $\sim 1 \times 10^{-9}$  Torr of H<sub>2</sub>CO was achieved within the chamber.

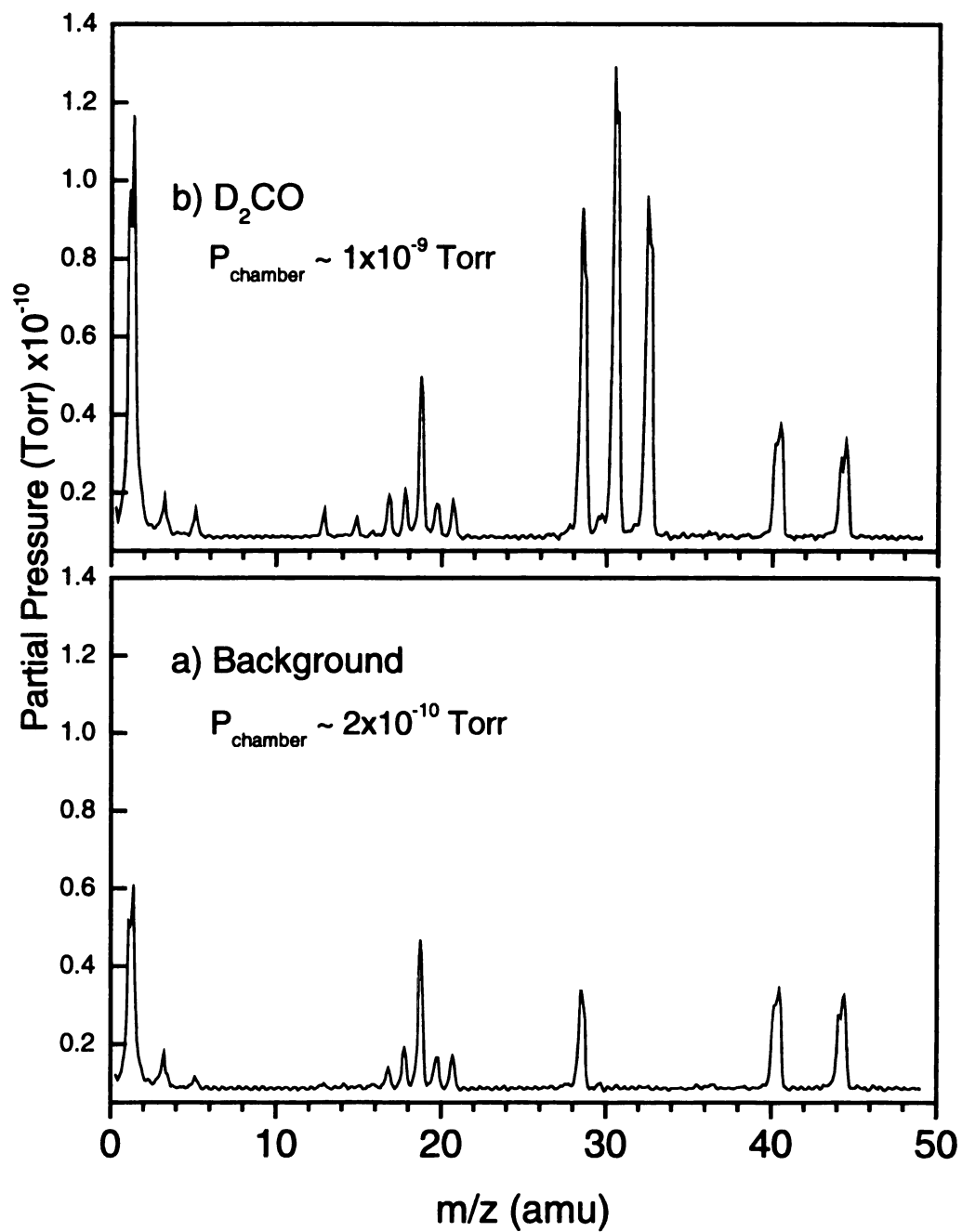


Figure A.2 Mass spectra of a) background vacuum prior to introduction of D<sub>2</sub>CO and b) after a pressure of  $\sim 1 \times 10^{-9}$  Torr of D<sub>2</sub>CO was achieved within the chamber.

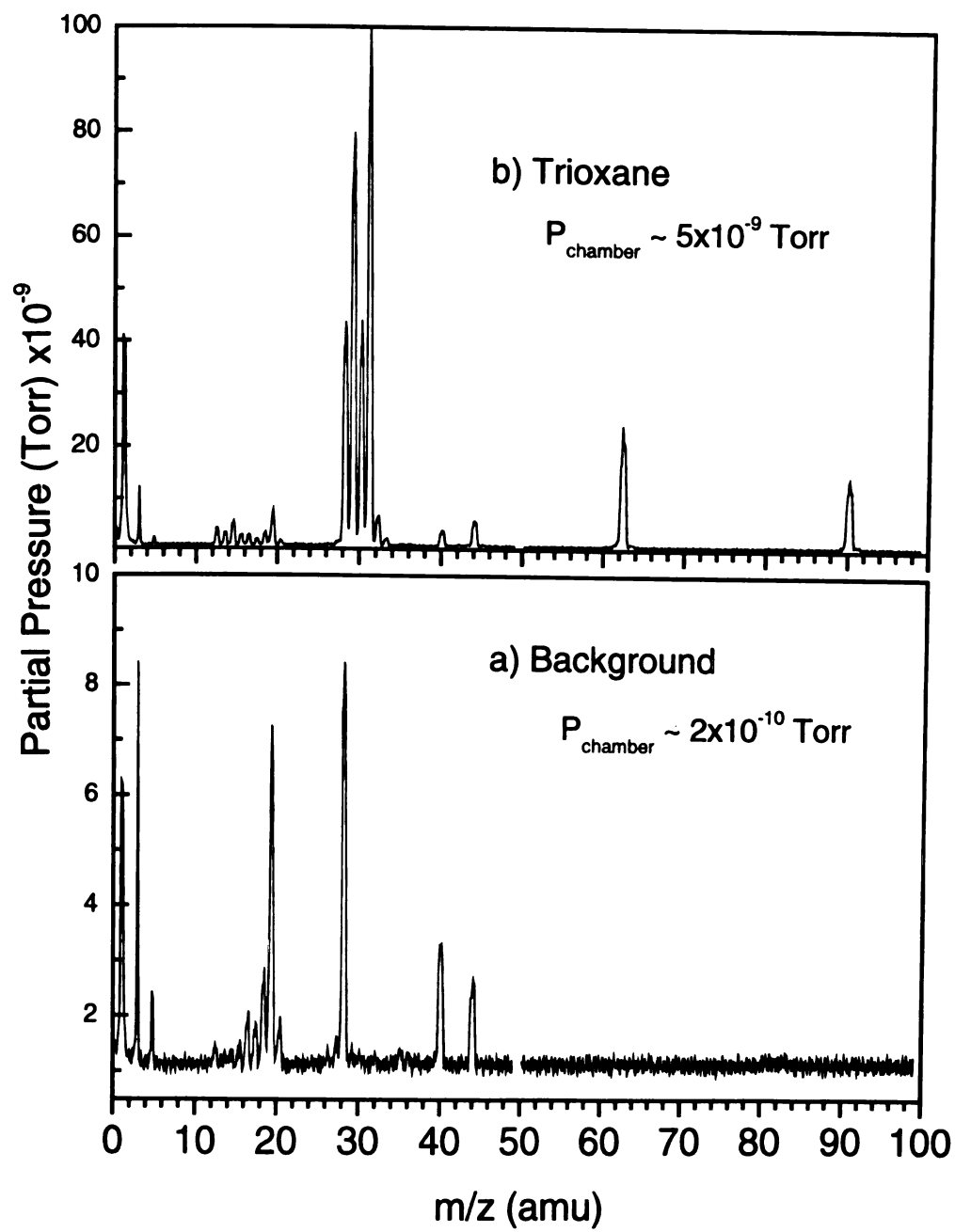


Figure A.3 Mass spectra of a) background vacuum prior to introduction of trioxane ( $\text{C}_3\text{H}_6\text{O}_3$ ) and b) after a pressure of  $\sim 5 \times 10^{-9}$  Torr of trioxane was achieved within the chamber.

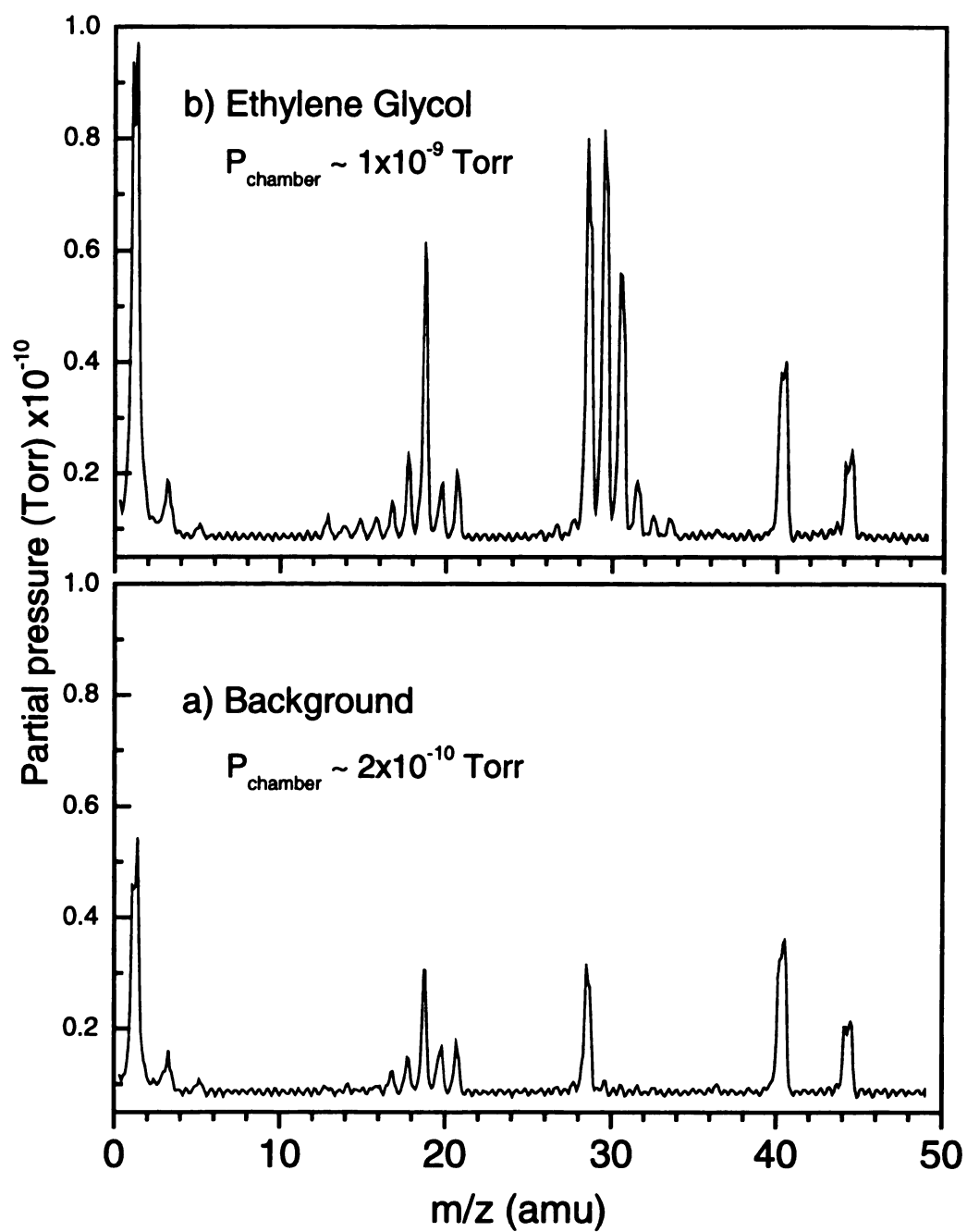


Figure A.4 Mass spectra of a) background vacuum prior to introduction of ethylene glycol ( $(\text{CH}_2\text{OH})_2$ ) and b) after a pressure of  $\sim 1 \times 10^{-9}$  Torr of ethylene glycol was achieved within the chamber.

## Appendix B Calculation of Electron Impact Ionization Cross-Sections

To calculate the purity of a compound accurately, based on the mass spectra presented in Appendix A, and quantitate surface species from TPD spectra, the electron impact (EI) ionization cross-section ( $\sigma_{EI}$ ) needs to be known. While the experimental  $\sigma_{EI}$  is known for a few of the compounds of interest ( $H_2O$ ,  $H_2$  and  $CO$ ),<sup>1,2</sup> the  $\sigma_{EI}$  for  $H_2CO$  is unknown to this author. However, binary-encounter-Bethe (BEB) theory has been shown to predict (within 10-15%) the  $\sigma_{EI}$  for small molecules using molecular orbital constants easily obtained from standard *ab initio* electronic structure programs such as GAMESS.<sup>2,3</sup>

The BEB theory combines the Mott description for hard electron-electron collisions with that of the dipole interaction theory that accounts for electron interaction at high incident electron energies. The theory provide a simple, analytic expression for the  $\sigma_{EI}$  per molecular orbital (MO) and the total  $\sigma_{EI}$  is then a sum over all MOs. Three orbital constants are needed: the binding energy  $B$ , the orbital kinetic energy  $U$  and the electron occupation number  $N$ . The expression, as a function of incident electron energy  $T$ , is:

$$\sigma_{EI} = \frac{S}{t+u+1} \left[ \frac{\ln(t)}{2} \left( 1 - \frac{1}{t^2} \right) + \left( 1 - \frac{1}{t} - \frac{\ln(t)}{t+1} \right) \right] \quad (B.1)$$

where

$$t = \frac{T}{B} \quad (B.2)$$

$$u = \frac{U}{B} \quad (B.3)$$



$$S = \frac{4\pi a_0^2 N R^2}{B^2} \quad (\text{B.4})$$

with  $a_0=0.5292 \text{ \AA}$  and  $R=13.61 \text{ eV}$ .

The orbital constants were calculated at the minimized geometry at the Hartree-Fock level with a 6-31G\* basis set using the GAMESS<sup>4</sup> code. The orbital constants for H<sub>2</sub>O and H<sub>2</sub>CO are summarized in Table B.1 and the  $\sigma_{\text{EI}}$  as a function of T is shown in Figure B.1. The  $\sigma_{\text{EI}}$  and orbital constants for H<sub>2</sub>O have been previously calculated and are compared to those calculated for this work as a measure of the error. The variation arises due to differences in basis set used (6-311G vs. 6-31G\*) and the use of the experimental ionization energy for the HOMO of water in the previous work.<sup>2</sup> All quantitation is done using calculated  $\sigma_{\text{EI}}$  to eliminate large discrepancies that may arise between experimental and calculated values.

Table B.1 Molecular orbital constants calculated at the Hartree-Fock level of theory with a 6-31G\* basis set. These constants were used to evaluate the electron impact ionization cross-section.

H <sub>2</sub> O <sup>a</sup>		
Molecular Orbital	Binding Energy (eV)	Kinetic Energy (eV)
2a <sub>1</sub>	36.46	70.14
1b <sub>2</sub>	19.12	47.78
3a <sub>1</sub>	15.47	58.73
1b <sub>1</sub>	13.52	61.89

H <sub>2</sub> O <sup>b</sup>		
Molecular Orbital	Binding Energy (eV)	Kinetic Energy (eV)
2a <sub>1</sub>	36.88	70.71
1b <sub>2</sub>	19.83	48.36
3a <sub>1</sub>	15.57	59.52
1b <sub>1</sub>	12.61	61.91

H <sub>2</sub> CO		
Molecular Orbital	Binding Energy (eV)	Kinetic Energy (eV)
3a <sub>1</sub>	38.56	73.68
4a <sub>1</sub>	23.59	44.02
1b <sub>2</sub>	18.95	36.77
5a <sub>1</sub>	17.74	61.17
1b <sub>1</sub>	14.69	47.46
2b <sub>2</sub>	11.83	54.58

a) this work

b) Reference 2

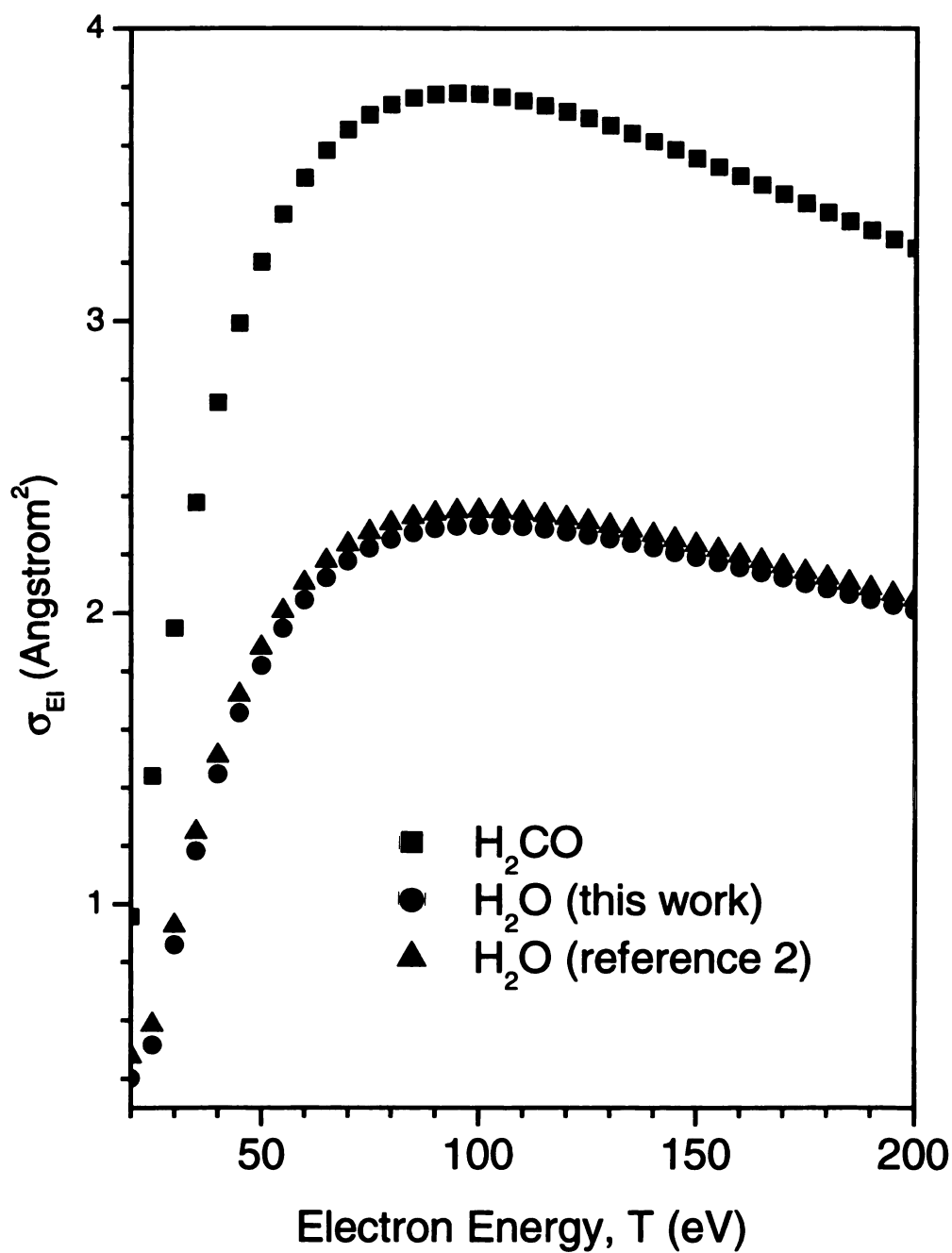


Figure B.1 Electron impact ionization cross-section ( $\sigma_{EI}$ ) as a function of incident electron energy for  $H_2CO$  and  $H_2O$  and a comparison to previous work done for water showing the small error introduced by using a smaller basis set.

## B.1 References

- (1) Beran, J.; Kevan, L. *J. Phys. Chem.* **1969**, *73*, 3866.
- (2) Hwang, W.; Kim, Y.; Rudd, M. *J. Chem. Phys.* **1996**, *104*, 2956.
- (3) Kim, Y.; Rudd, M. *Phys. Rev. A.* **1994**, *50*, 3954.
- (4) Schmidt, M. W.; Baldridge, K. K.; Boatz, J. A.; Elbert, S. T.; Gordon, M. S.; Jensen, J. H.; Koseki, S.; Matsunaga, N.; Nguyen, K. A.; Su, S. J.; Windus, T. L.; Dupuis, M.; Montgomery, J. A. *J. Comput. Chem.* **1993**, *14*, 1347.

## Appendix C Electron Energy Loss Spectrometer and Operating Voltages

Shown in Figure C.1 is a schematic of the ELS3000 electron energy loss spectrometer manufactured by LK Technologies, Inc. The operating voltages for the individual segments are shown in Table C.1. These voltages were used as initial parameters prior to tuning the spectrometer in the “straight through” geometry. The resolution obtained using these voltages was 3.2 meV ( $26\text{ cm}^{-1}$ ) full width half maximum (FWHM) and provided  $\sim 70\text{ pA}$  of current detected at the channeltron cone.

Table C.1 Operating voltages for the ELS3000 electron energy loss spectrometer.

Setting		Setting	
Cathode		Monochromator	
Filament, V	3.22	M1	2.639
Filament, A	1.90	M1-slit	-0.31
Beam, E	-6.09	M1-cover	-3.56
Emission Optics		$\Delta$ M1-cover	0.16
R	-2.71	M2	0.638
A1	46.22	M2-slit	0.12
$\Delta$ A1	-3.54	M2-cover	-0.16
A2	0.70	$\Delta$ M2-cover	0.03
$\Delta$ A2	1.60	M2-exit	0.49
A3	0.10		
$\Delta$ A3	0.56		
Lenses		Analyzers	
B1	0.78	AN1	0.572
$\Delta$ B1	0.04	AN1-slit	0.46
B2	3.05	AN1-cover	-0.43
B3	2.98	$\Delta$ AN1-cover	0.14
B4	0.67	AN2	0.576
$\Delta$ B4	0.11	AN2-slit	0.35
		AN2-cover	-0.43
Miscellaneous		$\Delta$ AN2-cover	-0.01
Shield	0.0		
Sample	0.003		
Ch-slit	1.00		
Ch-cone	0.51		
Scan	0.001		
Scan-step	3.41		
Offset	0.001		
B3 ramp	1.0		
B4 ramp	1.0		
C.S. ramp	1.0		

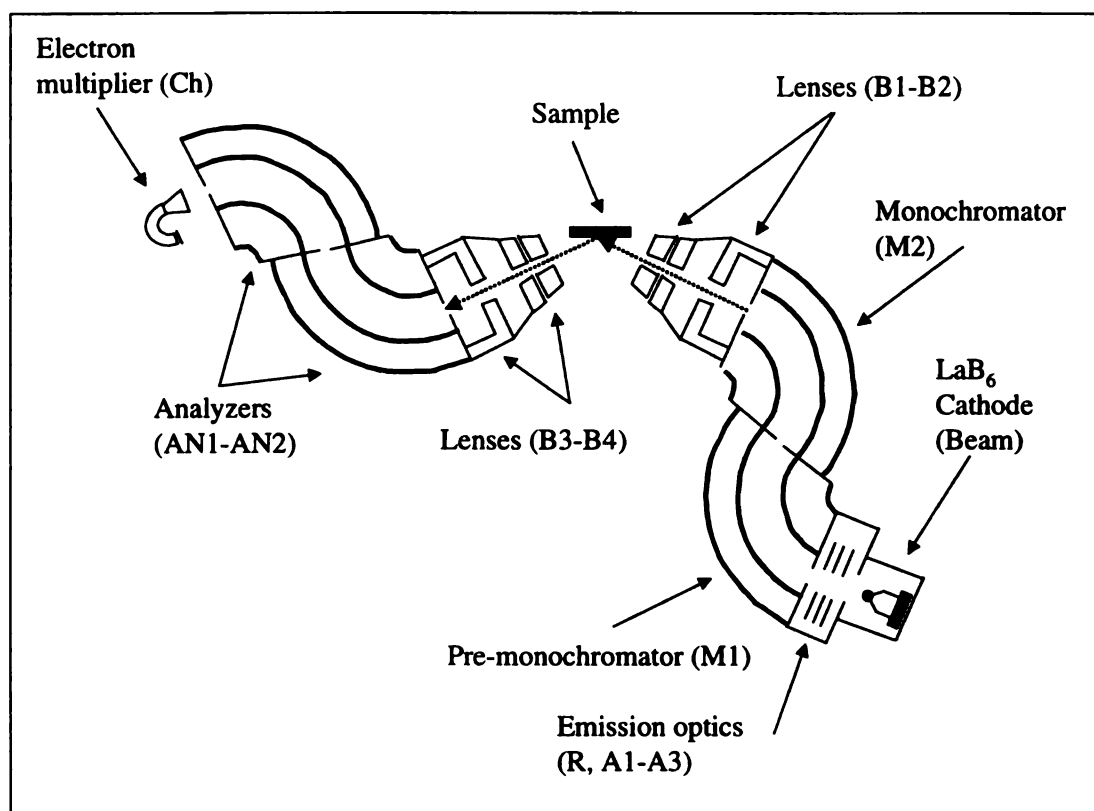


Figure C.1 Schematic of the ELS3000 electron energy loss spectrometer.

MICHIGAN STATE LIBRARIES



3 1293 02177 7721